Pore Pressure Generation Characteristics of a Liquefiable Sandy Layer in a Stratified Soil Deposit

by

Avik Saha

Exam Roll no:-M4CIV23005

Registration no: - 160038 of 2021-2022

Under the Guidance of

Dr. Narayan Roy, Assistant Professor, Civil Engineering Dept., Jadavpur University

SUBMITTED IN PARTIAL FULFILMENT OF THE REQUIREMENTS FOR THE AWARD OF THE DEGREE OF MASTER OF ENGINEERING IN CIVIL ENGINEERING IN THE FACULTY OF ENGINEERING AND TECHNOLOGY

JADAVPUR UNIVERSITY

(2023)

DEPARTMENT OF CIVIL ENGINEERING

JADAVPUR UNIVERSITY

KOLKATA-700032

INDIA

JADAVPUR UNIVERSITY

FACULTY OF ENGINEERING AND TECHNOLOGY

DECLARATION

I hereby declare that, this thesis contains literature review and original research works by the undersigned candidate, as a part of his Master of Civil Engineering in Soil Mechanics and Foundation Engineering studies. All the information in this document has with academic rules and ethical conduct.

I also declare that, as required by these rules and conduct, I have fully cited and referenced all material and results that are not original to this work.

Thesis Title:-Pore Pressure Generation Characteristics of a Liquefiable Sandy Layer in a Stratified Soil Deposit.

Date:-……

Place:-……

……

(Avik Saha)

Exam Roll no:-M4CIV23005

Registration no:- 160038 of 2021-2022

Class Roll no:-002110402024

Jadavpur University

JADAVPUR UNIVERSITY
FACULTY OF ENGINEERING AND TECHNOLOGY
DEPARTMENT OF CIVIL ENGINEERING

CERTIFICATE OF RECOMMENDATION

I hereby recommend that the thesis entitled **"Pore Pressure Generation Characteristics of a Liquefiable Sandy Layer in a Stratified Soil Deposit"** submitted by **Avik Saha** carried out under our supervision and guidance be accepted in the partial fulfilment of the requirements for the degree of "**Master of Engineering in Civil Engineering"** in Jadavpur University.

.

Thesis Supervisor

(DR. NARAYAN ROY)
Assistant Professor
Dept. of Civil Engineering
Jadavpur University
Kolkata-700032

Countersigned by

DEAN
Faculty of Engineering and Technology

H.O.D.
Faculty of Engineering and Technology

JADAVPUR UNIVERSITY

FACULTY OF ENGINEERING AND TECHNOLOGY

DEPARTMENT OF CIVIL ENGINEERING

CERTIFICATE OF APPROVAL

The foregoing thesis is hereby approved as a creditable study of an engineering subject carried out and presented in a manner of satisfactory to warrant its acceptance as a pre-requisite to the degree for which it has been submitted. It is understood that by this approval, the undersigned do not necessarily endorse or approve any statement made, opinion expressed and conclusion drawn therein but approve the thesis only for the purpose for which it has been submitted.

COMMITE OF FINAL EXAMINATION FOR

EVALUATION OF THE PROJECT WORK

1. **---------- (Signature of the Examiner)**
2. **---------- (Signature of the Examiner)**
3. **---------- (Signature of the Examiner)**

ACKNOWLEDGEMENT

It is my greatest fortune to perform the thesis work in the Civil Engineering Department, Jadavpur University. I express my heart-felt gratitude to my esteemed guides Dr. Narayan Roy, Assistant Professor, Dept. of Civil Engineering, Jadavpur University. It is because of his noble and continuous guidance, encouragement as well as valuable advices at every aspect and strata of the problem from the embryonic to the development stage that my thesis has been in the light of the day. My special thanks to Head of Civil Engineering Department for allowing me to carry out the research investigation with various facilities of the department. I am also grateful to all research scholars and appreciate the support of librarian, technicians and other staffs of our department for their cordial assistance throughout my thesis work. I express my appreciation to my friends for their understanding, patience and active co-operation throughout my course. I feel pleased and privileged to fulfil my ambition of my parents and I am greatly indebted to them for their scarification in nurturing me and bearing the inconvenience throughout my academic course. Any omission in this brief acknowledgement does not mean lack of gratitude.

(Avik Saha)

Department of Civil Engineering

Exam Roll no:-M4CIV23005

Registration no:-160038 of 2021-2022

Class Roll no:-002110402024

MCE Student (Specialization: Soil Mechanics and Foundation Engineering)

Department of Civil Engineering

Jadavpur University

Kolkata:-700032

Pore Pressure Generation Characteristics of a Liquefiable Sandy Layer in a Stratified Soil Deposit

Contents

List of Tables

Abstract

Soil liquefaction is one of the most dangerous threats to civil engineering structures constructed in sandy grounds when earthquakes occur. Due to the disastrous effect of liquefaction phenomena, in last few decades the study focused on the factors responsible behind such behaviour of soil and ways to mitigate the cause had been studied intensively. This parametric study is done to determine the pore pressure generation characteristics of a stratified sandy soil under seismic loading. Pore pressure generation characteristics will help us in removing the excess pore pressure generated in soil under seismic loading. This study is conducted using nonlinear finite difference software FLAC 2D. The parametric variation of intensity of input motion, type of motion, embankment loading and variation in height of liquefiable layer. From the study it was found that the pore pressure generation increase with the increase in intensity of the earthquake. Power amplitude of input motion also affect the extent of pore pressure generation. With the increase in the length of the embankment the pore pressure generation intensity also increases and cause failure of soil. As the height of liquefiable soil increases the, depth of soil liquefaction also increases. To overcome this pore pressure generation proper ground improvement must be done before starting construction work.

CHAPTER 1

INTRODUCTION

1.1 Liquefaction

Liquefaction is the phenomena that has been simultaneously used with Earthquake to understand and study the effect of cyclic loading on the soil deposit caused during earthquake. Past study of liquefaction shows that the cyclic loading in the soil caused by seismic force generate excess pore pressure, which ultimately reduce the effective earth pressure causing the failure of soil and the structure above it. The soil Liquefaction causes huge damage. So the study of the way a soil deposit will behave under cyclic loading and excess pore pressure generation in the soil is of high importance. Understanding the pore pressure generation patterns in a soil will help us in preventing liquefaction in soil as well as to take better preventative measure against it.

There are basically three possible ways to reduce the damage caused by liquefaction hazard.

1. Avoid Liquefaction Susceptible Soils: The first possibility, is to avoid construction on liquefaction susceptible soils. There are various criteria to determine the liquefaction susceptibility of a soil. By characterizing the soil at a particular building site according to these criteria, susceptibility to liquefaction of a soil can be decided and therefore the unsuitable soil can be avoided.

2. Build Liquefaction Resistant Structures: After detecting the susceptibility of a soil the structure should be redesigned to prevent or counteract the effect of pore pressure generation in the soil. Redesigning of the structure is not always suggested as it is not suitable for smaller projects.

3. Improve the Soil: The best way to prevent the soil liquefaction is to improve the property of the soil that causes the liquefaction. Following are the few of the important parameters that effect the liquefaction in soil i.e. density of the soil, ground water level, permeability of the soil, finesses content of the soil, void ratio of the soil etc. Various ground improvement technique such as sand drain, stone column and vibro-flotation are used to improve soil property.

Kolkata is situated in the eastern part of India. It has located linearly along the banks of the Hooghly River. Kolkata is currently known as the capital city of West Bengal. The Kolkata Municipal Corporation (KMC) has an area of 187 sq km and housing a population of 4.6 million, it is the largest urban local body in West Bengal and also one of the largest in India. Kolkata is situated over a huge pericratonic tertiary basin with enormous thickness of fluvial-marine sediments. The basin can be divided into three structural units: The westernmost shelf or platform, the Central hinge or shelf/slope break and deep basinal part in the east and south east that open in the present Bay of Bengal.(Roy and Chattopadhyay, 1997). The KMC area has been developed geologically by deposition of sediments carried by big river system, so the soil below the ground is basically erratic in nature. Geomorphologic-ally the area have been divided into fluvial plain, tidal flat, natural levee and aggravated channels **(Nandi 2007)**. From the past study, It was also observed that the study of the upper thick sticky clay, overlaying the

thicker coarse sandy unit up to a depth of 30-60m of Kolkata soil are very important in understanding the behavior of soil toward the earthquake shaking and liquefaction potential ((Nath 2006).

In recent years the rapid growth of population in Metropolitan city like Kolkata has led to increase in construction of building in the marshy areas like that of Saltlake and Rajarhat. This rapid constructions of residential building, hospitals, schools and shopping complexes in marshy regions are the main concern for the increase in the vulnerability toward the liquefaction of Kolkata soil in the event of the Earthquake. As per IS code the IS 1893 – Criteria for the design of Earthquake Resistant Design of Structures, Kolkata lies in the seismic zone III with a zone factor 0.16. Over the past Kolkata had experienced shaking and damage to buildings by both far and near source earthquakes. Notable amongst them are 1906 Calcutta Earthquake of intensity of order VI- VII based on Rossi- Forel Scale, 1969 Sagar Island Earthquake of order VII on MMI scale (Modified Mercalli Intensity), 1897 Assam Earthquake of order VIII o MMI scale, 1918 Srimangal Earthquake, 1934 Bihar Nepar Earthquake of order VI on MMI, 1964 Contai earthquake which had intensity of VIII (MM scale), recent 2006 Sikkim Earthquake and many more.

1.2 Origin of the Problem

From our study of literature on Liquefaction potential of Kolkata soil, based on the article from **Nath et al [2017]** on "Earthquake induced liquefaction hazard, probability and risk assessment in the city of Kolkata, India: its historical perspective and deterministic scenario" where he performed an extensive micro zonation study on Kolkata soil using stochastic simulation of 1934 Bihar-Nepal and 1897 Shillong earthquakes. The study suggest that the Liquefaction Risk Index I_R of various locations of Kolkata mainly ranges from high to very high. From the study he also concluded New Town—economic and finance centre of the city and part of skyscraper inhabited in Rajarhat to be more susceptible to soil liquefaction and, therefore, are at high Liquefaction risk. So based on the analysis on **Nath et al [2017]** we have selected soil profile of Rajarhat site for the parametric analysis of pore pressure generation. Study of pore pressure generation will help us in better designing of structure above the soil deposit of Kolkata.

1.3 Objective of the Parametric Study

The objective of this study is to investigate the pore pressure generation behaviour of a liquefiable sandy layer in a stratified soil deposit under seismic condition.

1.4 Scope of the Study

The present investigation studies the seismic response and pore pressure generation of a liquefiable sandy layer of a stratified soil deposit with varying thickness of liquefiable layer, intensity of shaking, type of input motion and surcharge loading using FLAC 2D.

1. A parametric study has been performed by varying the thickness of liquefiable layer to 5m, 9m, 15m and 20m.

2. The study is conducted to investigate the effect of intensity of input motion. In this regard the intensity of Loma Prieta earthquake is scaled to 0.05g, 0.1g, 0.2g and 0.357g and used as input motion in the analysis.

3. To study the effect of different input ground motion, Mammoth lake Earthquake, North Ridge Earthquake and Loma Prieta Earthquake have been used in the analysis as a scaled motion of intensity 0.2g.

4. To study the effect of surcharge on pore pressure generation behaviour, an embankment loading is used and the width of the embankment (4m height) is varied to 10m, 20m and 30m.

CHAPTER 2

LITERATURE REVIEW

Over the past few decades the of pore pressure generation in soil under cyclic and seismic loading had been studied. Based on the study various researchers have developed numerous numerical models of pore pressure generation in soil. A few of the suitable theories and relevant literature review have been discussed in brief in this chapter.

2.1 Method of analysis of the generation and dissipation of Pore pressure.

Seed et al. (1975) in his report on "the generation and dissipation pore water pressure during soil liquefaction" present a means for analysing the development and redistribution of pore water pressures in a horizontally stratified deposit of sand, both during and following the periods of earthquake shaking. There was two methods of expressing the rate of build-up of pore water pressures in soil deposit subjected to cyclic loading. 1. By means of test data on the rate of settlement of dry sand under cyclic loading conditions combined with a knowledge of the rebound characteristics and the stress-deformation characteristics of the sand, analyses could be made to predict the rate of pore pressure development due to any sequence of cyclic stress applications. 2 By observing the rate of pore pressure development in cyclic loading tests. it has been found that the rate of build-up generally lies within a fairly narrow range when plotted in the normalized form as concluded from the test results of cyclic triaxial test data of Lee & Albaisa and De Alba et al (Fig 1 and 2) .

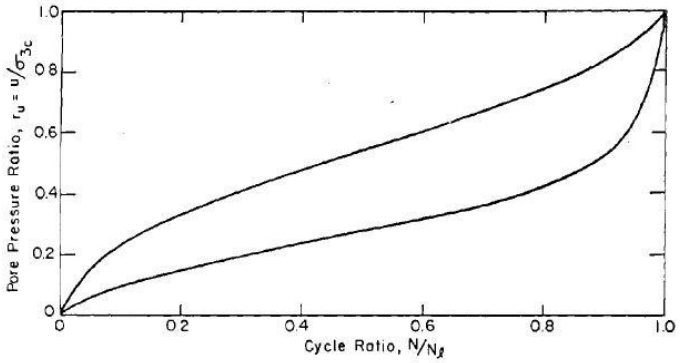

Fig 1: rate of pore pressure build -up in cyclic triaxial tests, (Lee and Albaisa)

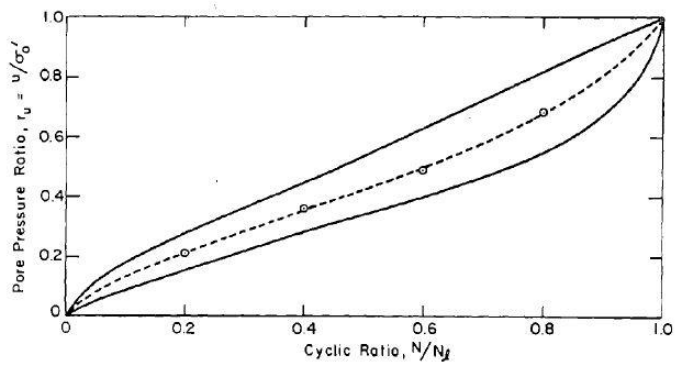

Fig 2: rate of pore water pressure build-up in cyclic simple shear tests. (otter De Alba et al.)

As derived from the results of cyclic triaxial test data of different sands done by Lee and Albaisa (1974), shows that the results are falling within the band shown in Fig. 1. Similarly cyclic simple shear tests on sand at different relative densities done by De Alba, et al. (1975) shows that the data is falling within the band shown in Fig. 2. From Fig. 2, he then considered that the curve shown by the dashed line representative of sands with a relative density of about 60%, provides the best general representation of the rate of pore pressure development in sands exhibiting a serious liquefaction potential problem. Using the assumption that other sands will exhibit similar characteristics. The dashed curve has been adopted as a convenient basis for predicting the rate of pore pressure generation. He proposed the following equation for pore pressure generation.

$$r_u = \frac{1}{2} + \frac{1}{\pi} \arcsin\left(2r_N^{\,1/\alpha} - 1\right) \quad (1.1)$$

$$r_N = \left[\frac{1}{2}\left(1 - \cos \pi r_u\right)\right]^{\alpha} \quad (1.2)$$

Here

r_u is the pore pressure ratio

r_n is cycle ratio

α = recommended to be functions of soil properties and test conditions with an average value of 0.7; and

N = number of equivalent uniform loading cycles.

After this he had discussed the procedure for the evaluation of pore pressure generation and dissipation along with the incorporation of pore pressure in finite difference analysis. He had also discussed the effect of depth of water table on pore pressure generation in soil and effect of soil permeability and grain size on liquefaction response. From his study he also concluded that improving the drainage capability of a sand deposit by the installation of a highly pervious continuous drainage system may thus provide an effective means of stabilizing a potentially unstable deposit. The simplified theory presented above offers the potential for predicting changes in pore water pressures with sufficient accuracy for many practical purposes where extreme accuracy of test data is not required. This approach depends upon the accuracy of establishing soil properties data.

2. Martin et al. (1975) in his journal on Fundamentals of liquefaction under cyclic loading proposed an alternative framework on the basis of strain controlled cyclic test performed in dry sand. The author produced an semi empirical formula relating tendencies of volumetric straining and excess pore water pressure of dry and fully saturated sand subjected to strain cycles. The expression was proposed as

$$\Delta u = E_r \cdot \Delta \varepsilon_{vd} \quad (1.3)$$

Here

Δu = increase in excess pore-water pressure;

E_r = tangent modulus of the one-dimensional (1D) unloading curve corresponding to the initial effective vertical stress; and

$\Delta \varepsilon_{vd}$ is the change in volumetric strain attributable to cyclic shearing

For determination of pore pressure the author had provided steps of calculation

1. The available initial condition prior to each loading are the shear stress amplitude, vertical effective stress, accumulated volumetric slip strain and pore water pressure from previous cycles.

2. Calculation of shear strain amplitude for corresponding shear stress amplitude is done by using the graph (Fig 3) or using the equation.

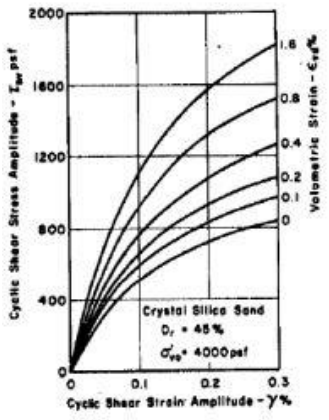

$$\tau_{hv} = \frac{(\sigma'_v)^{1/2}}{a+b} \qquad (1.4)$$

Fig 3: Effect of Cyclic shear strain amplitude and volumetric strain on Drained stress strain amplitude (Martin et al, 1975)

3. Calculation of increment of the volumetric slip strain ($\Delta\varepsilon_{vd}$) from the calculated shear strain amplitude using

$$\Delta\varepsilon_{vd} = C_1 \cdot (\gamma - C_2 \cdot \varepsilon_{vd}) + \frac{C_3 . \varepsilon^2_{vd}}{\gamma + C_4 . \varepsilon_{vd}} \qquad (1.5)$$

4. Calculation of the unloading modulus Er.

$$\bar{E}_r = \frac{d\sigma'_v}{d\epsilon_{vr}} = \frac{(\sigma'_v)^{1-m}}{mk_2(\sigma'_{vo})^{n-m}} \qquad (1.6)$$

σ_v' and σ_{vo}', respectively = vertical and initial vertical effective stresses;
γ = induced cyclic shear strain;
ε_{vd} = accumulated volumetric strain; and
Ci, m, n, k_2 = model coefficients/ constant
5. Substituting the value of Er and $\Delta\varepsilon_{vd}$ in Δu equation.

Then author had computed the increase in pore water pressure for undrained stress controlled cyclic stress and determined that the pattern shows a similarity with that generated in experimental study. The result for a case with initial vertical stress σ_{vo}' 4000Psf and various value of τ/ σ_{vo}' is shown below (Fig 4).

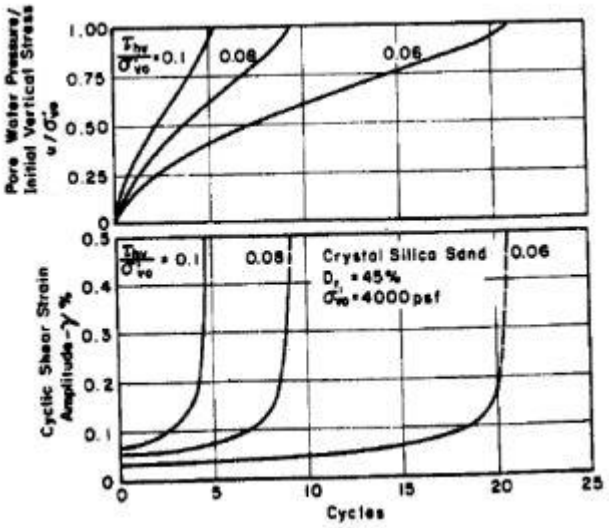

Fig 4: Results for undrained stress controlled cyclic simple shear test on Crystal silica sand (Martin et al, 1975)

3. Byrne (1991). Proposed a modified and simpler volume change model with two calibration parameters. The governing equation was expressed as:

$$\frac{\Delta\varepsilon_{vd}}{\gamma} = C_1 \cdot \exp(-C_2 \cdot \frac{\varepsilon_{vd}}{\gamma}) \tag{1.7}$$

Where; C_1 and C_2 are model constants. Byrne also proposed a correlation between these constant and relative density D_r of the soil.

$$C_1 = 7600(D_r)^{-2.5} \tag{1.8}$$

$$C_2 = \frac{0.4}{C_1} \tag{1.9}$$

The shear induced volumetric strain for constant amplitude of cyclic shear strain predicted by this formula is plotted versus number of cycles in Fig 5. The formula predicts an increase in shear-induced (compactive) volumetric strain with the level of cyclic shear-strain. Also, for a given strain amplitude, γ, the rate of accumulation decreases with the number of cycles.

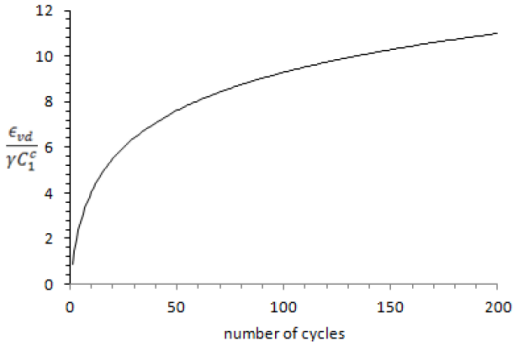

Fig 5: Byrne formula- constant cyclic shear strain amplitude (Byrne 1991)

2.2 Study of Factors affecting Pore pressure generation in soil.

Over the past decade researchers have studied the pore pressure generation in sand by both experimental and theoretical modelling methods. The past studies have suggested the below mentioned factors affecting the pore pressure generation in cohesionless soil.

a. Shear strain of soil
b. Relative Density of the cohesion less soil
c. Confining pressure
d. Frequency of the Cyclic Loading
e. Percentage of fines
f. Number of loading cycles

1. **Sitharam & Govindaraju (2007)** in their paper on "pore pressure generation in silty sands during cyclic loading", geomechanics and geoengineering had conducted an experimental investigation by strain controlled cyclic loading test to study the pore water pressure response in liquefiable soil. The experimental study was conducted on sand from 3 different locations as Bhuj, Ahmeadabad and Assam (Table 1). Dry deposition method had employed to prepare the soil specimen for strain controlled cyclic triaxial test.

Table 1: Index property of soil used in the experimental analysis of Sitharam and Govindaraju (2007).

	Location of soil sample		
Index property	Bhuj	Ahmedabad	Assam (Beltaghat)
Specific gravity	2.67	2.66	2.66
Gravel (%)	NIL	NIL	NIL
Coarse sand (%)	NIL	NIL	NIL
Medium sand (%)	35	37	48.8
Fine sand (%)	43	53.4	45
Silt size (%)	20	9.6	6.2
Clay size (%)	2	NIL	NIL
Liquid limit (%)	21.6	NP	NP
Plasticity index (%)	3.8	NP	NP
Maximum void ratio (e_{max})	0.68	0.67	0.91
Minimum void ratio (e_{min})	0.42	0.54	0.53

The tests were conducted to determine the effect of change in Relative Density, cyclic strain, confining pressure and frequency on pore pressure generation in 3 different types of soil. The parameters selected for the test was as mentioned below.

Table 2: Test parameters selected by Sitharam and Govindaraju (2007) in their analysis of pore pressure generation in sandy soil

Material	Relative density (%)	Confining pressure (kPa)	Frequency (Hz)	Shear strain (%)
Bhuj sand	8.9, 56.5 and 80	100	1	0.18 to 0.61
Ahmedabad sand	30, 50 and 70	100	1	0.15 to 0.64
Assam sand	20, 50 and 75	100	1	0.14 to 0.77
Assam sand	50	25, 50, 100 and 200	1	0.13 to 0.77
Assam sand	50	100	0.2, 0.5, 1, 2 and 3	0.22 to 0.77

After comparing the result of several tests they concluded that the pore pressure ratio upto a level of effective confining pressure is a function of both cyclic stress and number of cycles.

The graph drawn between pore pressure and number of cycles showed an increase in rate of pore pressure ratio build up with shear strain at constant relative density. (Fig 6)

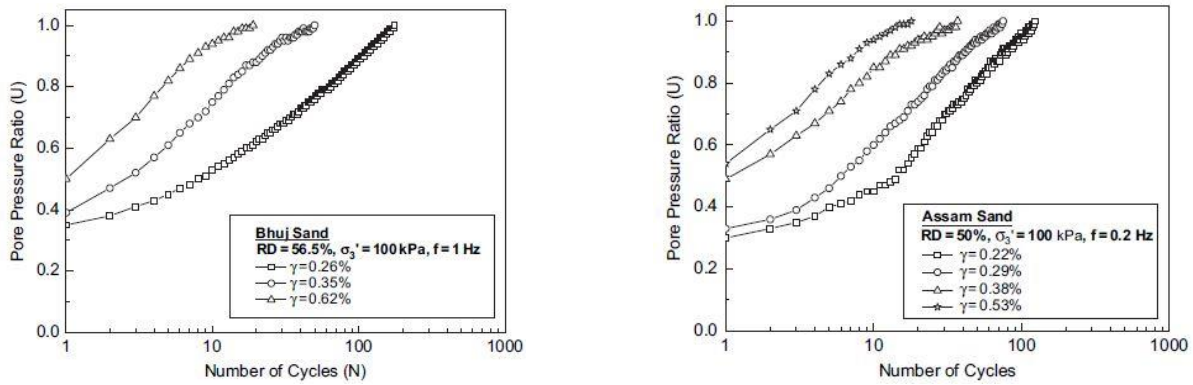

Fig 6: Results of Plot between Number of cycles and Pore pressure for Bhuj Sand (at RD-56.5% and frequency 1Hz) and Assam sand (at RD- 50 and frequency 0.2Hz)from the experimental analysis of Sitharam and Govindaraju (2007) showing similar pattern to change in shear strain.

They also concluded that when the same pore pressure ratio was plotted with respect to the Cycle ratio they provide a relationship independent of the amplitude of cyclic strain at a constant relative density (Fig 7).

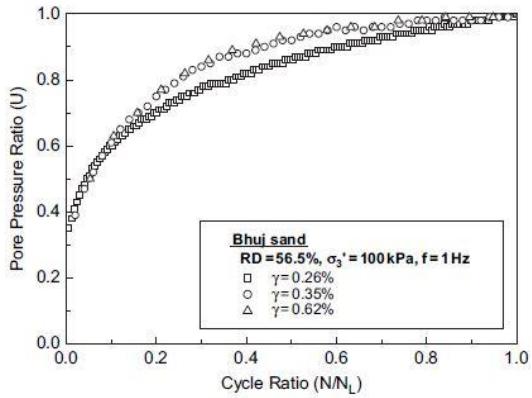

Fig: 7 Shows the plot of pore pressure ratio vs Cycle ratio at Constant and RD and variable strain for Bhuj sand

The **Effect of Relative Density** was also concluded by them from the plot of pore pressure ratio vs of number of cycles (Fig- 8), as the relative density increases the rate of pore pressure ratio buildup decreases. But the decrease of rate of pore pressure ratio is not much significant when the same data was plotted on pore pressure ratio vs Cycle ratio as seen from the above plotted graph. Here the data represent a relationship independent of relative density for constant strain, confining pressure and frequency.

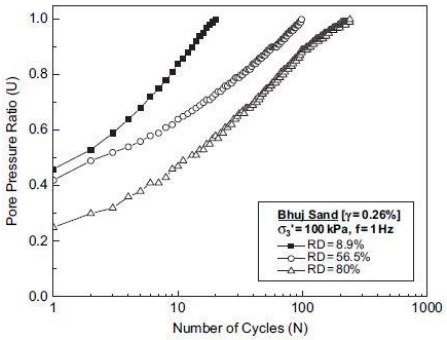

Fig: 8 Shows the plot of pore pressure ratio vs Number of Cycles of Bhuj Sand at Constant confining pressure, frequency Strain and variable RD

The Effect of confining pressure was also studied by them from the plot of pore pressure vs Number of cycles at constant RD, strain and frequency, from which they arrive to the observation that the rate of pore water pressure ratio increases, with the decrease in confining pressure (Fig 9). However when the same was plotted against cycle ratio, it show a unique relation between pore pressure ratio and cycle ratio which was independent of the confining stress (Fig 10).

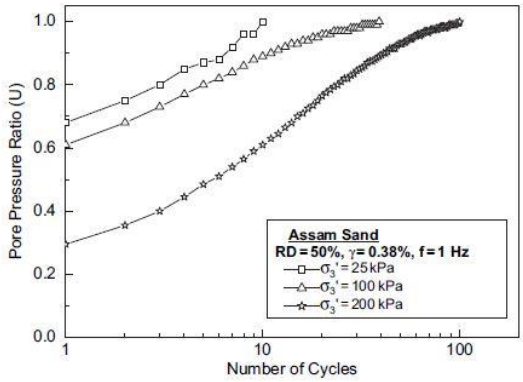

Fig: 9 Shows the plot of pore pressure ratio vs Number of cycles at Constant RD, strain, frequency and variable confining stress

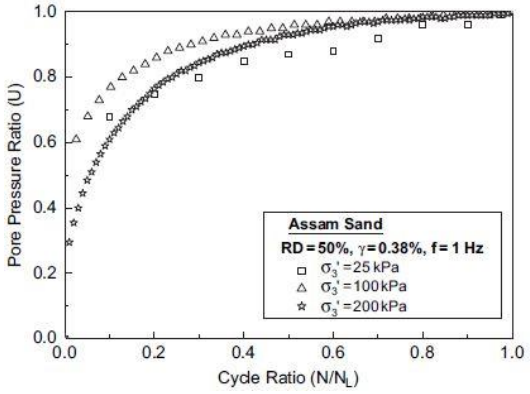

Fig: 10 Shows the plot of pore pressure ratio vs cycle ratio at Constant RD, strain, frequency and variable confining stress

The **Effect of Frequency of the cyclic loading on the pore pressure build up:** From the plot drawn in pore pressure ratio vs Number of cycles at constant relative density, confining pressure, strain and variable loading frequency ranging from 0.2Hz to 3 Hz. From the outcome it was proposed that the pore water pressure build up in sand was independent of the frequency of the loading (Fig 11). Similar result was observed when the same had been plotted on pore pressure vs cycle ratio. It shows a unique relation between pore pressure ratio vs Cycle ratio which was independent of frequency of loading (Fig-12).

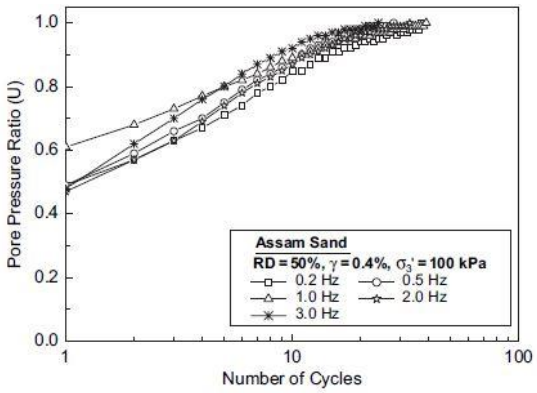

Fig: 11 Shows the plot of pore pressure ratio vs Number of cycles at Constant RD, strain, confining stress and variable frequency

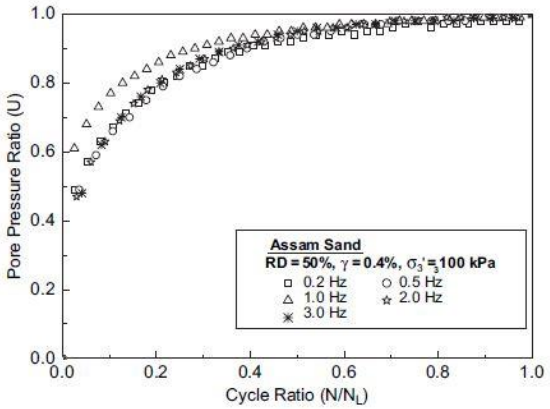

Fig: 12 Shows the plot of pore pressure ratio vs Cycle ratio at Constant RD, strain, confining stress and variable frequency

They also compared the test result of both Bhuj Ahmedabad and Assam sand of wide range of relative density with the relation given by Talaganov (1996) and it was observed that all the results are well within the upper and lower bound range (Fig-13). Talaganov (1996) obtained a best fit of all the data by grouping the results and proposed an analytical expression using regression analysis for the purpose of defining the mean relationship between normalized pore water pressure ratio and normalized cycles for the prediction of pore water pressure build-up in sands. The equation was presented as

$$\mathbf{Y = X(A + BX)/(C + DX)} \qquad (1.10)$$

Y = U & X = N/NL

A= 1.1218,

B= 0.1143

C= 0.14

D=1.2809

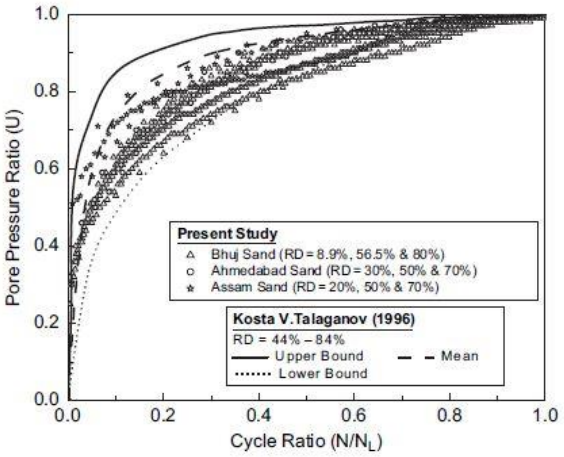

Fig 13 : Comparison done by Sitharam and Govindaraju (2007) of the results obtained from the experimental study with the rage of pore pressure ratio proposed by Kosta V .Talaganov (1996)

From the Fig 13 it was clear that most of the data falls close to the lower bound curve of Talaganov. So they performed a regression analysis to define a mean relationship between pore

pressure ratio and cyclic ratio. They also proposed analytic solution for each to define the relation between pore pressure ratio and cyclic ratio. The equation was expressed as below.

$$Y = \frac{A\left(\frac{N}{N_L}\right)}{B + \left(\frac{N}{N_L}\right)} \quad (1.11)$$

Here A and B are the parameters obtained by regression analysis for different sands and Y is the Pore pressure Ratio
For Bhuj Sand the value of A= 1.0494 and B = 0.0824
For Ahmedabad Sand the value of A = 1.0379 and B = 0.0569
For Assam Sand the value of A = 1.0494 and B = 0.0457.

2. Derakhshandi et al.(2007) in his journal of " The Effect of Plastic fines on the pore pressure generation characteristics of saturated sands" had done an experimental investigation to determine the effect of plastic fine (kaolinite) in the pore pressure generation of saturated sand by strain controlled cyclic triaxial test. His selection of strain controlled method was justified with the reason that it reduces the effect of different method of sample preparation and also the rearrangement of the soil particle under undrained condition is well characterized by shear strain. For this study they had used a mixture of Monterrey #0/30 sand and Kaolinite. The index property of the mixture is presented as below by them. (Table 3).

Table 3: Index properties of the Mixture of Monterrey #0/30 and Kaoliite used by Derakshandi et el(2007) in their study

Index properties	Fines content (FC)				
	0%	10%	20%	30%	100%
G_s	2.64	2.633	2.628	2.622	2.58
e_{min}	0.577	0.394	0.3	0.304	–
e_{max}	0.848	1.049	1.319	1.824	–
LL	–	8.8	11.5	15.3	41.7
PL	–	–	9.6	10.3	26.2
PI	–	–	1.9	5	15.5
%< 5 μm	0	7	14	21	70
USCS classification	SP	SP-SM	SM	SC-SM	CL/ML

The specimens for testing was prepared with initial relative density of 50% and consolidated with an isotropic confining pressure of 100 Kpa and subjected to the 50 sinusoidal circles of axial strain at the loading rate of 0.1Hz. Relative Density was kept constant throughout the test for variable fines as it does not significantly affect the pore pressure generation in clean sand when using strain controlled test. The effect of fines content in pore pressure is determined by conducting a strain controlled test at strain variable strain level of 0.03%, 0.1% and 0.3% and fines content between 10 to 30%. The data obtained from the test was plotted in excess pore pressure vs Number of Cycles and presented as below in their study. (Fig 14)

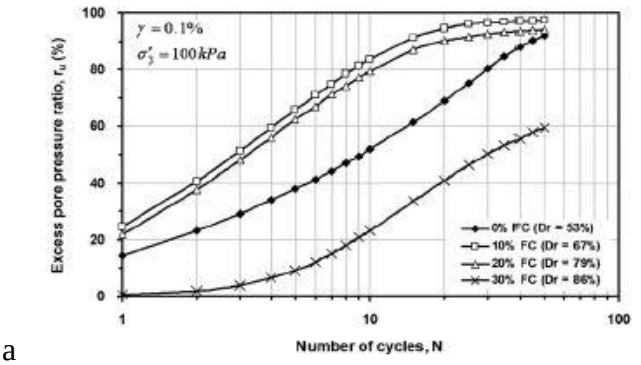

a

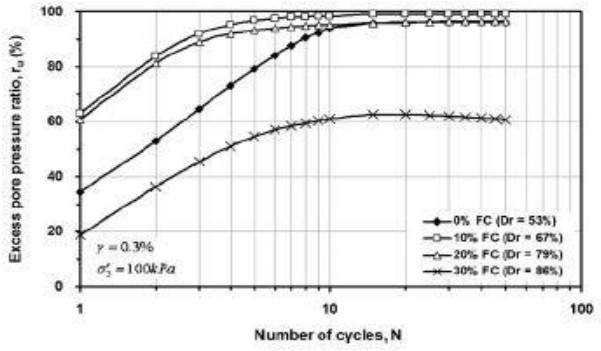

b

Fig 14: Show the variation of excess pore pressure ratio with number of cycles a) for strain 0.1% and b) for strain 0.3% at variable finesse content of 0% , 10%, 20% and 30% as presented by Derakhshandi et al.(2007).

From the above data they concluded the pore pressure generated for 10 to 20% fines are greater than no fines. Whereas for the 30% fines the excess pore pressure generated is much less than that for zero fines in both 0.1% and 0.3% strain. The justification for such behaviour is given by the fact that for 10% and 20% fine the void ratio is smaller and the sand skeleton void ratio is governed by the larger void ratio of the specimen. Whereas for the 30% fine the sand skeleton void ratio is governed larger voids of kaolinite, which makes the sand to behave more like clay. As the fines are added the sand skeleton void ratio increases even though the void ratio decreases. At this stage the soil behave more like that of sand. When the added fines content are increased beyond limit the sand skeleton void ratio is larger than the maximum void ratio of clean sand. In this condition the sand no longer behaves like sand and the fine control the soil behaviour.

This is the same reason that cause the decrease in the number of cycles for liquefaction on addition of fines 10 to 20% and the liquefaction is never reached for 30% fines as at 30% fines soil behaves like clay.

3.Dash and Sitharam (2016) in their journal on Effect of frequency of cyclic loading on liquefaction and dynamic properties of saturated sand, have studied the effect of frequency on pore pressure generation in sand. In their study of Effect of Frequency they have considered Ahmadabad sand collected from excavated pits close to the Sabarmati river belt. The index property of the sand considered for study is as given below by them (Table 4).

Table 4: Index properties of the Ahmadabad Sand given by Dash and Sitharam (2016) in their journal

Soil type	Original Ahmadabad sand
Is classification symbol	SP
Maximum grain size (mm)	2.36
Mean grain size D_{50} (mm)	0.29
Minimum grain size (mm)	<0.075
Uniformity coefficient (C_u)	5.067
Coefficient of gradation (C_z)	0.789
Specific gravity (G_s)	2.65
Minimum index density (kN/m³)	15.79
Maximum index density (kN/m³)	19.82
Minimum index void ratio (e_{min})	0.34
Maximum index void ratio (e_{max})	0.678
Liquid limit (%)	NP
Plastic limit (%)	ND
Plasticity index (%)	NP

ND – not determinable; NP – non-plastic.

This soil specimen used for test is prepared by dry deposition method and subjected to stress controlled cyclic triaxial test after consolidating the specimen to a confining pressure of 100Kpa. The specimen have a relative density of 54 % post consolidation and at constant confining pressure of 100 Kpa it was subjected to variable frequency ranging from 0.1 to 0.5 Hz.

Table 5: Test parameter selected by Dash and Sitharam (2016) for their study

Approach adopted	Post-consolidation relative density	Soil type	Effective confining pressure (σ'_{3c}) (kPa)	Frequency (Hz)	Range of cyclic stress ratio (CSR)	Total no. of expts
Effect of frequency	RD_c = 54%	Original Ahmedabad sand	100	0.1, 0.2, 0.3 and 0.5	0.077–0.154	12

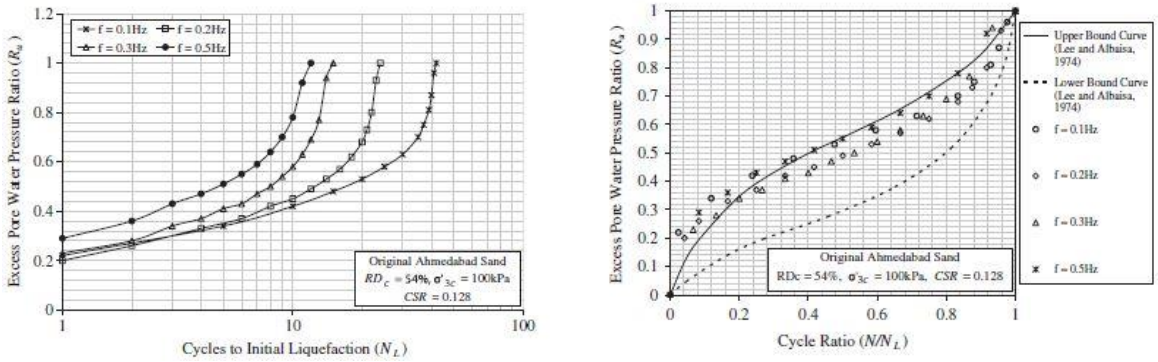

Fig 15: Shows the results of the experimental study done by Dash and Sitharam (2016)

Using the above plots (Fig 15) they concluded that with the increase of frequency the rate of pore pressure ratio generation also increases, thereby causing initial liquefaction of sample specimen at much lower number of cycle. Thus increase in frequency leads to the reduction of the liquefaction resistance of the soil. The finding of this journal that the cyclic resistance ratio of the soil decreases with increase in frequency contradicts with the study done by Sitharam & Govindaraju (2007) where they have shown that the frequency of locating has no major implication in pore pressure generation and reduction in cyclic resistance ratio of soil. The reason behind such abrupt natural behaviour is may be due the production of double the static stress under impact loading at higher frequency

2. **Kanth and Maheshwari (2017)** in their paper on "Effect of Frequency of Loading on Pore Pressure in Solani Sand" . They conducted an experimental study using the cyclic triaxial test to quantify the effect of frequency in pore pressure generation of Solani sand. The properties of Solani Sand used for the study is as mentioned below (Table 6).

Table 6: Index properties of the Solani Sand given by Kanth and Maheshwari (2017) in their journal

Soil type	C_u	C_c	*RD (%)*	e_{max}	e_{min}	G_s
SP	1.96	1.15	30, 50	0.85	0.54	2.68

They specimens Solani sand is prepared by water sedimentation method of relative density 30% and 50 %, at confining pressure of 50Kpa and shear strain of 1%. The specimens were tested at different frequencies of loading of 0.5 Hz, 1Hz and 2 Hz to find its effect on pore pressure causing liquefaction. The test was conducted as per the procedure mentioned in ASTM D 3999 (2003). They studied the effect of frequency by plotting the result of triaxial test in terms of pore pressure ratio vs time for different relative densities. The data obtained from the plotted graphs were summarized below. From the below table (Table 7) it was conclude by them that the rate of the pore pressure generation as the frequency of the loading increases. This increase in rate of pore pressure generation causes the reduction in CRR leading to the faster liquefaction of the soil.

Table 7: Number of Cycles required for liquefatction at a fixed RD and variable frequency of Solani Sand given by Kanth and Maheshwari (2017) in their journal

S.No.	*RD (%)*	*f (Hz)*	*t (s)*	*n (cycles)*
1.	30	0.5	7.116	3.558
2.		1.0	2.344	2.344
3.		2.0	1.142	2.284
4.	50	0.5	7.626	3.813
5.		1.0	3.260	3.260
6.		2.0	1.426	2.852

2.3 Relevant work in past on this field.

In this part we will cover an extensive review of the existing literature related to this study. The literature is going to cover analytical, empirical, numerical and experimental works in brief.

1. Seed and Idriss (1975) gave two parameters to determine the liquefaction resistance of the soil, (i) CSR or earthquake induced stress in the soil and (ii) CRR, which is the resistance against liquefaction.

$$CSR=(amax/g)*(\sigma 0/\sigma' 0)*rd \quad (1.12)$$

This CSR value should be reduced by 35% to represent the most significant cycles over the full period of loading.

$$rd=1.0 - 0.00765z \quad \text{for } z<9.15m \quad (1.13)$$

$$rd=1.174 – 0.0267z \quad \text{for } 9.15m<z<23m \quad (1.14)$$

Where, a max= maximum acceleration during earthquake

Z= depth of concern

2. Chkrobortty et al.(2004) In his paper on Liquefaction assessment for microzonation of Kolkata City had used more than 100 of the bore log data had been collected from different sources in Kolkata on the early seventies for the metro construction of Kolkata. These data was wide spread over the whole Kolkata region. He used neural nets developed specifically for interpolation / extrapolation of parameters essential for evaluation of liquefaction potential to determine the missing data from the bore log. Since Kolkata region lacks the records of any strong ground motion it was difficult for the author to prescribe a Peak Ground Acceleration Value, so he used the attenuation relationship suggested by Abrahamson et. Al.

$$\log(a) = -0.62 + 0.177\,M - 0.982\,\log(r + e^{0.284\,M}) + 0.132\,F - 0.0008\,Er \quad (1.15)$$

Where, a= Peak Ground Acceleration
r = Distance in Km to the closest approach of the zone of energy release
M= Magnitude of the earthquake
F= A Dummy variable - 1 for reverse or reverse oblique fault, 0 otherwise
E= A dummy variable - 1 for inter plate, 0 for intra plate events
The bore log data was then subsequently used for the determination of the liquefaction potential using both the Simplified Procedure suggested by Seed-Idriss and Method suggested by Seed, Idriss and Arango, for different depths at each borehole. A contour map of equipotential line at different depths were plotted and the below assumptions were made after their study.
1. River Channel deposit in South Kolkata area like Tolleygaunge, Kasba are found to be most susceptible to liquefaction. Extra care should be taken against liquefaction during construction of a structure upon this type of deposit.

2. The Salt Lake region being a reclaimed area has a top layer of very loose fine sand followed by soft to medium stiff / loose sandy silt or clayey silt mixed with decayed vegetations and this soil is also susceptible to liquefaction
3. The Normal Kolkata deposit in central Kolkata areas like Beliaghata, Sealdah generally are less susceptible to liquefaction.
4. From the study it is also concluded that if an earthquake of magnitude more than or equal to 7 on Richter Scale occurs in Kolkata or adjacent region then most of the areas will be extensively damaged due to liquefaction while only some part of Central Kolkata will be marginally damaged due to liquefaction at that magnitude.

3. **Ranjbar & Choobbasti [2008]** in their article on '**Mitigation of Liquefaction using Stone Columns'** compare the generation of the excess pore pressure in liquefiable saturated sandy soil with and without stone column. They used the FLAC 2D a finite difference software for their investigation. From the data generated of their study as presented below, they concluded that Stone columns are highly effective in reducing the pore pressure generation in soil and suggested that the same can be used along the Caspian Sea beach.

Table 8: Summary of the result of the analysis presented by Ranjbir & Choobbasti [2008] in their journal Mitigation of Liquefaction with Stone Column

PARAMETERS		A				B				C			
		WITHOUT STONE COLUMN		WITH STONE COLUMN		WITHOUT STONE COLUMN		WITH STONE COLUMN		WITHOUT STONE COLUMN		WITH STONE COLUMN	
		MAXIMUM	STABLE	MAXIMUM	STABLE	MAXIMUM	STABLE	MAXIMUM	STABLE	MAXIMUM	STABLE	MAXIMUM	STABLE
r_u	POINT 1	0.98	0.96	0.85	-	0.8	0.65	0.71	-	0.997	0.955	0.95	0.75
	POINT 2	0.892	0.674	0.74	-	0.71	0.64	0.65	-	0.9	0.69	0.3	0.25
	POINT 3	0.864	0.8	0.34		0.69	0.62	0.54	-	0.69	0.61	0.275	0.18
	POINT 4	0.821	0.75	0.19		0.75	0.69	0.32	-	0.588	0.52	0.212	0.102
	POINT 5	0.96	0.91	0.964	-	-	-	-	-	0.55	0.51	0.87	0.84
	POINT 6	0.91	0.891	0.958	-	-	-	-	-	0.563	0.5	0.55	0.53
	POINT 7	0.931	0.874	0.947	-	-	-	-	-	0.8	0.78	0.72	0.6

4. Zandian et al.(2009) in their paper on "modelling sand behaviour using a critical state model implemented in flac" have conducted an experimental study to check the validation of a critical state constructive model developed by University of Alberta for the prediction of the behaviour of sand using FLAC software. The model was verified by comparing the predicted and generated value of the triaxial test on Toyoura and Syncrude sands and also in full scale level by modelling the field event of the CANLEX Project. The results predicted by FLAC for Tourya Sand subjected to triaxial test with void ratio 0.833 and confining pressure 2000kpa was compared with the experimental result (Fig 16) and it show both results were quite similar. The comparison is shown as below

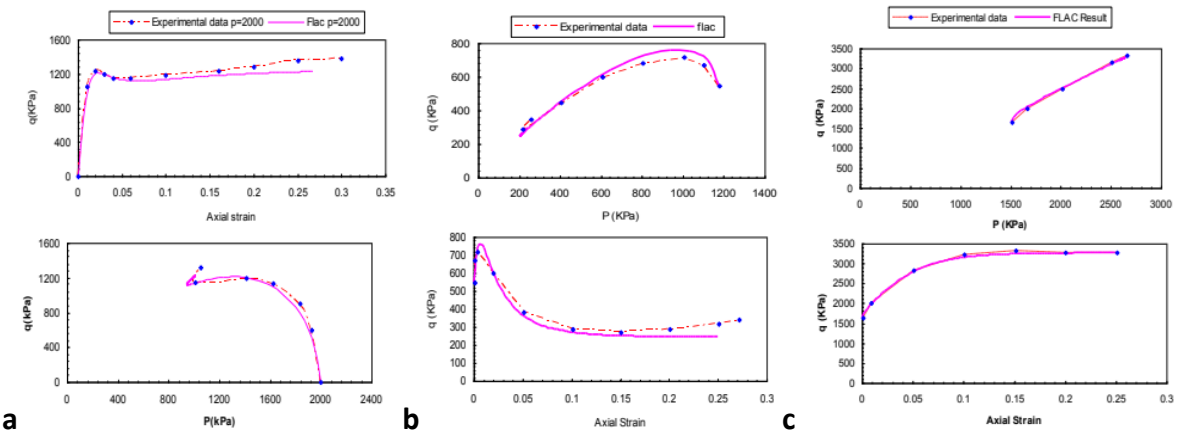

Fig 16: Comparison of data predicted by FLAC and experimental analysis for Toyoura sand (Zandian et al, 2009)

But they noticed that at higher the experimental data shows increase in strength with strain whereas the data from FLAC show a decrease in the value. They explained this behaviour is caused by the formation of shear bands in triaxial specimen which causes the increase in strength. Similarly they had also modelled for Syncrude sand and compared the FLAC values with the experimental data. Both the data shows similarity in their trend. These two models were then used by the author to predict the pore pressure generation in CANLEX project. The predicted pore pressure generation was then compared with the one previously used. From the above they concluded that the study

showed the importance of using an appropriate soil constitutive model which takes into account soil anisotropy, and taking into account the simultaneous pore pressure generation and dissipation during loading.

5. Debabrata Giri and A Sengupta [2010] compared the results of shake table test with the results of models, which were created in FLAC software. For modeling purpose they used uniform sand with the relative density of 60% and friction angle of 35º. Before the test of shake table, calibration was done to check the effect of amplification of input motion. They monitored the development of the sliding surface and crest settlement with the progress of the test and found that the failure surfaces in both the cases were shallow and rotational and the deformations along the width of sliding surface were more or less uniform. They also observed that the crest settlements of the numerical models were reasonably well but they do not predict the heaving and outward movement of the toe of the slopes.

6. Shooshposh & Bagheri [2012] in their article worked on to determine the effect of surcharge on liquefaction resistance of silty sand. They have adopted for Numerical analysis by finite difference method to investigate the effects. They used Mohr Coloumb elasto plastic model of FLAC 2D for static analysis and Finn & Bryne constitutive model to simulate the pore pressure generation & liquefaction phenomena. The author had varied the soil properties between Loose, medium and Dense sand and the input acceleration for their study and done a parametric study of the output. From their parametric study author concluded that even though the pore pressure ratio decreases under the higher loading, it can't be considered as a positive

factor toward higher factor of safety. Furthermore there was higher displacement at the edge of the loading than at the center causing uneven settlement, tilting & rotation of the structure which may cause lots of damage. From the parametric study author also concluded that the influence of the deformation criteria for evaluating potential liquefaction is very important component for geotechnical design of structure in earthquake prone area.

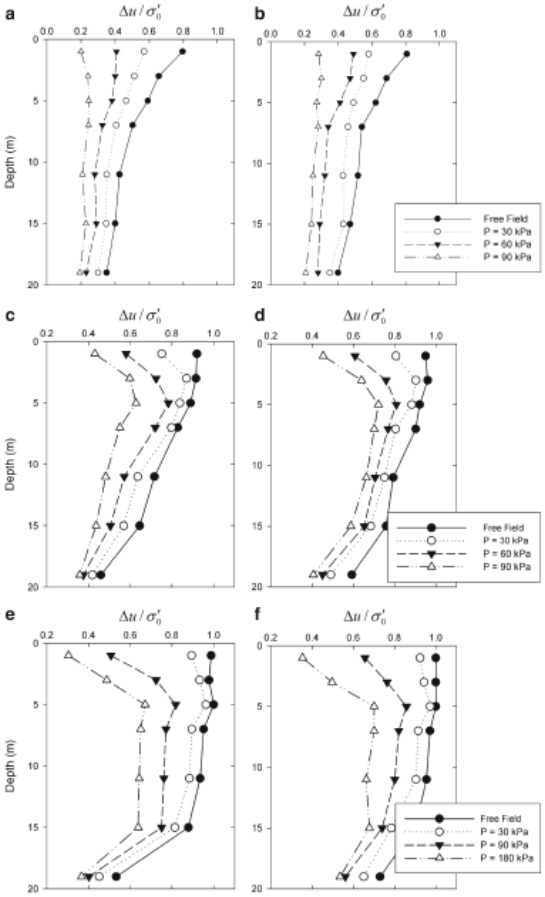

Fig 17: Variation of ru versus depth in silty sand deposits in critical points (along the edge of foundation) and subjected to two earthquakes. **a** Manjil earthquake Dr065 %, **b** Bam earthquake Dr065 %, **c** Manjil earthquake Dr045 %, **d** Bam earthquake Dr045 %, **e** Manjil earthquake Dr030 %, **f** Bam earthquake Dr030 % (Shooshposh & Bagheri [2012)

7. Chatterjee & Choudhury [2013] in their article on "Variations in shear wave velocity and soil site class in Kolkata city using regression and sensitivity analysis" they have done an extensive study on the data collected from 434 the bore hole data across 75 sites in the Kokata city. Using the data they provided a correlation between shear wave velocity and SPT n values for various soil profile of Kolkata City The regression coefficient for the provided relationship are in excess of 0.96, which indicates good prediction capabilities.

Table 9: Proposed correlations between shear wave velocity (Vs) and corrected SPT N values with magnitudes of R2, r and MSE obtained from nonlinear regression analysis Chatterjee & Choudhury [2013]

Soil type	Proposed correlation	Coefficient of regression (R^2)	Coefficient of correlation (r)	Residual mean square error (MS_E)
All soils	$V_s = 78.63(N_1)_{60}^{0.37299}$	0.9996	0.96614	0.000033
Clay	$V_s = 78.03(N_1)_{60}^{0.38344}$	0.9981	0.97021	0.000145
Silt	$V_s = 58.62(N_1)_{60}^{0.44791}$	0.9988	0.97591	0.000134
Silty sand	$V_s = 56.44(N_1)_{60}^{0.51104}$	0.9961	0.98511	0.000424

8. Asgari et al [2014] in their article on Numerical Evaluation of Seismic Response of shallow foundation on Loose Silty Sand have compared the dynamic behavior of loose deposit underlying a shallow foundation using Numerical simulation by FLAC software. The numerical simulation includes a liquefiable soil layer with variable thickness. The input motion was scaled at different intensity for application and parametric study. From their study they concluded that the soil under structure shows resistance to pore pressure generation and liquefaction, but if the intensity of the earthquake is high enough to overcome this resistance then the soil is will generate higher pore pressure. Minimum excess pore pressure ratio was observed under the foundation at shallow depth and the maximum pore pressure ratio was observed at greater depth. This ratios are always smaller than the one observed in free field conditions. Both type of soil under consideration i.e. loose silty sand and loose silty soil deposit undergoes huge deformation even when the pore pressure ratio is small. So they also suggest to consider displacement criteria for prediction of liquefaction potential rather than excess pore pressure generation. Even though the loose silty sand have higher mechanical properties than Loose silty soil, the pore pressure generation and deformation in former is larger than the later one. This is due to the fact that the loose silty sand have higher coefficient of permeability and lower cohesive strength than loose silty soil. They also observed that with the increase in thickness of Liquefiable soil layer the response get amplified, especially under heavier structure and stronger motions. Excessive displacement under structure cause uneven settlement, resulting in failure of structure. Significant effect of plastic fines on decrease of earthquake susceptibility of foundation soil was also observed

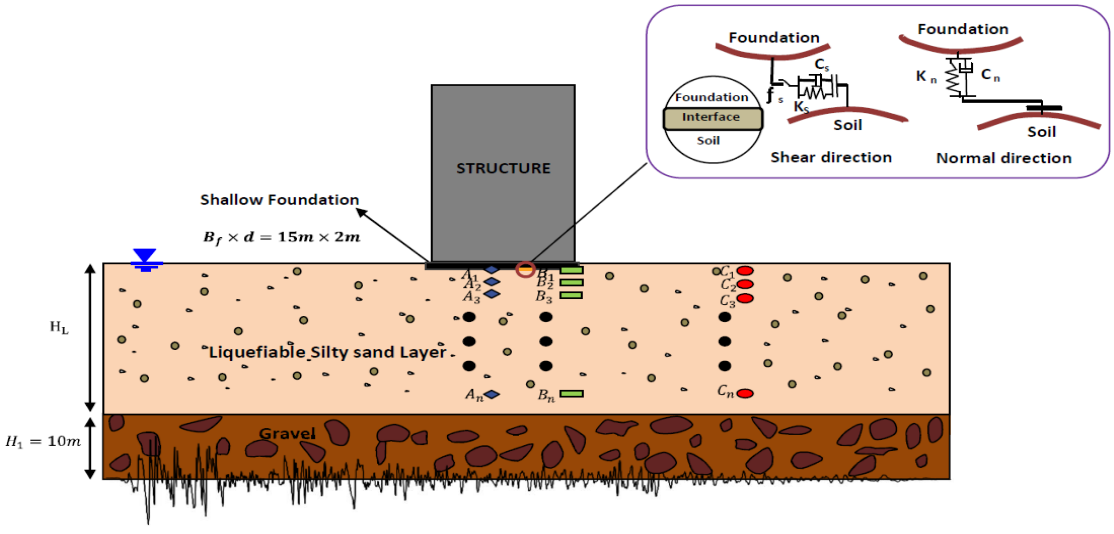

Fig 18: Schematic illustration of structure on shallow foundations subjected to earthquake and a details of the constitutive law of normal and shear contact forces at the interface between foundation and liquefiable soil (**Asgari et al [2014]**)

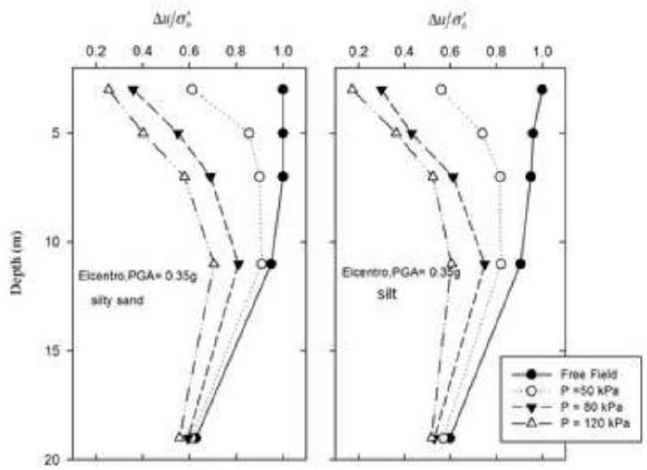

Fig 19: Variation of ru versus depth in silty sand and silt deposit in critical points subject to El Centro Earthquake (**Asgari et al [2014])**

9.Vargas et al (2014) in their paper on "Liquefaction Analysis Using Pore Pressure Generation Models During Earthquakes" they had performed a liquefaction analysis for a site using two-dimensional numerical models that take into account the irregular ground and the constitutive models that involve the dynamic pore-pressure generation from volumetric strain induced by seismic excitation. This paper highlights the means considerations of numeric model, as such as, input parameters, model calibration, steps calculations, among other. They have considered Hotel Sapanca site during the 1999 Kocaeli (Izmit) Turkey earthquake for their study. The site is located on the southern coast of Lake Sapanca, approximately 20 km of the Izmit Bay southwest of the city of Adapazary. Following earthquake parameter was used. The Kocaeli (Izmit) earthquake (Mw 7.4). The Sakarya strong motion had a peak ground acceleration of 0.37 g (Fig 20). Permanent lateral displacement of 1.50 m according to the measurements of ground fissures occurred

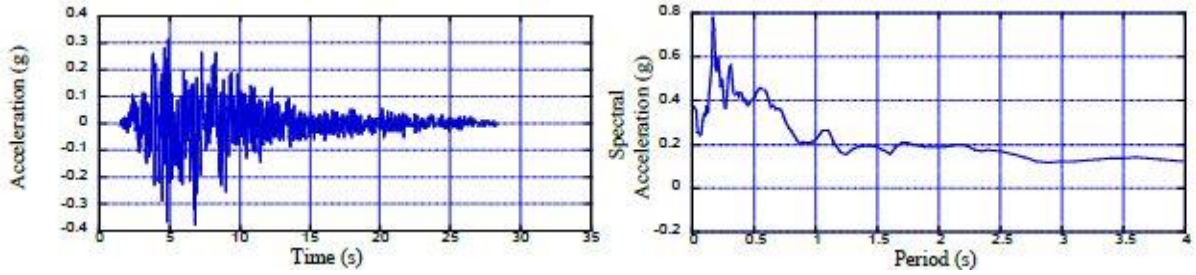

Fig 20 : Acceleration record and response spectra from Sakarya strong motion record.(Vargas et al, 2014)

The strength parameters were derived from the in-situ tests (SPT and CPT), which were carried out by researchers from different Universities. The dynamic soil properties such as shear wave velocity and shear modulus were estimated using the empirical relation based on direct measurements of in-situ tests depending on cone tip resistance. Then the model was developed considering horizontal layers as derived from bore hole data and the dynamic simulation was carried out using a Finite Difference Method with FLAC-2D software. The programme includes such process to calculate pore pressure generation under cyclic loading. The response

of the soil during earthquake, in terms of effective stress, excess pore pressure and excess pore pressure ratio as a function of the time, at a corresponding point is generated through FLAC.

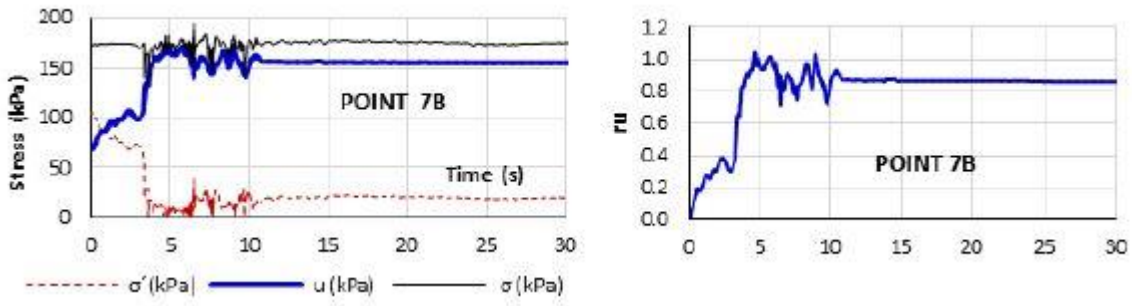

Fig 21: Shows the excess pore pressure ratio and the effective stress generated in the soil. (Vargas et al, 2014)

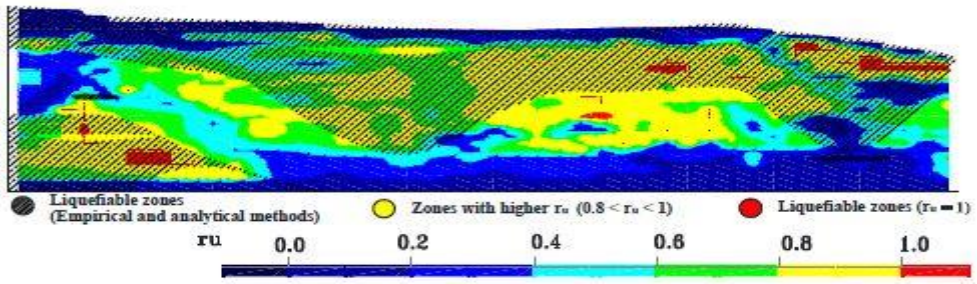

Fig 22: Shows the excess pore pressure ratio contours as generated by FLAC for Hotel Sapanca (Vargas et al, 2014)

He then compared the data from the FLAC to the actual result and arrived at the conclusion that the modeling should include three steps: 1) Model calibration (Free Field), 2) Static equilibrium calculation for the site including the steady-state groundwater conditions and 3) Seismic calculation and dynamic pore pressure generation. From the above data the author concluded that more case studies should be analysed, in order to generalize the model results.

10. Assadi & Sharifipour [2015] investigated the liquefaction susceptibility of saturated sand under single concrete pile action in their article Numerical simulation of liquefaction susceptibility of soil interacting by single pile. They used FLAC 2D a finite difference software for their investigation. Investigation was carried out on three different soil of relative density 35% , 55% and 75% and a scale dynamic input of 0.2g to 0.4g of three different motion. Investigations led to the following conclusion that for all case the liquefaction susceptibility in low depth is more than the liquefaction potential at greater depth. Also the liquefaction potential of soil decrease in depth with the increase in relative density of soil. The pile provide soil reinforcement thus decreasing the large shear deformation and also prevent the soil from reaching liquefaction. Liquefaction start sooner for input acceleration with higher peak value. Increased in amplitude of frequency also led to higher value of horizontal displacement and settlement. It was also evident from the study that the liquefaction susceptibility of soil decreases as the predominant frequency of the input motion increases.

11. Bhatnagar, Kumari & Sawant [2015] in their article on 'Numerical Analysis of Earth embankment resting on Liquefiable soil and Remedial measure' have presented a discussion on the results of Embankment founded on Liquefiable deposit using Plaxis 3D finite element software. Their objective was to provide a numerical analysis to predict the response of the Liquefiable strata with proper counter measure. As a counter measure they have used sheet pile and soil column to analyses the extent and their performance in reducing the liquefaction susceptibility of the soil. From their parametric study data they concluded that a reduced strain and cyclic mobility was observed in case of soil column. Soil Columns are also most effective in reducing the excess pore pressure generation in soil beneath the embankment. The excess ore pressure and displacement value tends to decrease with increase in the width of the soil column. Even though the foundation soil undergoes huge liquefaction, the sheet pile were effective in protecting the embankment due to their confining effect.

12. LIN Yu-liang et al. (2016) in his case study on Numerical analysis on seismic behavior of railway earth embankment studied, the full scale model of earth embankment in Yun Gui Railway in south west of China was studied. He adopted for the full scale numerical model instead of prototype one as they had few limitations such as in the shaking table test, the test model was built in a reduced scale in the geotechnical engineering while the 1g gravity field cannot be altered. Similarly in dynamic centrifugal test is also limited due to the size of the prototype model. On the contrary the numerical method of analysis is much more economical and accurate. He constructed a full scale mode of earth embankment by numerical simulation code in FLAC 3D and it was studied for horizontal acceleration response, the vertical acceleration response, the dynamic displacement response, and the block state of earth embankment.

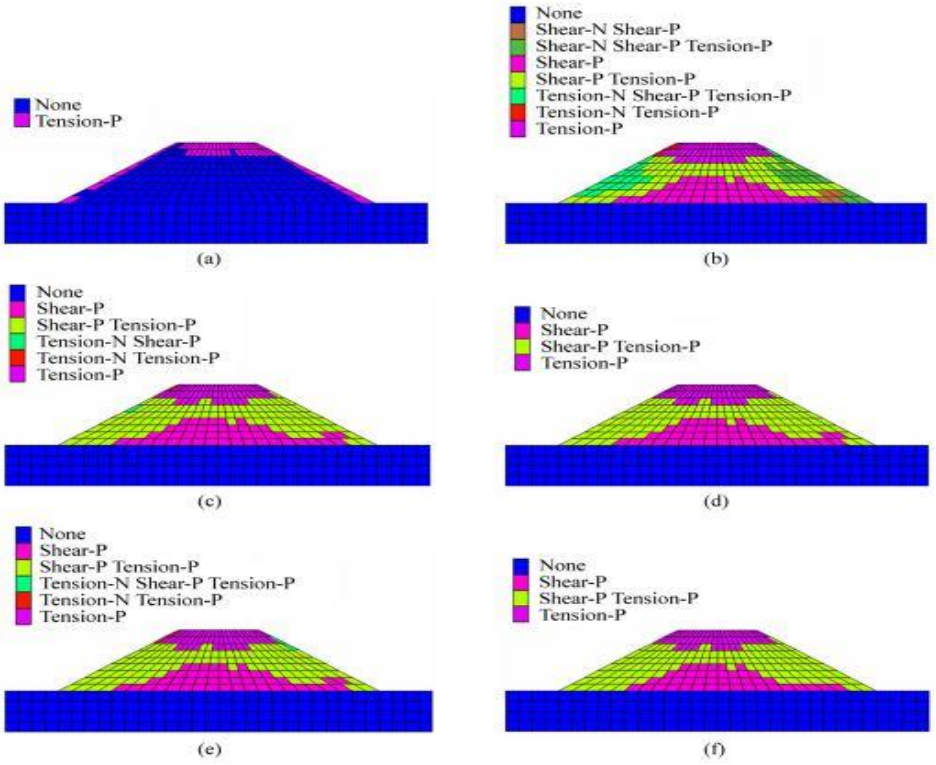

Fig 23: The output figure of the experimental study of LIN Yu-liang et al for the State of embankment body during WC7 (Axmax=1.0g) excitation: (a) t=5 s; (b) t=10 s; (c) t=15 s; (d) t=20 s; (e) t=35 s; (f) t=50s (LIN Yu-liang et al., 2019)

The below mentioned conclusions had been drawn after the study:-
The ground motion gets amplified whenever the seismic motion travels through the embankment for most of excitation events. The acceleration get more magnified near embankment slope surface than that in the internal body. The top zone of the embankment was more sensitive to the intensity of the ground motion. The vertical acceleration gets less influenced by the intensity of the ground motion than the horizontal acceleration. The maximum deflection occurs in the middle of the embankment slope surface. They also concluded from the above figures that the upper part of embankment experiences tension failure without shear failure, and the bottom area of embankment around the symmetry-axis of embankment mainly experiences shear failure under the earthquake loading.

13. Dinesh et al. (2016) in their paper on "study of constitutive models for cyclic liquefaction in sand" had done a comparative study on the sand models UBCSAND and PM4SAND. They have compared the principle operation behind this models. From their comparative study and comparing with the results of Cycle Direct simple shear Test (Fig 24) they concluded that the PM4SAND can predict the pore pressure generation in sand better than that done by UBCSAND model on the ground of significance of fabric dilatancy tensor, means of representing the soil in numerical model and ease of the calibration of the model.PM4SAND can easily be calibrated and deployed due the ease with which the input parameter are designed and correlated.

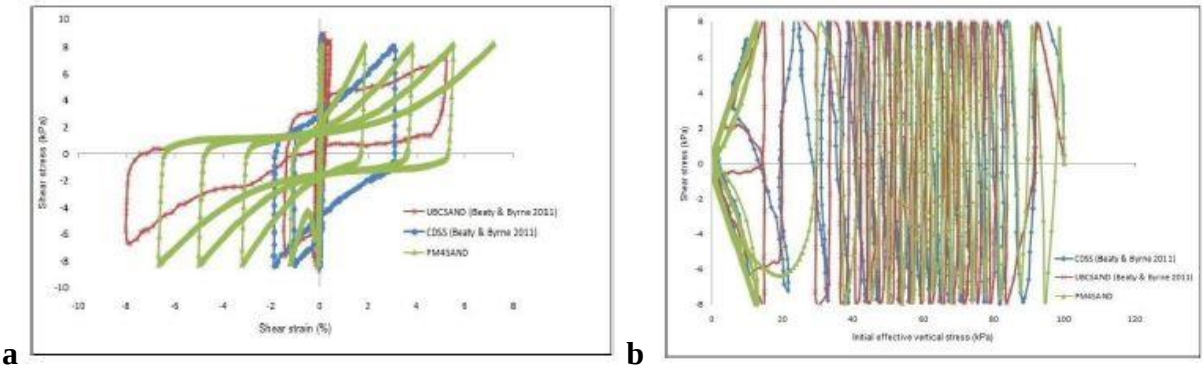

a **b**

Fig 24: a) Comparison of simulated stress-strain responses b) Stress path for single element simulations of CDSS (Dinesh et al, 2016)

14. Assefa & Sachpazis [2017] in their journal on slope stability evaluation of the railway Embankment using stochastic finite element and Finite difference method investigated the stability of Ethiopia railway embankment by using different stochastic approaches with commercially available finite element and finite difference programs. Their investigation led to the following conclusions, the probabilistic assessment is more efficient than the deterministic approaches, as the determisitic approaches are solely relied on the safety factor. They also suggested that the pseudo-static analysis can be used for the analysis of Ethiopia railway embankment as there is no considerable strength loss by cyclic loading.

15. Banerjee et al [2017] in his article on **'Shake Table Tests and Numerical Modelling of Liquefaction of Kasai River Sand'** investigated the liquefaction potential of Kasai River sand due to ongoing constructions. Shake Table test at 1g was studied for laboratory and Numerical analysis was done by Finite Difference software FLAC. Investigation had led to the conclusions that the lateral spread and vertical settlement for liquefied sand is 2.6 – 2.5 times of dry state. Laboratory and Numerical analysis results shows a vertical displacement of 10mm for dry sand whereas this displacement increase t 26mm for liquefied sand. Liquefied sand also show a great increase in volumetric strain compared to that of dry sand i.e around 4% for liquefied sand and 1.5% for dry sand. Amplification of PGA at ground surface of Liquefied was also reported by the author. This results led him to the conclusion that huge destruction of superstructures could happen if Kasai Sand undergoes liquefaction.

16. Oblak et. Al [2019] analyzed liquefaction induced deformation of traffic embankment using FLAC software and PM4Sand model. They used fragility curveto show the effects of crest width, height of embankment, thickness of liquefiable layer, density of liquefiable layer on crest settlement, which was used as damage state parameter. From their developed fragility curve it was clearly understood that crest settlement will be decreased with increase in width of crest, decrease in height of embankment, decrease in thickness of liquefiable layer and increase in density of it.

17. Surya P & Midhun Raj S N (2019) in their paper on the **"**Analysis for Pore Pressure Buildup Using UBC- Sand Model" they focused on the pore pressure buildup in the foundation soil for bridge abudment by using UBC SAND constitutive soil model into the finite element GT Software. They have done the seismic analysis of bridge foundation in liquefiable soil by using MIDAS GTS NX software. They have used the following soil model and earthquake parameter for the study as mentioned below.

Table 10: Soil properties & Earthquake Details (Surya P & Midhun Raj S N, 2019)

a

ID	1	2	3	4	5
Name	Embankment	Clay	Weathered Rock	Soft Rock	Abutment
Model Type	Mohr Coulomb	Modified Ubc sand	Mohr Coulomb	Mohr Coulomb	Elastic
Modulus of elasticity (ton/m^2)	4000	850	15000	30000	232,000
Poisson's ratio (v)	0.35	0.3	0.35	0.27	0.19
Unit weight γ, (ton/m^3)	1.8	1.7	2	2.4	2.5
Unit weight (Saturated ton/m^3)	1.9	1.8	2.1	2.5	2.5
cohesion(c) (ton/m^2)	1.5	5	20	45	-
Internal Friction Angle,ϕ	25	20	32.5	35	-
Damping Ratio	0.05	0.05	0.05	0.05	0.05
K0	1	1	1	1	1

b

EarthQuake Details	
Origin Time	18:41:28
Latitude.	26.6 N
Longitude	93.0 E
Depth (km)	20.0
Magnitude	5.4
Region	Assam
Record Station Detail	
Station Code	GOL
Station Latitude	26.516 N
Station Longitude	93.972 E
Station Height (m)	93
Record Time	11.05.2012
Sampling Rate	200. Hz
Record Duration	66.690 Sec.
Direction	E-W (E positive)

They have presented their study output in the form of pore pressure ratio and different stages of Liquefaction in the soil under the pile foundation subjected to Assam Earth Quake. The output result are as shown below.

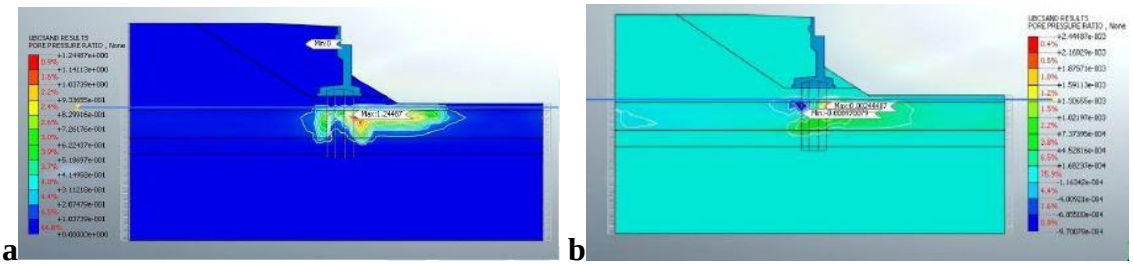

Fig 25: a) Location of Liquefaction b) Stages of liquefaction in Soil profile (**Surya P & Midhun Raj S N, 2019**)

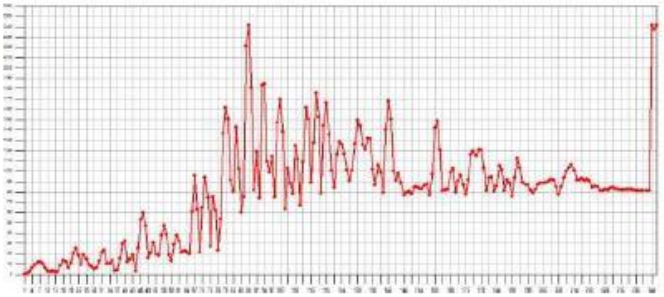

Fig 26: excess pore pressure curve (**Surya P & Midhun Raj S N, 2019**)

The variation of excess pore pressure is plotted in Fig 26 which show the increment of pore water pressure and it stabilizes at the end. The maximum excess pore pressure is obtained as 57.74 kN/m2 as. In the liquefied soil profile the red region and some of the yellow region as the area identified as the region where liquefaction has occurred (Fig 25). The author also concluded that occurrence of liquefaction in saturated sand deposits underlying the pile foundation of structure can cause a wide range of structural damages starting from minor settlement, and leading to general failure due to loss of bearing capacity.

18. Ales et al. (2020) in his article on Fragility assessment of Traffic Embankments exposed to Earthquake induced liquefaction had studied the vulnerability of the road and railway embankment due to liquefaction caused by seismic loading. For the sand profile modelling he had used FLAC 2D and PM4Sand software to simulate the behavior of a liquefiable soil. The output of these model was used for numerical calculation to obtain a set of fragility curves. He had conducted incremental dynamic analysis approach considering a set of at least 30 ground motion and 8 intensity level. The fragility curve was determined for 3 damage state: 1) minor 2) moderate and 3) extensive.17 variable model in terms of embankment shape and soil profile

stratigraphy was analysed to determine the stability of embankment. The variable details and the soild details used in the study is given below.

Soil ID	H_C—Thickness of Crust Layer [m]	H_L—Thickness of Liquefiable Layer [m]	H_B—Thickness of Base Layer [m]
S1	1	7	24
S2	0	7	24
S3	1	2	24
S4	1	4	24

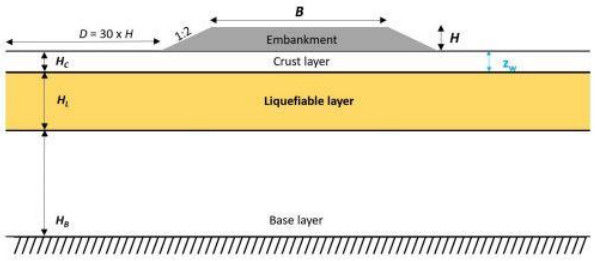

Fig 27: Soil profile stratigraphy variation (Ales et al, 2020)

Table 11: Geometric variation (Ales et al, 2020)

No. of Model Variations	1	2	3	4	5	6	7	8	9	10	11	12	13	14	15	16	17
Embankment height—H [m]	4		2				4				6				8		
Crest width—B [m]	6	12	24														
Soil profile ID	S1		S1	S2	S3	S4	S1	S2	S3	S4	S1	S2	S3	S4	S1	S3	S4

Table 12: Soil properties (Ales et al, 2020)

Layer	ρ_{dry} [kg/m^3]	k [m/s]	Mohr–Coulomb					PM4Sand		
			K [MPa]	G [MPa]	c_u [kPa]	φ' [°]	c' [kPa]	D_r [/]	G_0 [/]	h_{po} [/]
Crust layer	1784	$8{\cdot}10^{-8}$	64	30	80					
Liquefiable layer—medium dense	1486	$1.6{\cdot}10^{-5}$	/	/	/	/	/	0.60	760	0.55
Liquefiable layer—loose	1486	$1.6{\cdot}10^{-5}$	/	/	/	/	/	0.35	476	0.5
Base layer	1436	$1{\cdot}10^{-9}$	227	105	150	/	/	/	/	/
Embankment	1800	$1.18{\cdot}10^{-5}$	83.3	38.5	/	35	5	/	/	/

Notations: ρ_{dry}—dry density, k—soil permeability, K—bulk modulus, G—shear modulus, c_u—undrained shear strength, φ'—friction angle, c'—cohesion, D_r—relative density, G_0—shear modulus coefficient, h_{po}—contraction rate parameter.

For the purpose of fragility analysis set of 30 ground motions was selected from the database of Next Generation Attenuation (NGA). They scaled the ground motions to 8 intensity level to cover the entire fragility curve in terms of maximum acceleration at bedrock motion. Upon conduction of the study they concluded the following by the study of the specific points on the embankment. They suggested that increase in both the height of embankment and liquefiable layer increases the vulnerability, while increase in relative density and crest width reduces vulnerability of the embankment. The top layer of clay crust have positive effect in the stability of the embankment. The settlement of midpoint of the crest is correlated with maximum settlement at the edges of the crest and their horizontal displacement.

19. Sulaiman and Sengara [2020] have investigated on the pore pressure generation and stress deformation of the embankment soil under seismic action in their paper 'Nonlinear Dynamic Analysis Adopting Effective Stress Approach of an Embankment involving Liquefaction Potential'. They conducted a parametric study to identify the effect of height, input motion intensity and soil characteristics on evaluation of liquefaction susceptibility of the soil. From their study they observed that the liquefaction susceptibility of soil decrease in depth with the increase in the relative density of the soil. Excess pore pressure generation of the soil also decreases with the increase in relative density of soil. Increase of intensity in input motion generates higher pore pressure and horizontal displacement for a given relative density. They have also presented their data in form of charts, so that it can be used to estimate the density and embankment height in the preliminary design stage of embankment.

20. Jishnu & Ayothiraman [2021] studied the seismic behaviors of Delhi metro tunnels in the liquefiable soil by using site specific artificial ground motions at different cover depth to identify the major factors of concern. They have conducted their investigation on a Finite Difference Software FLAC 2D and drew following conclusions. They suggested that the incorporation of increment in thrust and uplift during the design stage is very important. This upthrust occurs due to the transfer of earth load from liquefied zone of soil. Ignoring the same could lead to unpredictable tunnel loads and serviceability issue. The liquefaction patterns shows the liquefaction tends to occurs in soil with less cohesion, especially at top layers due to the low confinement and lesser deformation modulus at these layers. Their study also suggest that the up thrust tends to decrease with the increase of cover depth, cohesion also contribute to lesser this thrust. Thus the inclusion of this thrust in the liner of the tunnel at design is must.

Chapter 3

Methodology

In this chapter the study of the seismic response and pore pressure generation in stratified soil deposit is performed using finite difference software FLAC 2D forming a full scale model of the subsoil strata and load conditions. In this study basically a parametric study has been performed considering the variation in intensity of seismic motion, loading intensity and soil stratification and their consequent effect is studied in pore pressure generation of the soil. After generating the full scale model of the soil strata it is solved for static analysis and then the dynamic loading is applied in form of shear stress wave derived from acceleration history. Acceleration history from low to high intensity was applied by scaling the PGA of the original input motion at the base of the model.

3.1 Brief Description on FLAC and its features.

FLAC 2D (Fast Lagrangian Analysis of Continua) is a two-dimensional software based on Finite difference principle used to solve complex and full scale engineering mechanics problem. It was first developed on in 1986 by Peter Cundall specifically to perform analyses on microcomputers operating on Microsoft Windows systems. The material in FLAC is represented as the elements which forms the grid of the model and it can be fit to the shape in accordance of the user defined model. Each element of the model behave according to the properties assigned to them and the boundary condition of the model. FLAC is based on Lagrangian model which is suitable for modeling of large distortion models. This software is primarily developed for geotechnical and mining engineering problems. It also offers several built in models that allows simulation of nonlinear irreversible response that are representative of geologic or similar material.

In addition, FLAC contains many special features

- interface elements for separation
- Ground water and consolidation (fully coupled) models;
- Plane strain, plane stress, and axisymmetric geometry modes;
- Structural element models to simulate structural support
- Fully dynamic analysis capability
- Visco-elastic and visco-plastic models for creep analysis
- Thermal modeling capability
- Extensive facility for generating plots of virtually any problem variable in FLAC

FLAC also has inbuilt programming language FISH to extend its usefulness. In FISH, the user can write their function and own constitutive models if needed. It can be operated as either a menu driven or command-driven program. A menu-driven command is useful for new users, but a command-driven program requires much more knowledge of the FISH language. The plastic collapse and plastic flow are modeled with the mixed-discretization scheme. This is more accurate than the reduced integration method that is usually used by the finite element techniques. The FLAC uses an explicit solution scheme that follows arbitrary nonlinearity in stress/strain laws in almost same computing time as in case of linear laws, unlike implicit solution techniques that take quite large time for solving non-linear problems. FLAC tracks its

elements in row-column numbering fashion rather than sequential fashion. It is easier to identify elements when interpreting outputs and assigning properties.

FLAC is most suitable for large-strain or non-linear problems. The time to solve a problem containing a composite material system depends upon the ratio of the longest natural period to the shortest natural period. This causes trouble to solve certain problems and solution time is very large. The basic mode of FLAC is a two-dimensional plane strain model analysis. This condition is well conformed to the long structures, excavation with constant sectional features along the length and subjected to the loading in the plane of its cross-section. This software also offers a plane-stress mode for analysis of plate-like structures. For our project the dynamic behavior of the soil strata has been investigated in two dimensional environment using the non linear effective stress dynamic analysis. Taking in consideration of the geometrical condition and the loading of the problem all analysis has been done considering the plain strain mode.

3.1.1 Brief discussion on Finite Difference Method

The behavior of the liquefied soil can be understood using the numerical finite difference method. The finite difference methods are based upon approximations which allows replacing differential equations by finite difference equations. These finite difference approximations are algebraic in form; they relate the value of the dependent variable at a point in the solution region to the values at some neighboring points. Thus a finite difference solution basically involves three steps: 1.Dividing the solution region into a grid of nodes. 2. Approximating the given differential equation by finite difference equivalent that relates the dependent variable at a point in the solution region to its values at the neighboring points. 3. Solving the difference equations subject to the prescribed boundary conditions and/or initial conditions. The course of action taken in three steps is dictated by the nature of the problem being solved, the solution region, and the boundary conditions.

The Finite difference code software FLAC 2D allows us to model the soil liquefaction phenomena. The advance constitutive model included in the software generates realistic soil behavior in liquefaction conditions. For our project the Finn Byrne liquefaction model developed by Byrne is used to model the liquefiable soil and Mohr Coulomb's constitutive model is used to model the non-liquefiable soil layers. In Finn- Byrne model, the excess ore pressure build up is obtained by calculating the permanent volumetric strain during the dynamic analysis.

3.1.2 Numerical Modelling of Stratified Soil

The numerical modelling of a soil strata is about selecting and focusing on the important aspects of the problem considered. A good model is the one that is fabricated to represent the key aspects of the soil behavior.

For the static analyses of the stratified soil the Mohr Coulomb's model was used to represent the constitutive behavior of all material zone of the stratified soil.

For Dynamic analyses the Finn model has been chosen to simulate the constitutive behavior of granular soil zone and Mohr Coulombs has been applied to the base layer and non-liquefiable

layers of soil. Also for the dynamic analysis part, we have linked up this constitutive model with the hysteresis damping properties of the material to enable a realistic analysis.

Mohr Coulomb's model is a simple linear elastic perfectly- elastic model that only requires five inputs that are the Young's Modulus, Modulus Poisson's Ratio, friction angle, cohesion and dilatency angle.

For ground water properties only to inputs are required that are porosity and hydraulic conductivity of the soil. Since liquefaction is a small time process it is mostly considered as undrained situation. To simulate this in numerical model the flow calculation should be turned off during static and dynamic analysis.

For Finn Model FLAC contains both Martin et al (eq.1.5) and Bryne model (eq.1.7) incorporated into the standard Mohr Coulomb's Plastic models. It can also be modified by the user based on their requirements.

$$\Delta\varepsilon_{vd} = C_1 \cdot (\gamma - C_2 \cdot \varepsilon_{vd}) + \frac{C_3 . \varepsilon^2_{vd}}{\gamma + C_4 . \varepsilon_{vd}} \tag{1.5}$$

$$\frac{\Delta\varepsilon_{vd}}{\gamma} = C_1 \cdot \exp(-C_2 \cdot \frac{\varepsilon_{vd}}{\gamma}) \tag{1.7}$$

The suitable Eq can be selected by setting the parameter ff_switch = 0 or 1 respectively. In addition to the usual parameters model needs the four constants for Eq 1.5 and three constant for Eq 1.7. In Fin model there is a logic t detect the strain reversal in I the general case. The Finn model is implemented in FLAC model with the MODEL Finn command. The model must be configured for dynamic analysis and large strain to apply the Finn model.

3.2 Description of Stratified soil and parametric variation in Model

In this chapter for the study of the pore pressure generation in stratified soil the model parameter and material properties are provided. The variation in input motion, application of the loading and progression of loading intensity are provided in details. A brief discussion is also provided on scaling, filtering and baseline correction of the input motion for their proper wave propagation in the numerical model.

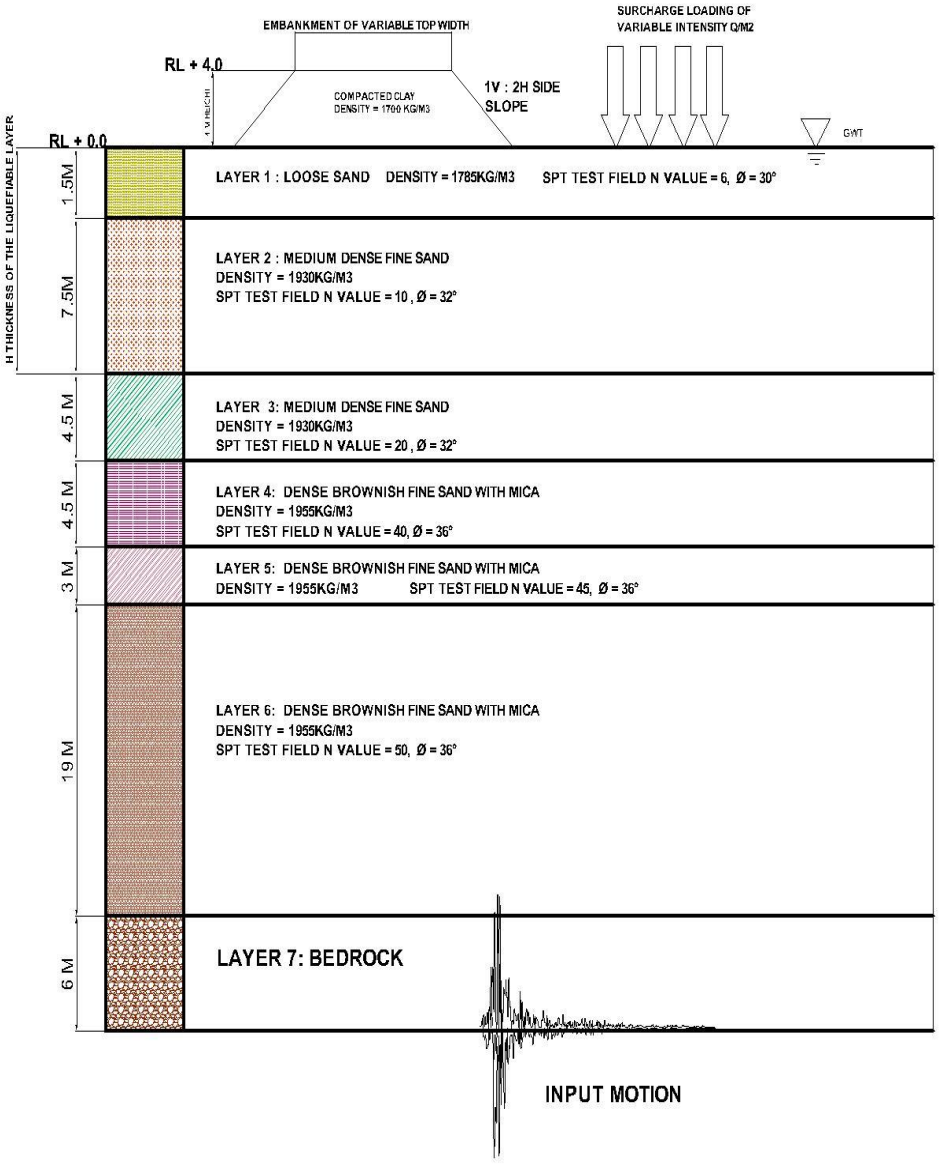

Fig 28: Schematic diagram of the model to be used for study of pore pressure generation derived from Bore hole data of Rajarhat site. (not in scale)

In the Fig 28 a schematic diagram of the soil strata (not in scale) based on the bore hole data collected from Rajarhat site is shown. The geometrical description of the soil strata is provided. The soil strata is composed of three sand layers of thickness that is Loose sand of 1.5 m, Medium Dense sand of depth 12 m and Dense Brownish fine sand with Mica of depth 26.5m. The loosest sand layer is at top and densest at the bottom. Additionally we have considered bedrock at the depth of RL-40 for this analyses. The Ground water table is considered at top surface of the stratified deposit (RL 0).The SPT test for different layers are provided based on the field test data. For our parametric variation we have used Loma Prieta of Peak Ground Acceleration (PGA) 0.357g and scaled it down to 0.05g, 0.1g and 0.01g. We have also used scaled Mammoth Lake earthquake of PGA 0.44g and North Ridge Earthquake of PGA 0.22g. For loading we have used Embankment loading and surcharge loading condition on foundation soil. Embankment width have been varied from 10m, 20m and 30m for particular Loma Prieta of 0.2g acceleration to identify the pore pressure generation pattern across the span. The Embankment have a slope of 2H: 1V and a height of 4m.. For our last variation we have changed the thickness of the liquefiable layer from actual 9m to 5 m, 15m and 20m to study the intensity and pore pressure generation pattern. A total of 12 models have been prepared for this study. Table 13 presents the details of geometric specification and model variations considered for this study.

Table 13 Presents the details of geometric specification and model variations considered for this study.

SUBJECT : PARAMETRIC VARIATION FOR PORE PESSURE GENERATION IN MODEL

SL no.	Model Name	Soil Strata Geometry	Earthquake Used	Intensity of Earthquake	Loading Condition
1	MOD-1	Standard Bore Hole Data - **Liquefiable soil Height 9m**	LOMA PRIETA	0.05g	-
2	MOD-2	Standard Bore Hole Data - **Liquefiable soil Height 9m**	LOMA PRIETA	0.1g	-
3	MOD-3	Standard Bore Hole Data - **Liquefiable soil Height 9m**	LOMA PRIETA	0.2g	-
4	MOD-4	Standard Bore Hole Data - **Liquefiable soil Height 9m**	LOMA PRIETA	0.357g	-
5	MOD-5	Standard Bore Hole Data - **Liquefiable soil Height 9m**	MAMMOTH LAKE	0.2g	-
6	MOD-6	Standard Bore Hole Data - **Liquefiable soil Height 9m**	NORTH RIDGE	0.22g	-
7	MOD-7	Standard Bore Hole Data - **Liquefiable soil Height 9m**	LOMA PRIETA	0.2g	With Ebankment of **Top Width -10mtr**
8	MOD-8	Standard Bore Hole Data - **Liquefiable soil Height 9m**	LOMA PRIETA	0.2g	With Ebankment of **Top Width -20mtr**
9	MOD-9	Standard Bore Hole Data - **Liquefiable soil Height 9m**	LOMA PRIETA	0.2g	With Ebankment of **Top Width -30mtr**
10	MOD-10	Standard Bore Hole Data - **Liquefiable soil Height 5m**	LOMA PRIETA	0.2g	-
11	MOD-11	Standard Bore Hole Data - **Liquefiable soil Height 15m**	LOMA PRIETA	0.2g	-
12	MOD-12	Standard Bore Hole Data - **Liquefiable soil Height 20m**	LOMA PRIETA	0.2g	-

3.3 Material properties of the Soil strata and Embankment Soil

The Field SPT values of soil strata is corrected for Overburden correction and Dilatency correction (if N' is greater than 15) using IS code 2131 1981. The final properties of soil has been presented in Table 14.

This shows that there exist mainly 4 layers of soil. Top most Layer 1 is a loose sand of $N1_{(60)}$ values of 11, saturated density 1785kg/m3 and angle of internal friction 30^0

Layer 2 is a medium dense sand having low $N1_{(60)}$ values of 12, saturated density 1930kg/m3 and angle of internal friction 32^0.

Layer 3 is a Medium Dense fine sand with $N1_{(60)}$ value of 18 saturated density 1930kg/m3 and angle of internal friction 32^0 .

Layer 4 is a Dense Brownish fine sand with mica having $N1_{(60)}$ value of 26 saturated density 1955kg/m3 and angle of internal friction 36^0 .This layer extends to a depth of 26.5m.

Layer 5 is bedrock layer with high cohesion and tension values.

Embankment portion is a homogenous compacted clay. The cohesion is fixed at 40Kpa and the angle of internal friction is 20^0.

Table 14: Properties of layers in soil strata along with Embankment soil property

		Embankment	Loose Sand	Medium Dense Fine Sand	Medium Dense Fine Sand	Dense Brownish Fine Sand with Mica	Dense Brownish Fine Sand with Mica	Dense Brownish Fine Sand with Mica	Bedrock
Soil Depth in m		4 - 0	0 - (-1.5)	(-1.5) - (-9)	(-9) - (-13.5)	(-13.5) - (-18)	(-18) - (-21)	(-21) - (-40)	(-40) - (-46)
Soil Properties	Unit								
Dry Density	kg/m3	1700	1500	1650	1650	1700	1700	1700	2700
Saturated density	kg/m3		1785	1930	1930	1955	1955	1955	2876
Moisture Content	%		19	17	17	15	15	15	
N			6	10	20	40	45	50	
N1(60)			11	12	18	26	26	26	
Shear Wave Velocity	m/sec	200.00	196	201	247	295	295	295	1609
G	Pa	6.80E+07	5.75E+07	6.66E+07	1.01E+08	1.48E+08	1.48E+08	1.48E+08	6.99E+09
Poission		0.3	0.3	0.3	0.3	0.3	0.3	0.3	0.38
E	Pa	1.77E+08	1.49E+08	1.73E+08	2.62E+08	3.86E+08	3.86E+08	3.86E+08	1.93E+10
void ratio			0.50	0.45	0.45	0.40	0.40	0.40	
Porosity		0.35	0.33	0.31	0.31	0.28	0.28	0.28	
Permeability	m/sec	1.00E-06	7.56E-04	7.56E-04	7.56E-04	6.24E-05	6.24E-05	6.24E-05	
Hydraulic conductivity	m2/Pa* sec	1.02E-10	7.71E-08	7.71E-08	7.71E-08	6.36E-09	6.36E-09	6.36E-09	
Angle of Internal friction	Degree	20	30	32	32	36	36	36	27.8
Cohesion	Pa	4.00E+04	-						2.72E+07
Tension									1.17E+06

Shear velocity of different model is calculated using the equation presented by **Chatterjee & Choudhury [2013]** for Kolkata soil.

For silty sand Shear wave velocity (Vs) = $56.44 * (N1_{(60)})^{\wedge 0.511}$ (1.16)

Shear modulus of different material in different layer is calculated using equation 1.17

Shear Modulus Gmax = ρVs^2 (1.17)

Density of material = ρ

3.4 Mesh Generation

After creating material file for each layer along with the embankment and bedrock the next sep is to generate mesh. Generation of mesh is dividing the numerical model into small elements which are needed for subsequent analysis under different loading and boundary condition. These small elements are quadrilateral in shape. For accurate results the mesh needs to as fine as possible. But with fine meshing, the calculation time increases significantly and sometime. So a balance to be maintained in choosing the mesh element size and calculation time. Among the three options available in the software, we obviously use the fine mesh generation option for accurate results. But, in our study, the dynamic (seismic) loading is associated with the analysis. So, only the fine meshing cannot guarantee accurate analysis. The element size is also to be checked in association with the frequency content of the input acceleration history. The significant frequency of the motions are presented below.

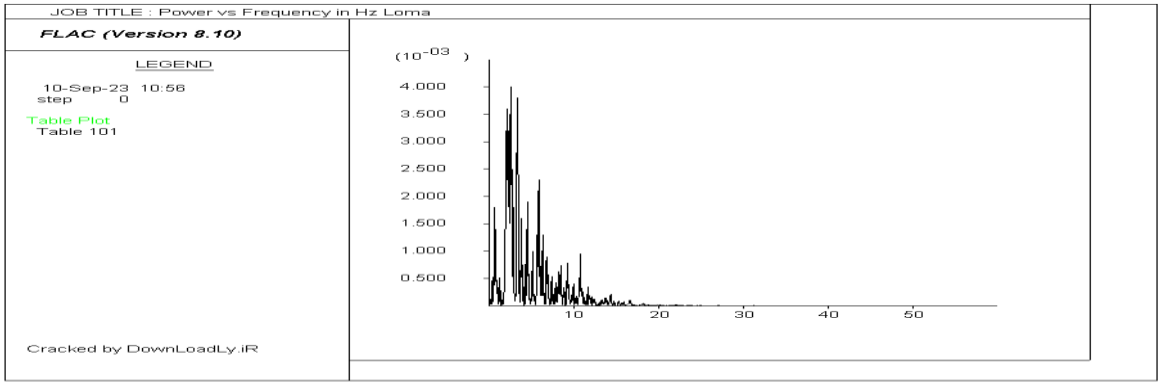

Fig 29: Power spectrum of Loma Prieta Earthquake acceleration history for maximum acceleration of 0.357g

Since the Loma Prieta Earthquake is scaled it to different PGA values, the significant frequency range for all scaled input motion would be similar like the original. The same stands true for Mammoth Lake power spectrum. From the power spectrum of the acceleration time history for all different acceleration it is clearly visible that maximum power dissipation lies below the frequency of 8 Hz.

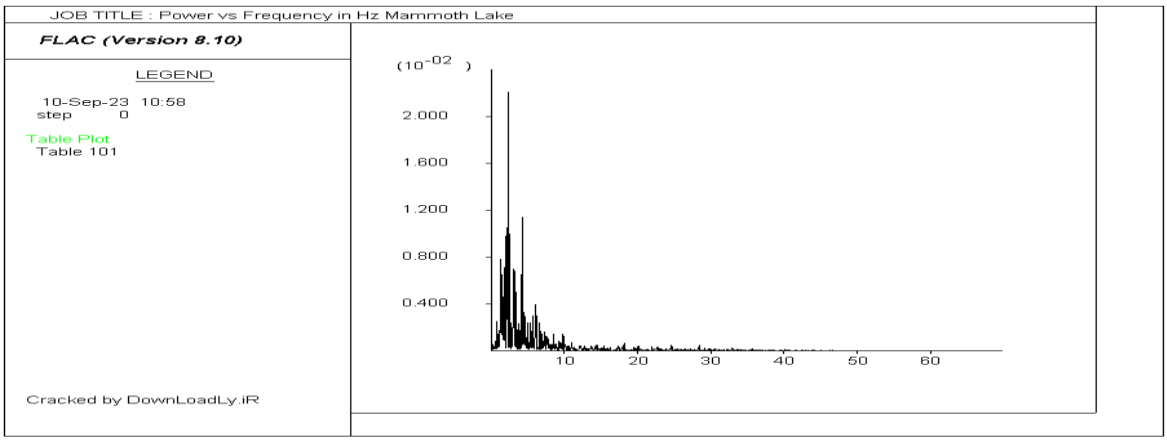

Fig 30: Power spectrum of Mammoth Lake Earthquake acceleration history for maximum acceleration of 0.44g

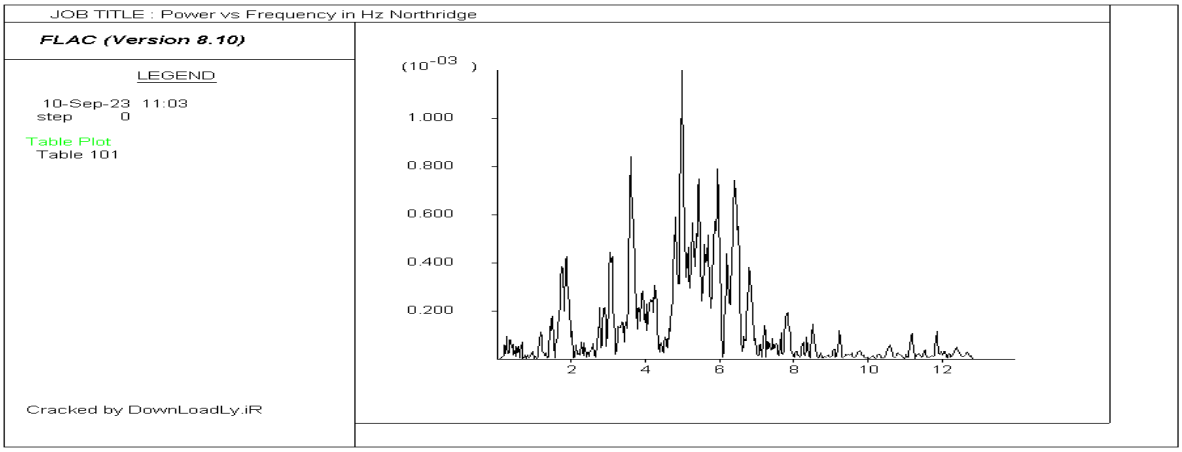

Fig 31: Power spectrum of Northridge Earthquake acceleration history for maximum acceleration of 0.17g

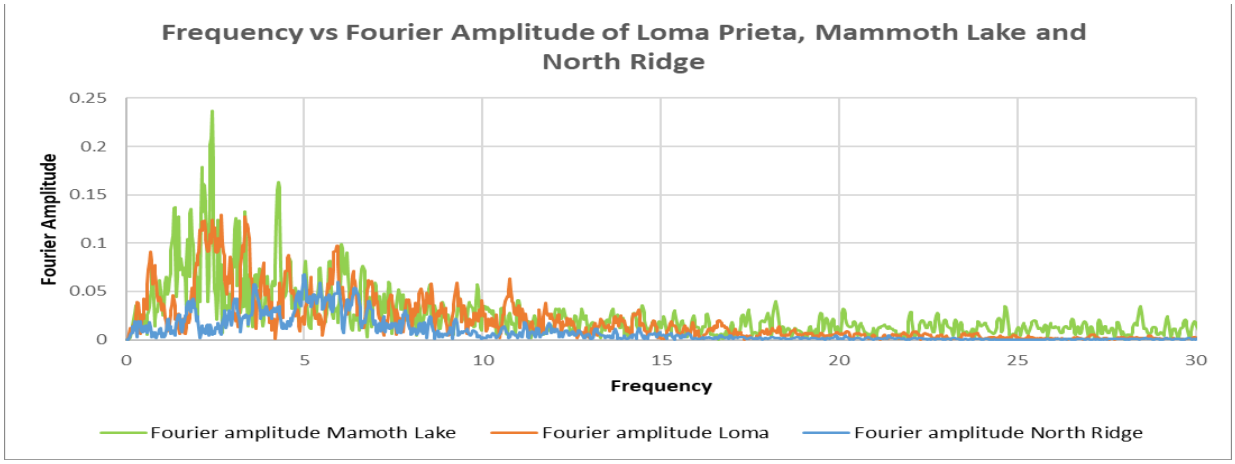

Fig 32: Frequency vs Fourier Amplitude comparison of Loma Prieta 0.357g, Mammoth Lake 0.43g and and 0.22 North Ridge.

So all the input earthquake records have to be filtered by a low pass filter to remove higher frequency content above 8 Hz. Now the 8 Hz can be used as the guiding frequency for fixing the mesh size. Kuhlemeyer and Lysmer (1973) showed that for an accurate representation of the wave transmission through the soil model, the spatial element size, Δl, must be smaller than approximately one-tenth to one-eighth of the wavelength associated with the highest significant frequency. The mesh size is decided based on maximum frequency content and least shear velocity of the material. Now, the minimum shear velocity belongs to the top sand layer and the velocity is 196m/sec.

$$\text{Wave length } (\lambda) = \frac{Shear\ wave\ velocity(\frac{m}{\sec})}{Significant\ maximum\ frequency(Hz)} = \frac{196}{8} = 24.5\text{m} \qquad (1.18)$$

Maximum element side length (Δl) is taken as one-tenth of the wavelength i.e.24.5m/10 =2.4m. So the maximum size of the mesh could be 2,4m for better accuracy of the analyses we have considered mesh size of 1m for our analysis.

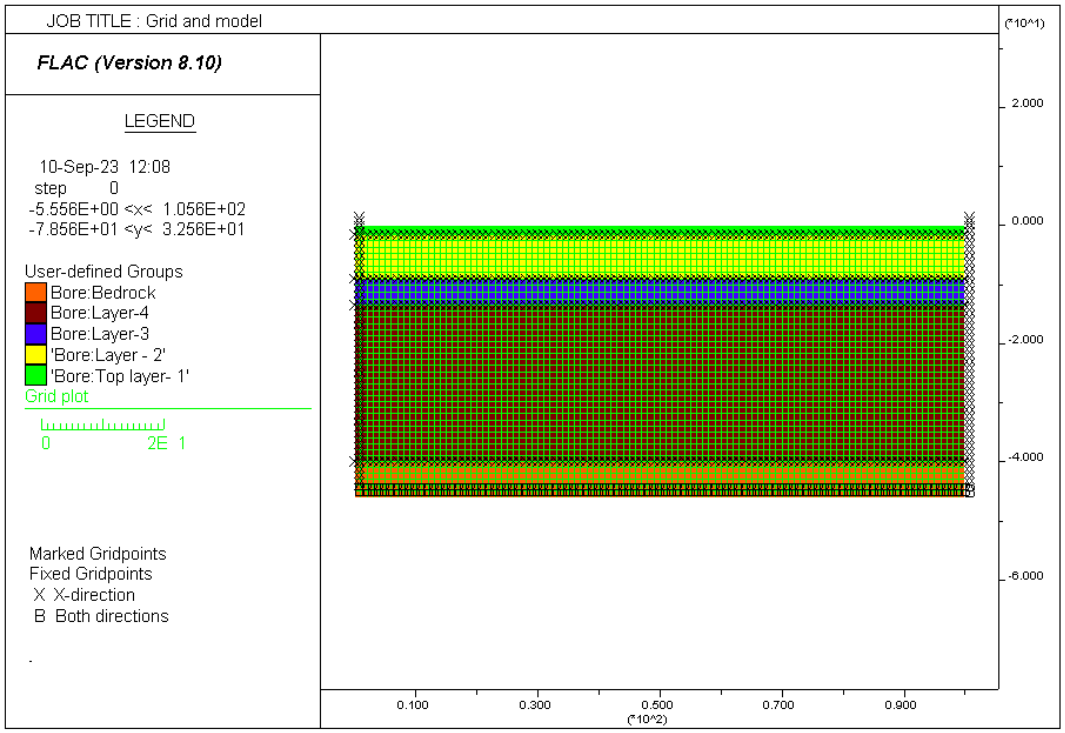

Fig 33: Soil strata model shown with mesh generated of 1mx1m

3.5 Input Motion: Scaling, Filtering and Baseline correction

3.5.1 Scaling of Input motion

The soil strata is subjected to three different kinds of loading that are Loma Prieta, Mammoth Lake and North Ridge. The details of the acceleration has been provided below table 15

Table 15: Acceleration details of the input motions

Earthquake Name	Loma Pietra	Mamoth Lake	Northridge
Peak Ground Acceleration	0.357g	0.43g	0.22g
Duration of Earthquake	40	30	40
Date of occurance	18.10.1989	25.05.1980	17.01.1994
Pre Dominanat Frequency	0.325hz	0.27hz	0.25hz
Moment Magnitude	6.9	6.5	6.6

From the soil property it is quite evident that the top soil layer will not be able to cope with peak acceleration of 0.357g of Loma Prieta and 0.43g of Mammoth Lake. So we have scaled down the acceleration of Loma Prieta to 0.05g, 0.1g, 0.2g. Similarly we have also scaled down the Mammoth Lake acceleration to 0.g for the analyses. The frequency content remains unchanged except for the amplitude of the power spectrum.

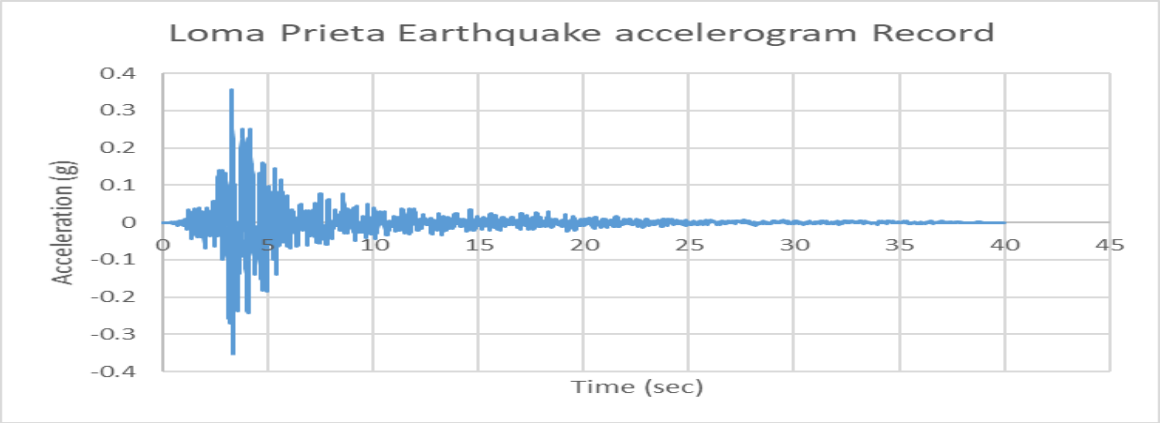

Fig 34: Loma Prieta Accelerogram record for PGA 0.357g

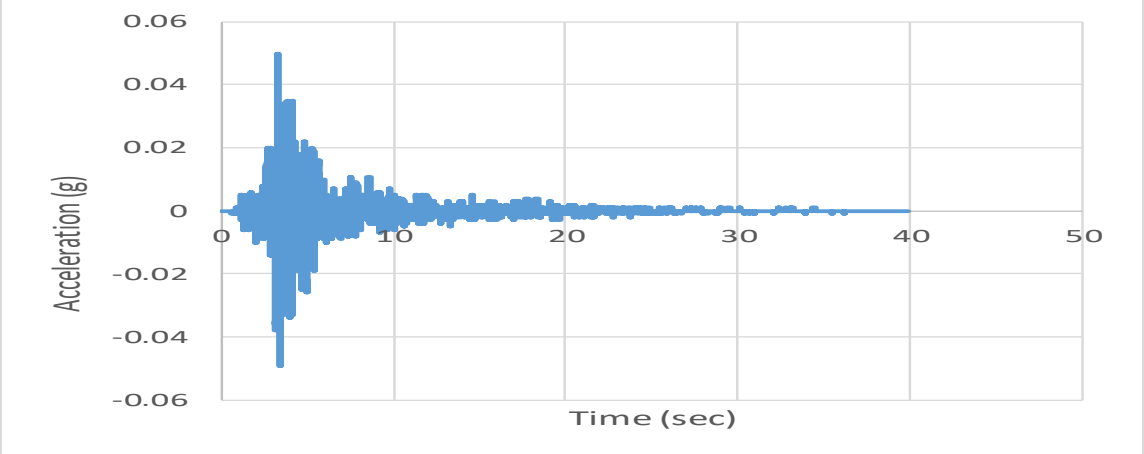

a

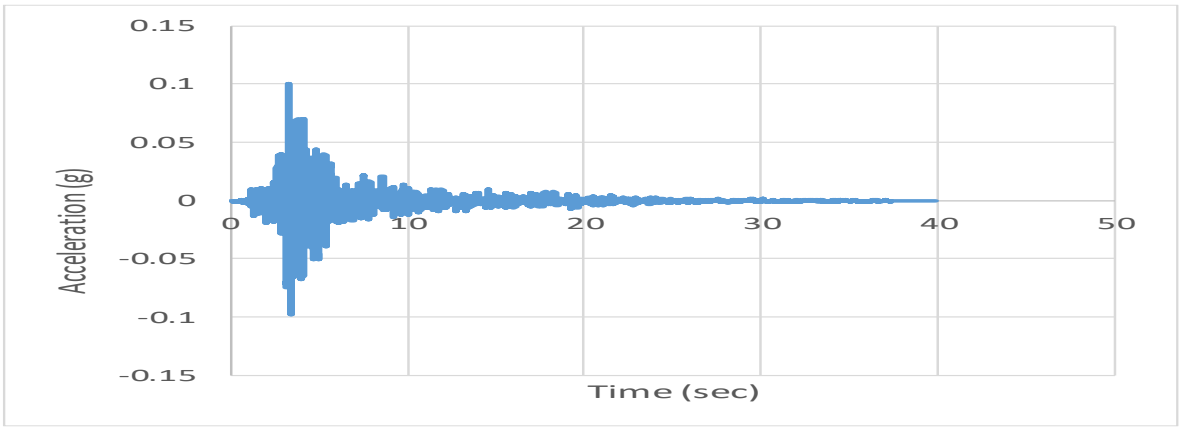

b

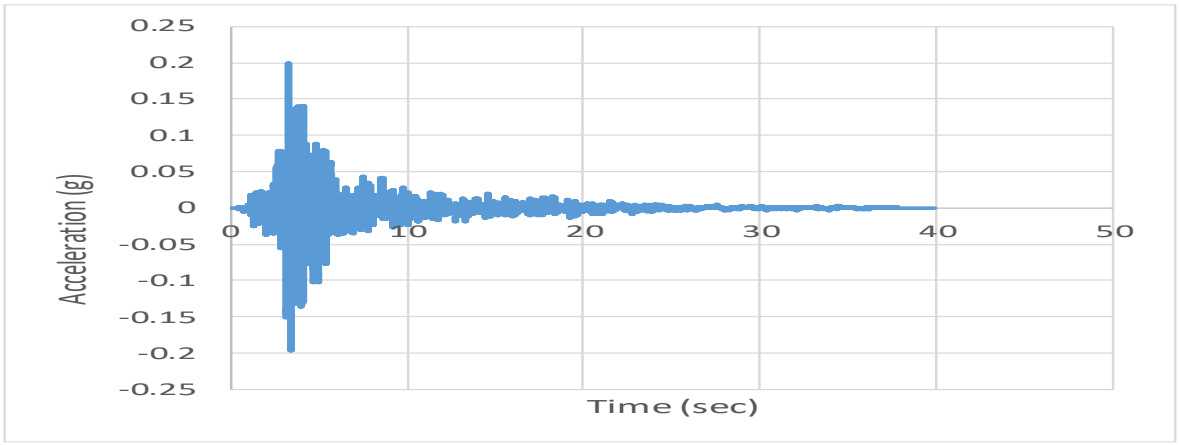

c

Fig 35: Scaled acceleration time history of Loma Prieta for a) 0.05g b) 0.1g and c) 0.2g

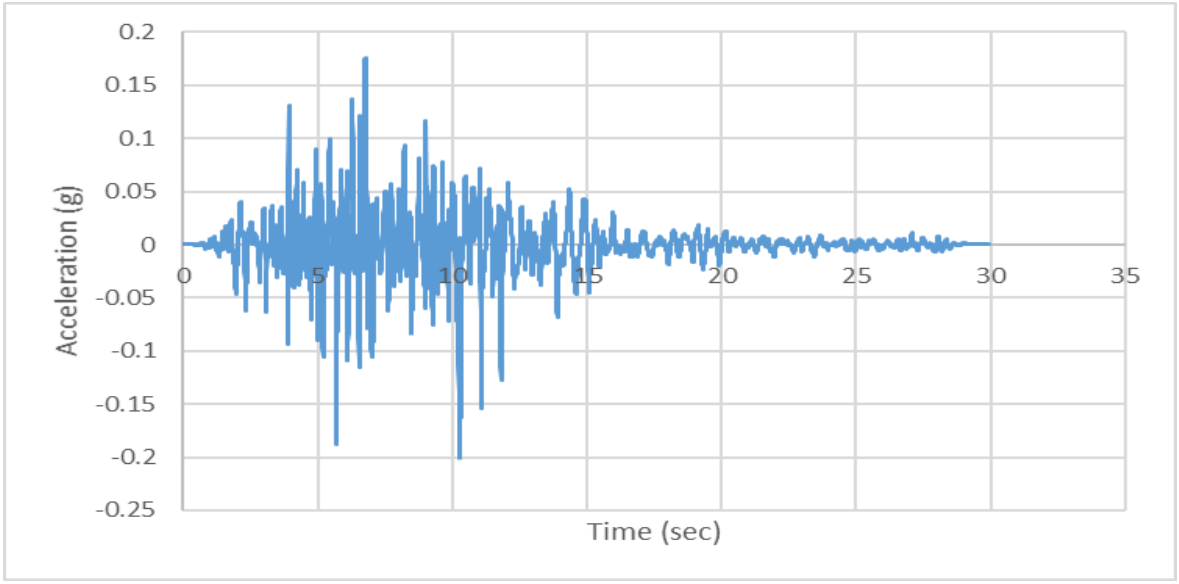

Fig 36: 0.2g Scaled acceleration time history of Mamoth lake Earthquake

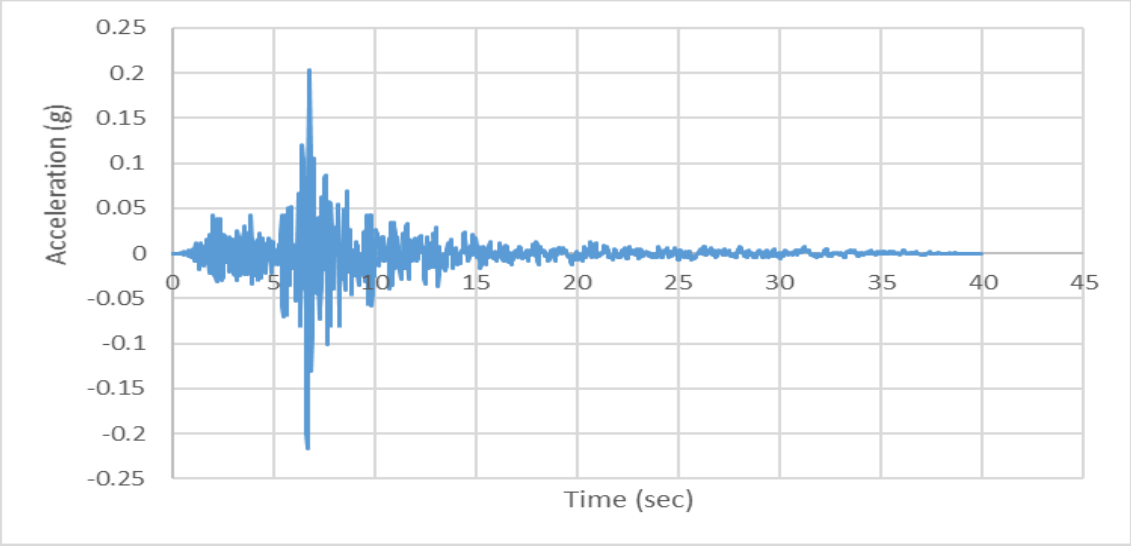

Fig 37: 0.22g acceleration time history of North Ridge Earthquake

3.5.2 Filtration of Input motion

As discussed in earlier section an 8 Hz frequency filter is selected to run the acceleration in the above numerical model. So all the input motions must be filtered for 8 Hz frequency before proceeding for baseline correction.

3.5.3 Baseline Correction of Input motion

The baseline correction of an acceleration time-history or velocity-time history needs to be done if raw data of those time histories are used in numerical input. This is because FLAC model may exhibit continuing velocity or residual displacements after the motion has finished. This condition arises from the integral of time -history is not zero. A low frequency periodic function is determined that is added to the site recorded time history to make final residual displacement zero. As, in this study the three velocity histories derived from the site recorded accelerogram data, a baseline correction is required to carry out for each of the motion.

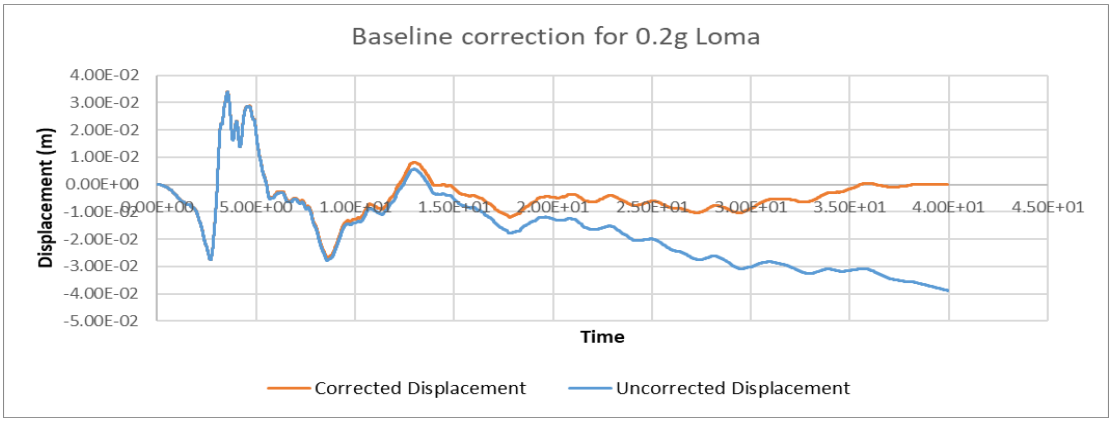

Fig 38: Baseline correction for 0,2g Loma Prieta

3.5.4 Boundary Condition of the Model

In the static analysis phase, the normal boundary condition for soil structures is subjected to the model. Along the base, the fixed boundary is assigned and the roller boundary is assigned in the sides of the model and top surface of the model is kept free. Roller boundary is not assigned at the base of the models in order to avoid the free sideways motion which will lead to the unrealistic failure mode. After completion of static analysis, the dynamic loading is applied. Before the application of dynamic loading, proper boundaries are to be applied to the model. The choices of boundaries depend on the mode of application of the input motion. In this study, the input motion is given at the model base (RL -46.0+) in the shear stress waveform. There are other modes of application of input motion (like acceleration-time history, velocity-time history) that will be discussed later in details. For the shear stress form of input motion, we can apply the most suitable boundary for seismic analysis that is available with FLAC2D. The "quiet" boundary criteria are applied along the base of the model (along RL-46.0) and the "free field boundary" criteria are applied along both the sides of the model (from RL -46.0 to RL 0.0 both sides). The top surface is kept free i.e. shear stress on the top surface is zero. The "quiet boundary" and "free field boundary" are discussed below in brief.

3.5.4.1 Quiet Boundary

The soil mechanics problem is modelled best when represented resting on an unbound medium which extends to infinite. But for numerical modelling purpose, it is quite unrealistic because to model an unnecessary large extent of the medium on which the main structure rests, it will take a very large solution time. The near-surface earth structures are assumed to rest on half-space. This is similar to the problem that is to be addressed in this study. Numerical methods relying on the discretization of a finite region of space require that appropriate conditions be enforced at the artificial numerical boundaries. In the case of static analysis, the fixed or elastic boundaries can be placed at some distance from the main structures. But in case of dynamic analysis, with this type of boundary conditions, the waves can be reflected back in the model instead of radiating out of the zone of interest. By using large it can be solved as material damping will nullify most of the reflected energy but it would not be computationally viable. The viscous boundary developed by Lysmer and Kuhlemeyer (1969) is used in FLAC2D. This boundary can be used in the time domain. The consistent boundary is most suitable for dynamic analysis but it works in frequency domain analysis. As this is an analysis done in the time domain, the quiet boundary is used in this analysis. The quiet-boundary scheme proposed by Lysmer and Kuhlemeyer (1969) involves dashpots attached independently to the boundary in the normal and shear directions. The dashpots provide viscous normal and shear tractions given by

$$t_n = -\rho\, C_p v_n \quad (1.19)$$

and $$t_s = -\rho\, C_s v_s \quad (1.20)$$

Where v_n and v_s are the normal and shear components of the velocity at the boundary; ρ is the mass density; C_p and C_s are the p- and s-wave velocities. In our model, the quiet boundary is applied in both x and y direction at the base of the model. This prevents the reflection of the wave back to the embankment that minimizes unrealistic amplification at the free surface.

3.5.4.2 Free Field Boundary

The seismic input is normally represented by plane waves propagating upward through the underlying material. The boundary conditions at the sides of the model must account for the free-field motion that would exist in the absence of the structure. The vertical boundaries should be placed at a significant distance from the zone of interest to minimize the wave reflections and to achieve free field condition. Sometimes this leads to the modelling of a significantly large model that in turn causes tedious calculations. An alternative procedure is to enforce the free field motion in such a way that boundaries retain their non-reflecting properties (i.e., outward waves originating from the structure are properly absorbed)

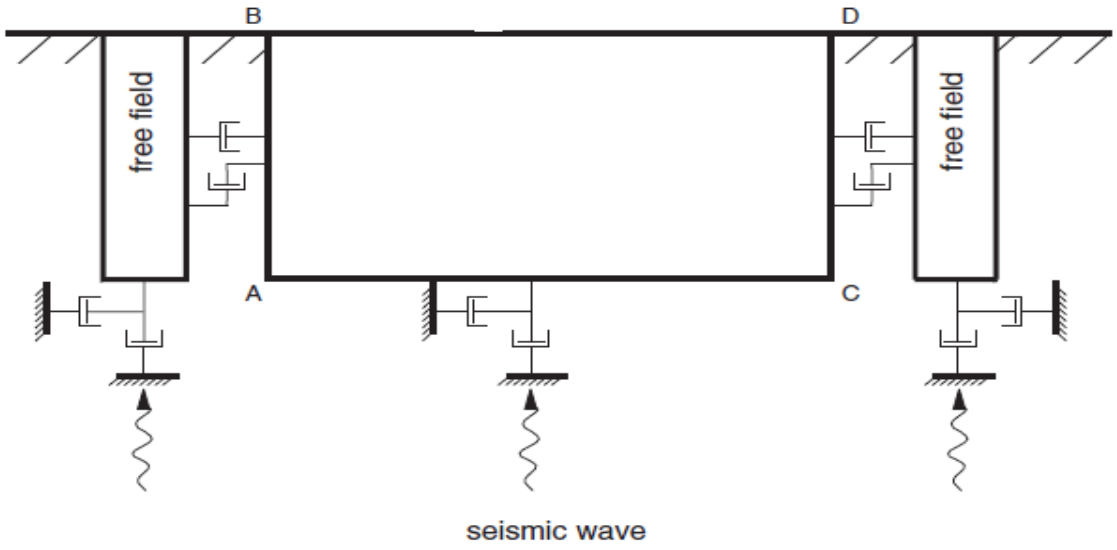

Fig 39: Soil strata with half-space and free field boundary (dashpot representation)

The lateral boundary of the model coupled with viscous dashpots create the condition of the quiet boundary that simulates the condition for infinite medium in the sideways and the unbalanced force is applied from free field to the main grid boundary. The plane waves that propagate upward is not distorted at the boundaries due to the free field condition that holds similar like an infinite model. The model is kept in static equilibrium before applying the free field condition.

3.5.4.3 Mode of Application of the Seismic Input Motion

The seismic input motion can be applied to the model in different ways like in the forms of acceleration-time history, velocity-time history, shear stress wave history etc. In the FLAC 2D version 8.1, all these modes of seismic load application are available. But the dynamic boundaries discussed in 3.5.4 cannot be suitably applied along with all modes of application of dynamic loading. For example, if the input motion is applied in the form of velocity-time history or acceleration-time history along the base, the quiet boundary cannot be along the base; it is a limitation of the software. The dynamic boundary is very important in the analysis of the seismic behaviour of embankment. So, the shear stress-wave history is used as input loading and the quiet boundary and input stress-wave history both can be applied along the same base grid of the model that is necessary for the accurate study of the soil strata. So, the acceleration time history will have to be converted into stress wave history. The conversion procedure is described below considering the boundary condition as well.

Step I: First, the acceleration time history is integrated to convert it into shear particle velocity history. (V_s)

Step II: In the second step, the shear velocity time history is converted into shear stress-time history by the following relationship.

$$|\sigma| = 2\rho C_s V_s \qquad (1.21)$$

In the above equation (1.21), |σ| = magnitude of shear stress; ρ = mass density of material; Cs = Shear wave velocity in the medium; vs is input particle velocity i.e. the velocity-time history derived from the acceleration time history. The values of the acceleration time history is now converted to the shear stress time history.

In the equation factor, 2 is taken for the input stress energy is divided between the upward and downward propagating wave in the medium. We are interested in the upward propagating wave from the base towards the surface.

Peak Acceleation	Modified Peak Acceleation after Filtering and Baseline correction	Acceleration time history	Velocity Time history
Loma Prieta			
0.05g	0.0445g	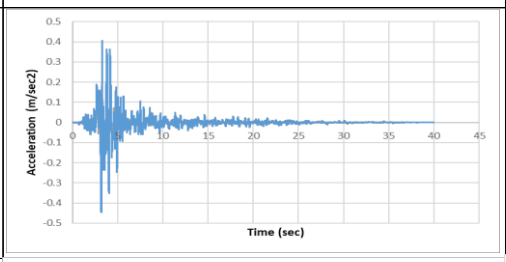	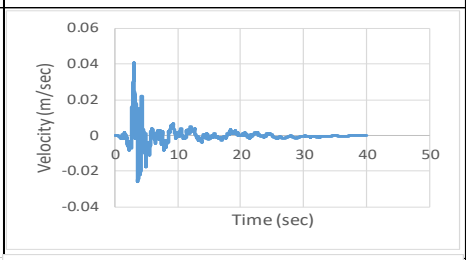
0.1g	0.089g	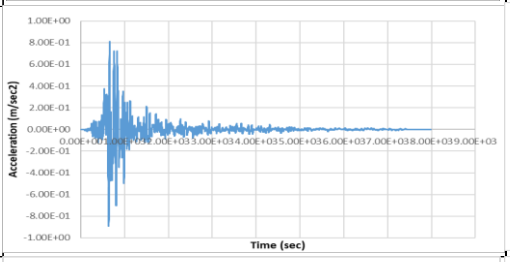	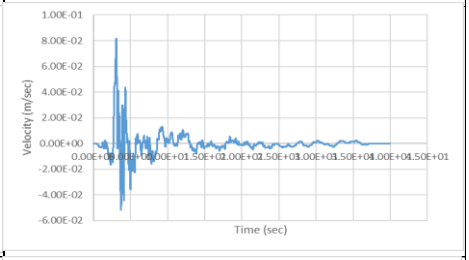
0.2g	0.178g	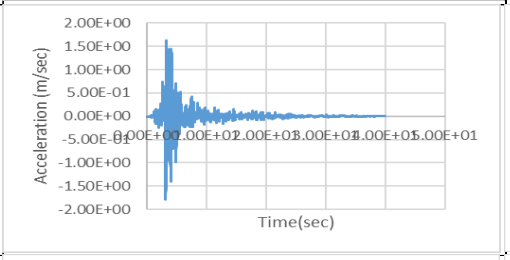	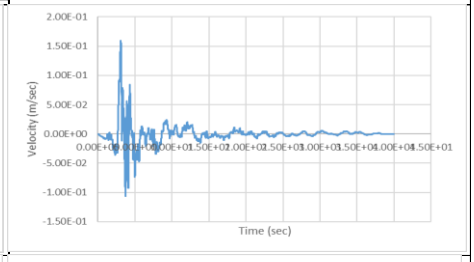
0.357g	0.328g	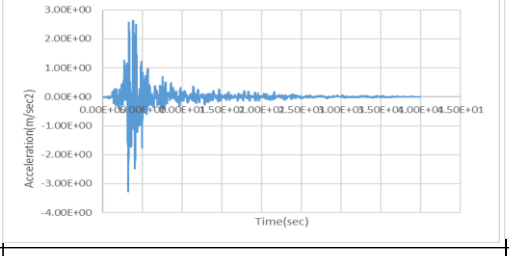	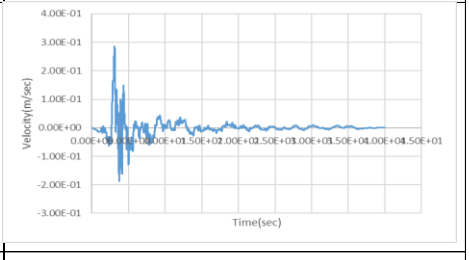
Mammoth Lake			
0.2g	0.14g	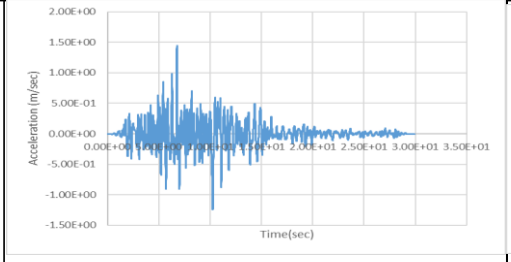	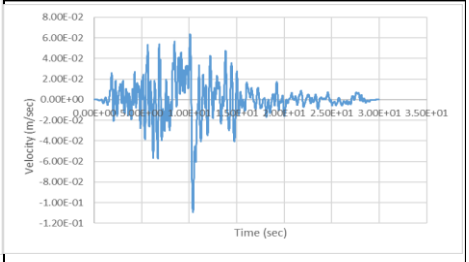
North Ridge			
0.22g	0.208g	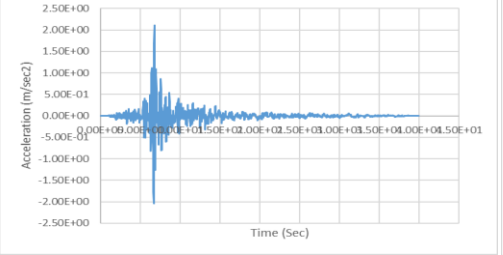	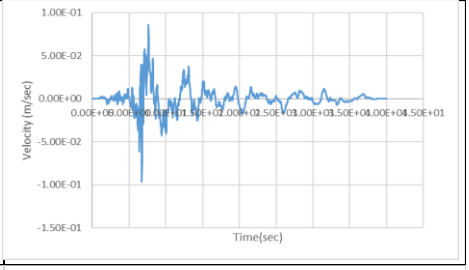

Fig 40: Acceleration tie history after filterating and baseline correction and their corresponding velocity

3.5.5 Damping and response of soil

Material damping in soil is mostly due viscosity, friction and plasticity development. The damping in the numerical dynamic analysis should produce energy loss in the system when subjected to dynamic loading. In soil and rock natural damping is mostly hysteretic. Numerically it is difficult to produce hysteretic damping because of two reasons. First simple hysteretic function do not damp all components equally when several waveforms are superimposed. Second, hysteretic functions are path dependent which makes them harder to intercept. In this study, the dynamic damping is provided by Hysteretic damping combined with small amount of 0.2% of Rayleigh Damping of stiffness proportional. This low level of Rayleigh damping is added to the Hysteretic damping in dynamic simulation to avoid low level oscillation and to remove high frequency noise

3.5.5.1 Rayleigh Damping

Rayleigh Damping is originally used for structures in elastic column to damp natural oscillation of the system.

A damping matrix, C, is used, with components proportional to the mass (M) and stiffness (K) matrices:

$$C=\alpha M+\beta K \tag{1.22}$$

α = the mass-proportional damping constant; and β = the stiffness-proportional damping constant. The stiffness-proportional term is analogous to a dashpot connected across each FLAC zone (responding to the strain rate. The two terms of Rayleigh damping (mass and stiffness) depends on frequency, but they are considered to be frequency independent over a range of predominant frequency.

The central frequency is found as below,

$$f_{min} = (\omega_{min}/2\pi) \tag{1.23}$$

The idea in the dynamic analysis is to adjust the centre frequency of the rayleigh damping so that it coincides with range of the predominant frequency. Predominant frequencies are the combination of natural frequencies and natural modes of the system.

Rayleigh Damping is mostly unpopular with the code user as it involves drastic reduction in time step and a consequent increase in solution time.

3.5.5.2 Hysteretic Damping

Over many years, the cyclic loading on soil or rock has been analysed in the equivalent-linear method that does not assume non-linearity effects of soil behaviour directly. It incorporates linearity in soil behaviour and average strain-dependent shear modulus is used in the solution process to approximate non-linearity. Different damping levels also can be assigned depending upon the different levels of strains in soils in the hysteretic damping algorithm in FLAC which makes the analysis more realistic; so it is more accurate than the response that is predicted in Rayleigh damping algorithm that uses average damping response. Hysteretic damping analysis also takes significantly less time than the Rayleigh damping.

Formulation of Hysteretic damping

In Figure 40, a shear modulus degradation curve for sand is shown with respect to the cyclic strain percentage. In this study, this strain-dependent modulus degradation curve is used for hysteretic damped analysis for all the soil layers in the absence of the laboratory test data regarding the damping and modulus degradation

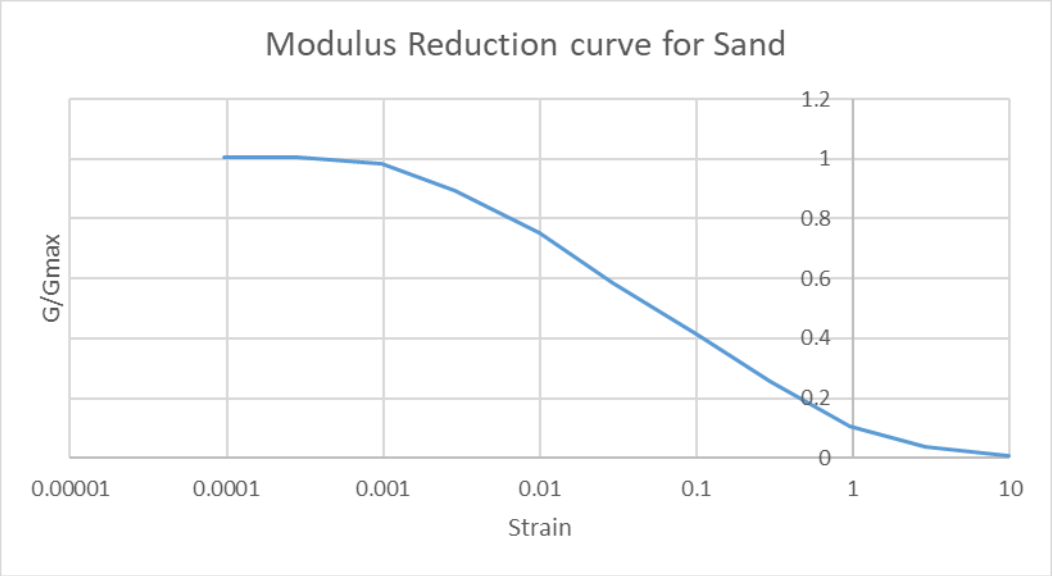

Fig 41: Modulus reduction curve of sand used for this study

The above Figure 40 implies a non-linear stress-strain relationship of soil. If an ideal soil is assumed for which stress is only dependent on strain not on the number of cycles, an incremental constitutive relation from the degradation curve, described by

$$\tau / (G_o \gamma) = M_s \quad (1.24)$$

G_o = Maximum Shear Modulus at small strain; γ = shear strain; M_s = strain-dependent normalised secant modulus.
The tangent modulus, M_t, is then obtained as

$$M_t = \frac{d\bar{\tau}}{d\gamma} = M_s + \gamma \frac{dM_s}{d\gamma} \quad (1.25)$$

Mt is normalised tangent modulus. The incremental shear modulus in a nonlinear simulation is GoMt.
The damping ratio and strain relationship that is used in this study for sand is shown in Figure 41. Similarly the Modulus reduction and Damping ratio curve for bedrock is generated using previous study [**Hanumantha Rao Ch 2014].** The Modulus reduction and strain relationship that is used in this study for rock is shown in Figure 42

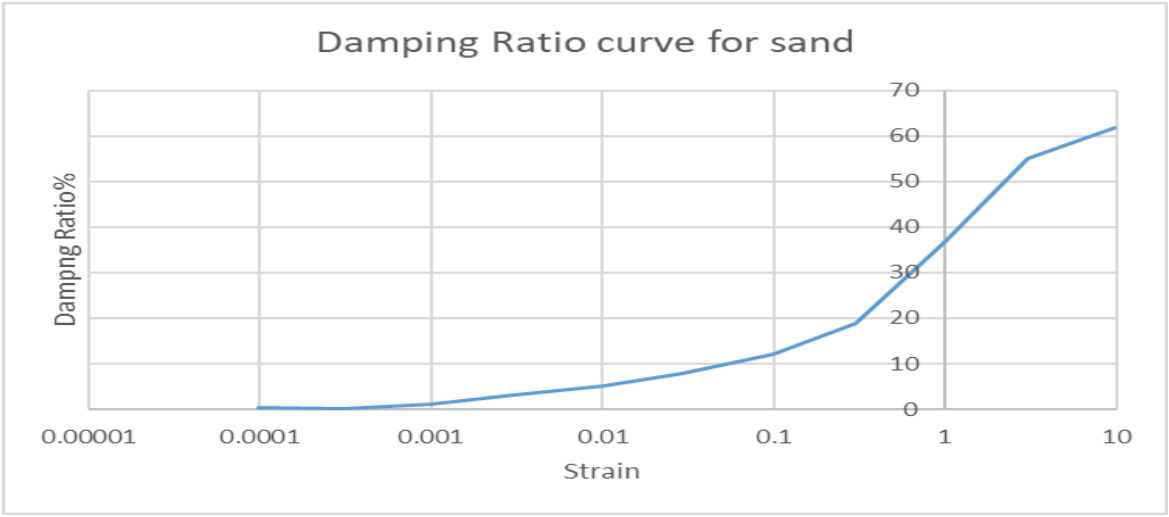

Fig 42: Damping Ratio curve of sand used for this study

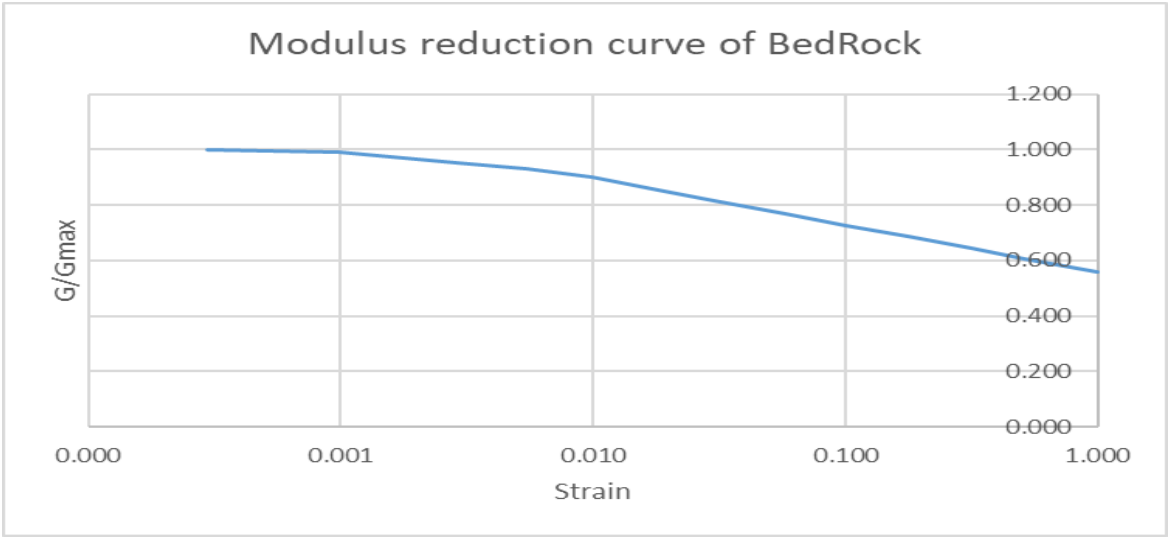

Fig 43: Modulus reduction curve of Bedrock used for this study

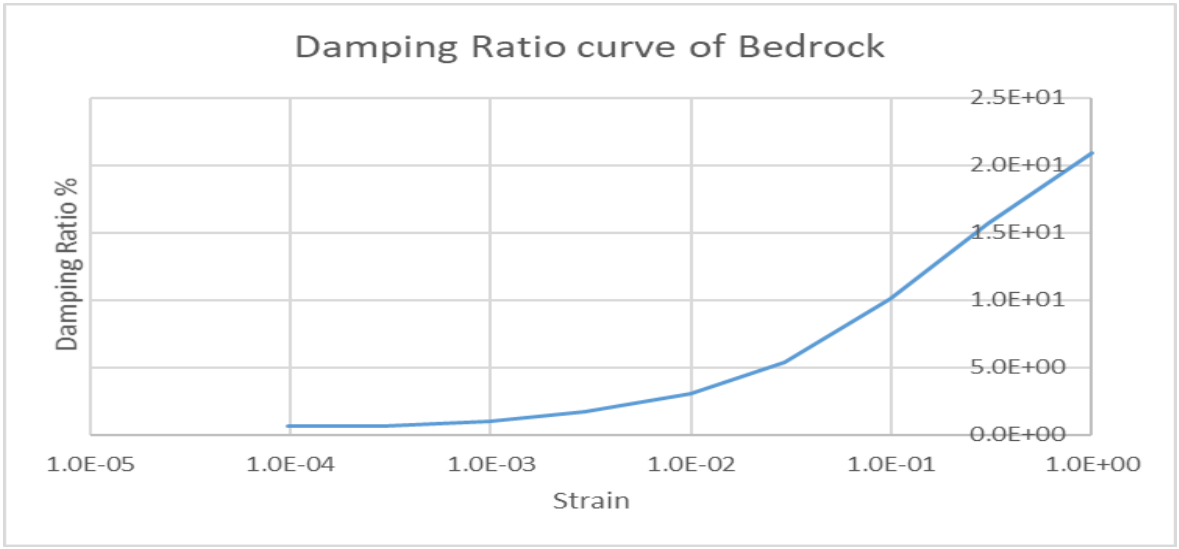

Fig 44: Damping Ratio curve of Bedrock used for this study

These curves are numerically linked with the basic constitutive algorithm of the Mohr-Coulomb model to simulate the actual condition of the soil materials under dynamic loading.

Chapter 4

Results and Discussions

4.1 Static Analysis

In this chapter the results of static analysis of the earthen embankment model are presented and discussed. The results of the analysis are subdivided into three parts, (i) Static analysis of soil strata (ii) Static analysis of soil strata with embankment, (iii) Static analysis of soil strata with Liquefiable layer height variation.

4.1.1 Static analysis of Soil Strata

Before doing dynamic analysis we need to check our model for geo-static stability. This helps us to check the accuracy of the model. As we have considered water table at GL (RL 0.0), the static pore pressure distribution is shown below and also the total and effective stress distributions are also shown and these value can be checked by hand calculation as well.

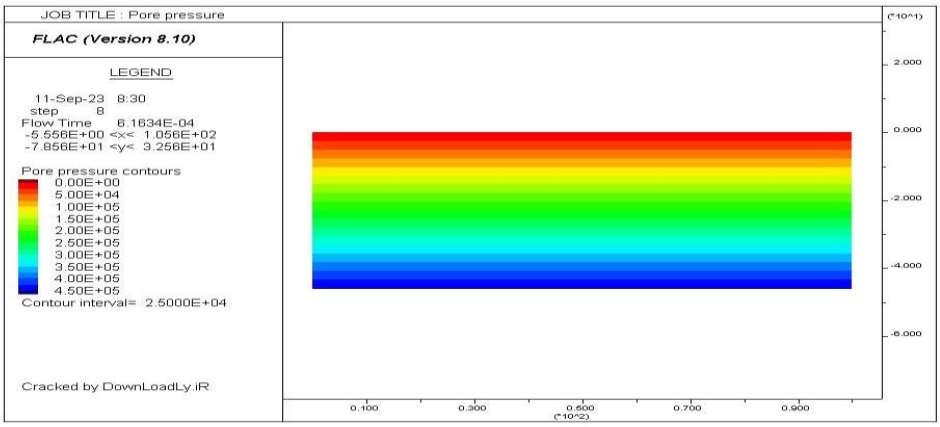

Fig 45: Static Pore pressure generation contour in soil

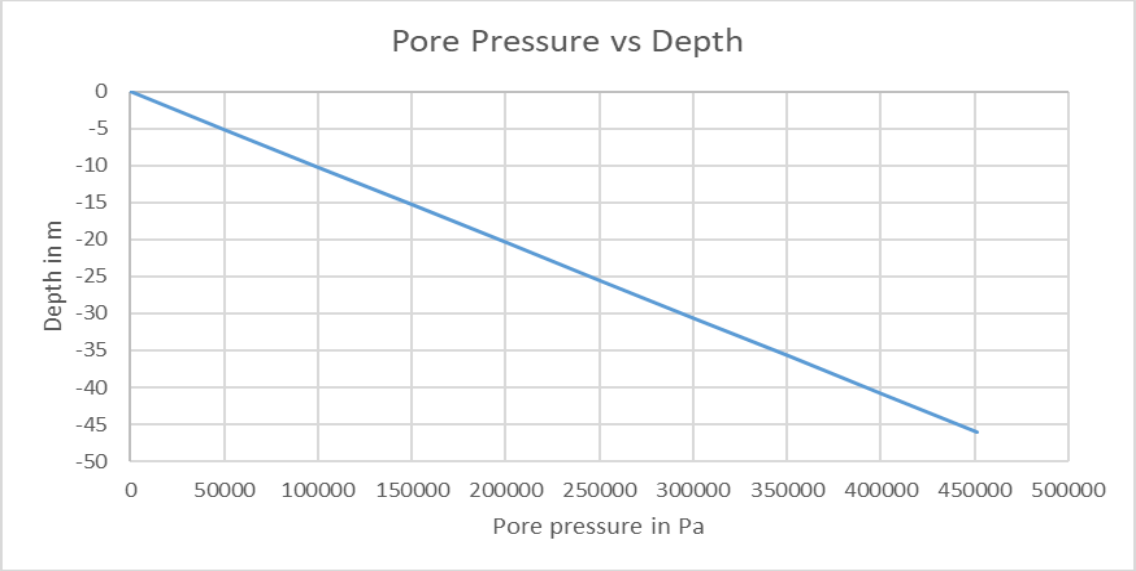

Fig 46: Pore pressure generation with depth in soil

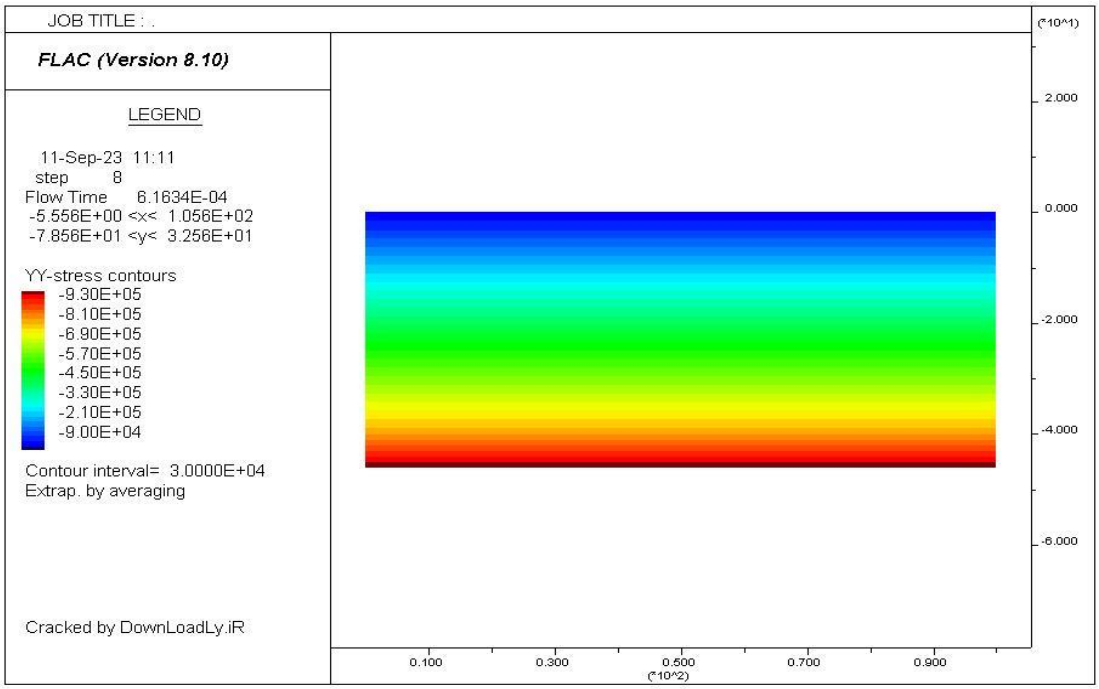

Fig 47: Total vertical Stress along y-y contour

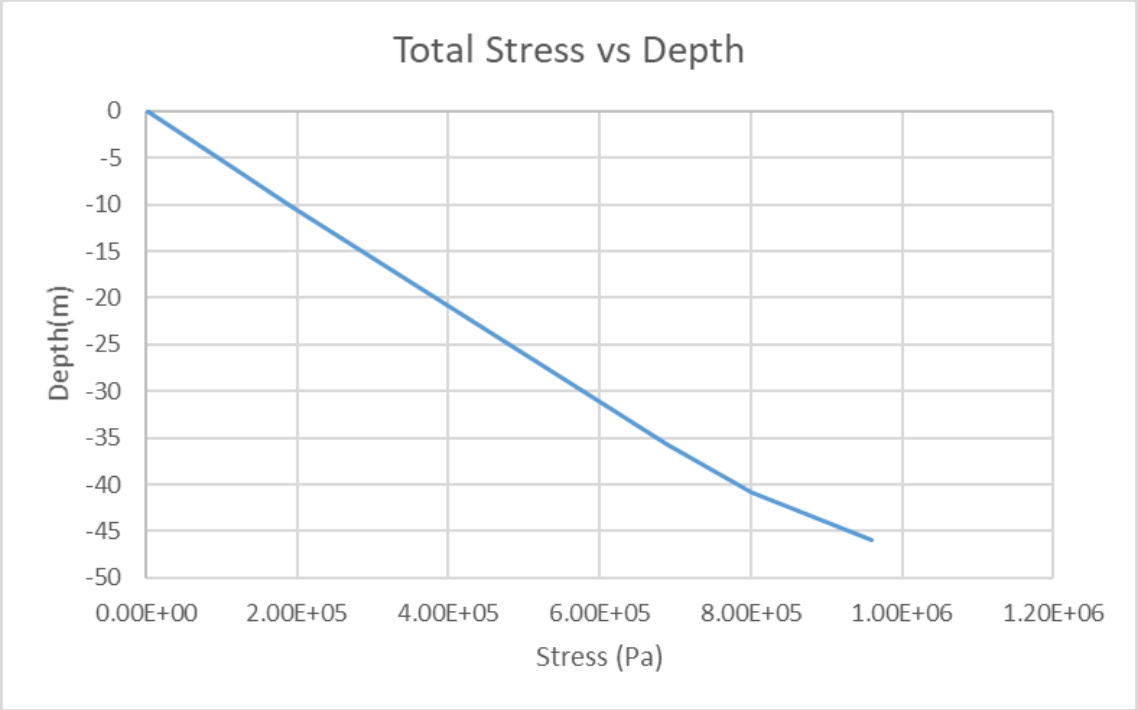

Fig 48: Total vertical Stress vs Depth

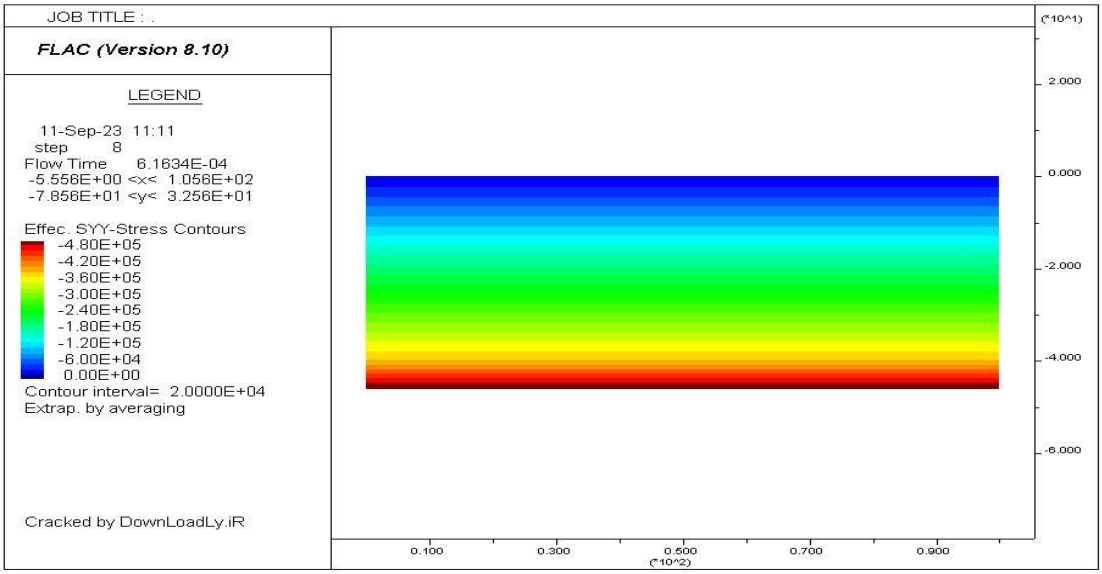

Fig 49: Effective vertical Stress along y-y contour

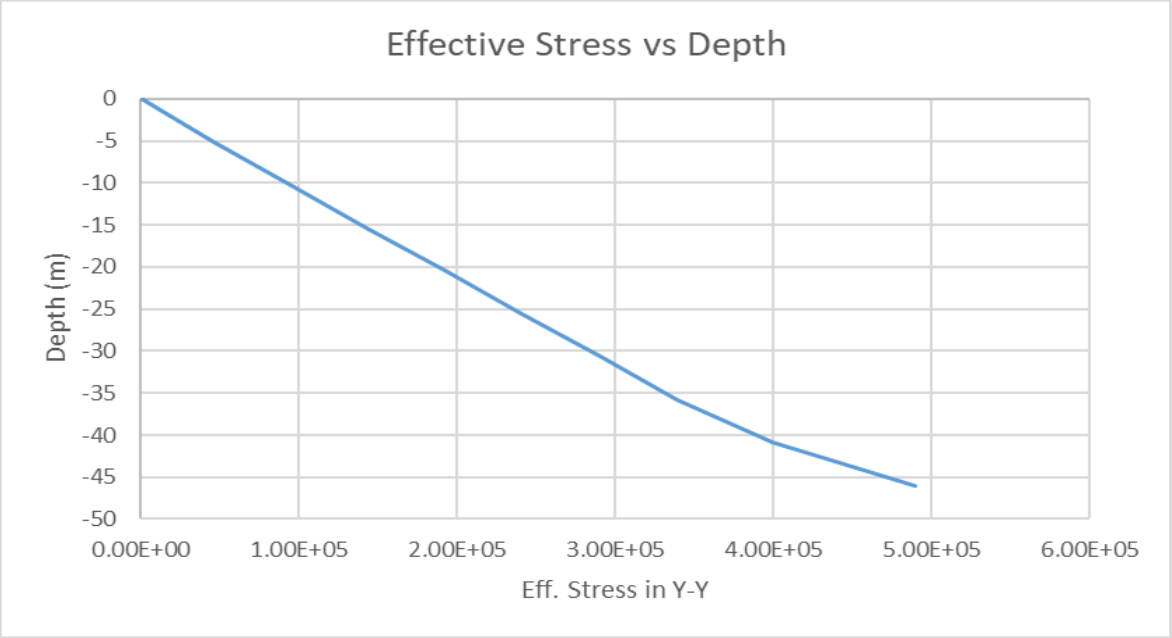

Fig 50: Effective vertical Stress vs Depth

4.1.2 Static analysis of Soil Strata with Embankment

After establishing the initial geo-static condition we have done the static analysis with the embankment and also the static stability of the embankment is checked by determining the static factor of safety. For this study we have varied the top width of the embankment ie mentioned in Table 13 MOD-7, MOD-8 and MOD-9 respectively. Factor of safety for all three models are 1.4. The pore pressure distribution, effective stress distribution, total stress distribution, x-displacement and y-displacement distribution etc. for each model are shown below.

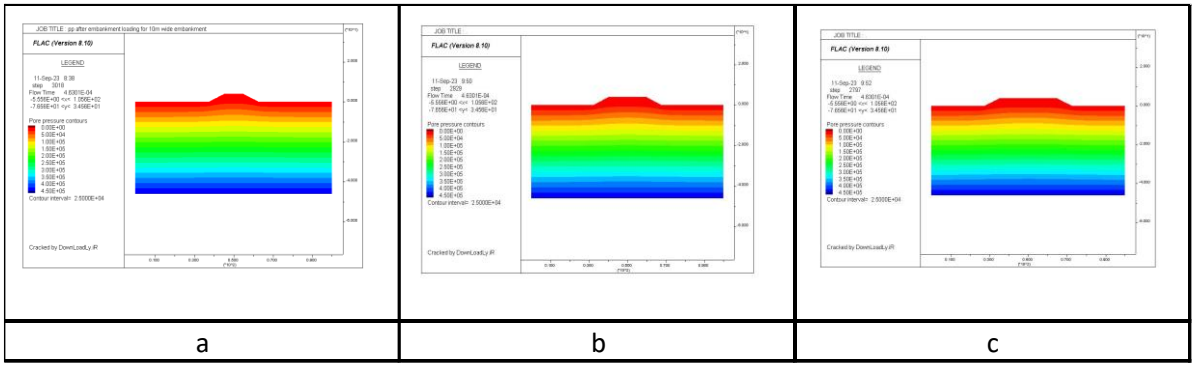

Fig 51: Pore Pressure distribution contour in a) MOD 7 b) MOD 8 c) MOD 9

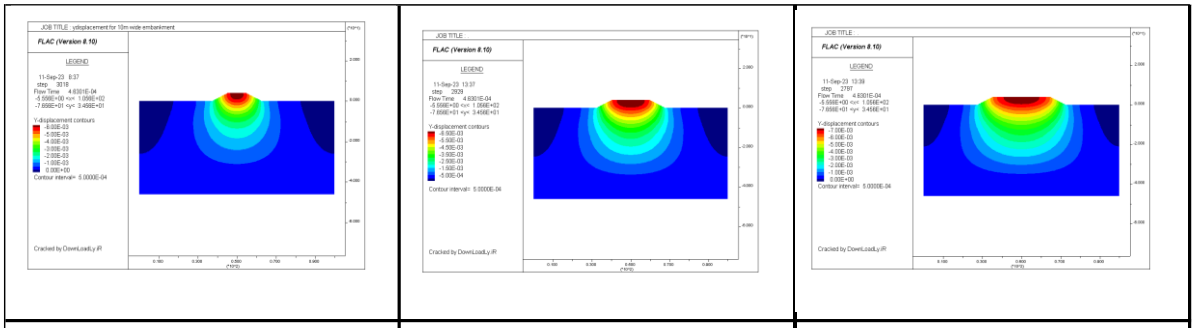

a	b	c

Fig 52: Y-displacement contour in a) MOD 7 b) MOD 8 c) MOD 9

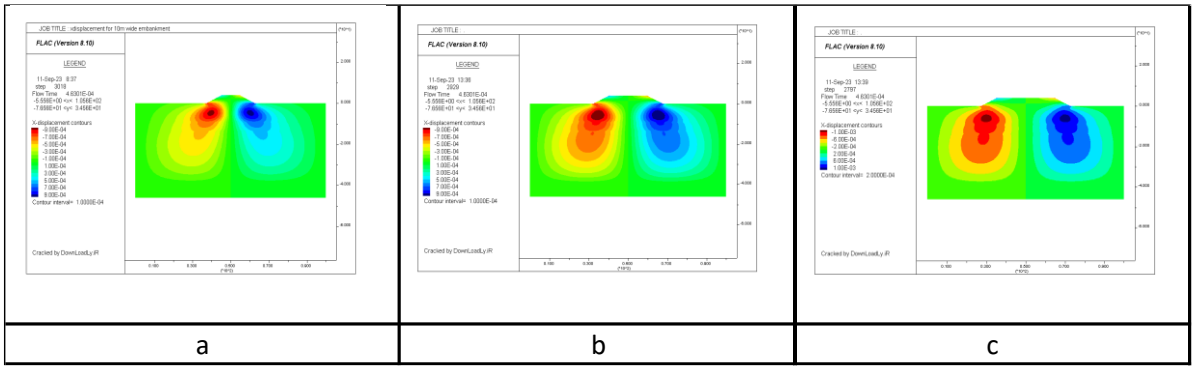

a	b	c

Fig 53: X-displacement contour in a) MOD 7 b) MOD 8 c) MOD 9

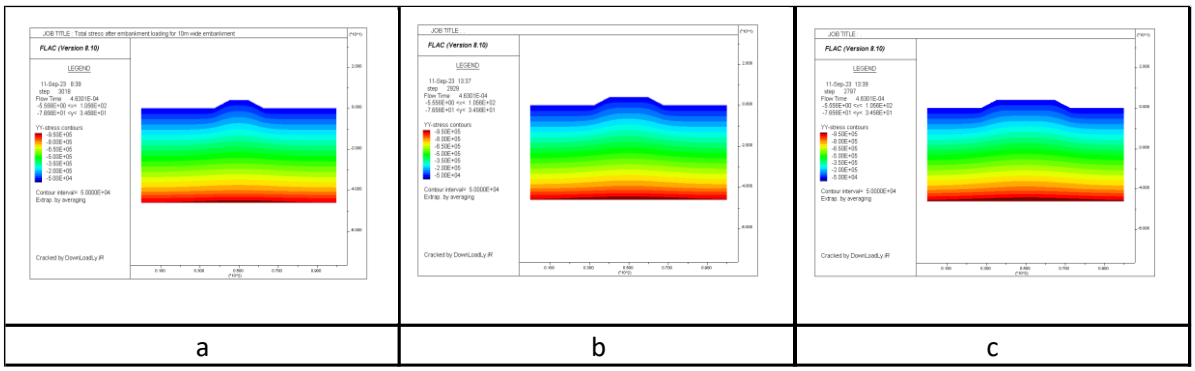

a	b	c

Fig 54: Total Vertical Stress contour in a) MOD 7 b) MOD 8 c) MOD 9

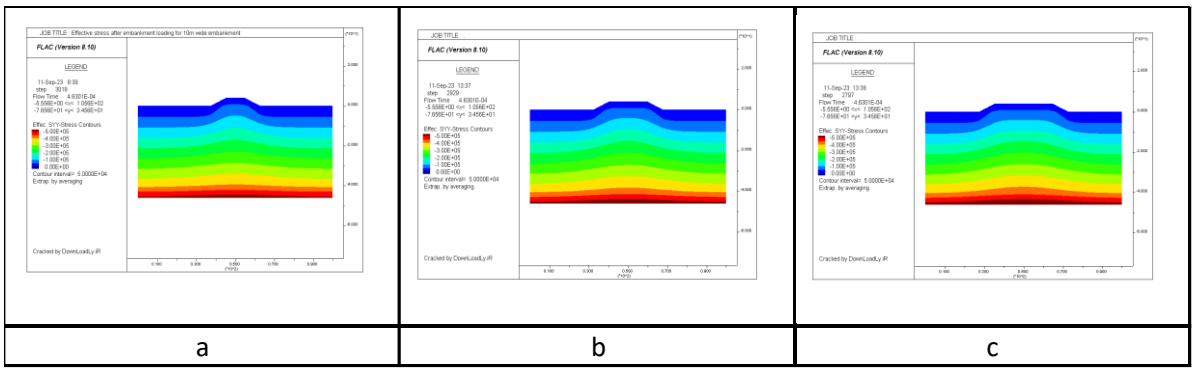

a	b	c

Fig 55: Effective Vertical Stress contour in a) MOD 7 b) MOD 8 c) MOD 9

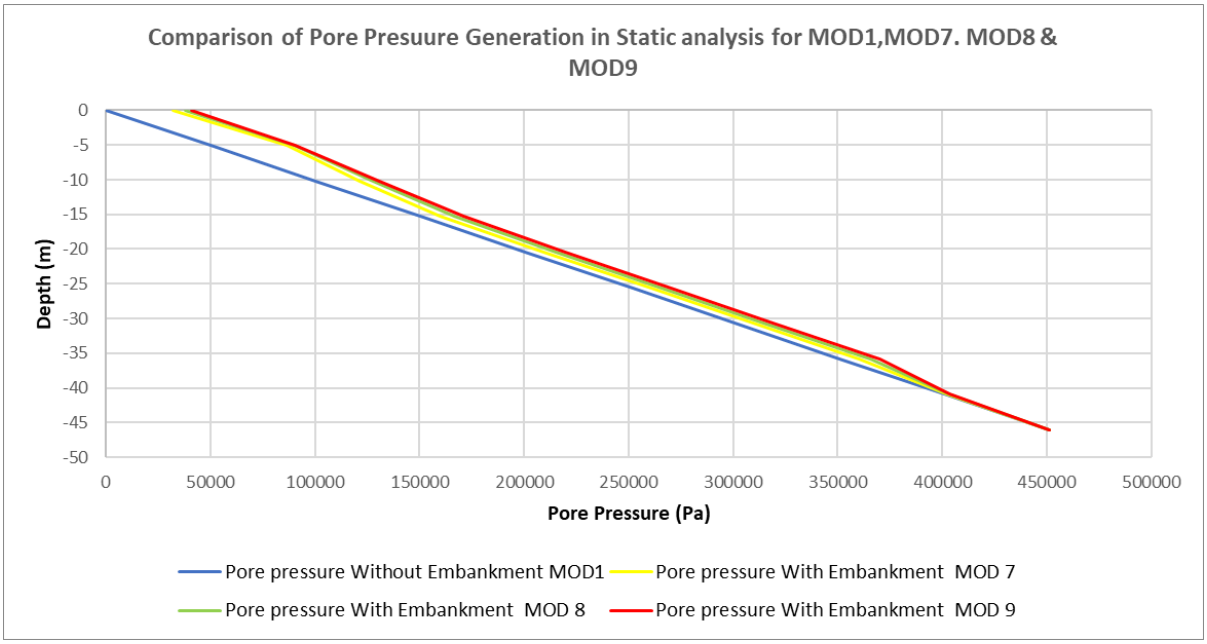

Fig 56: Comparison of Pore Pressure generation in MOD1, MOD7, MOD8 and MOD9

4.1.3 Static analysis of soil strata with Liquefiable layer height variation

In this study we have varied the Height of Liquefiable layers. Changing the height won't affect the pore pressure generation in static analyses but have major impacts in pore pressure generation under dynamic analyses. For static analyses the major difference will be in the Total and effective vertical stress of the model. The same has been presented for the Model MOD10, MOD11 and MOD 12 below.

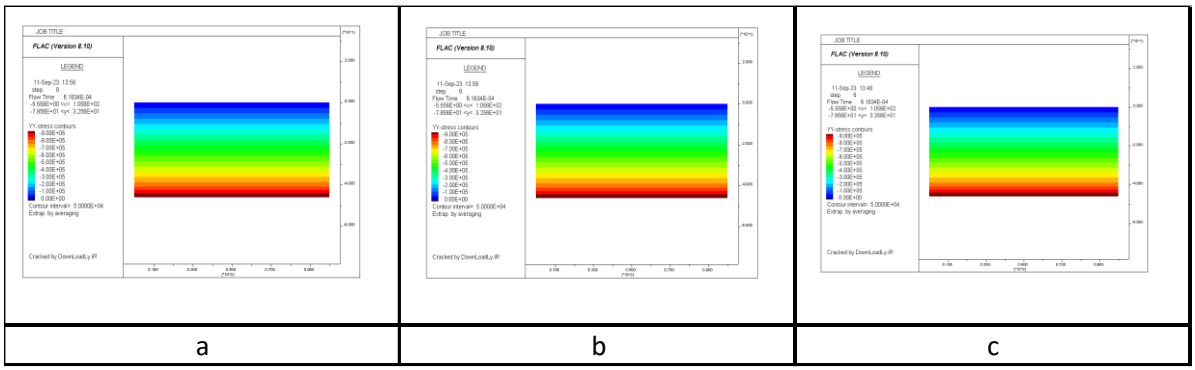

Fig 57: Total Vertical Stress contour in a) MOD 10 b) MOD 11 c) MOD 12

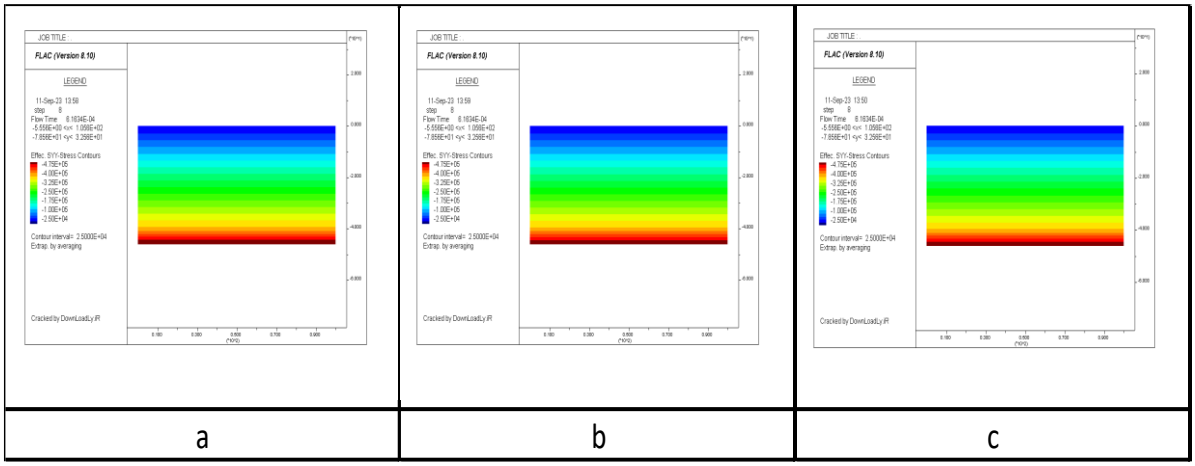

Fig 58: Effective Vertical Stress contour in a) MOD 10 b) MOD 11 c) MOD 12

4.2 Dynamic Analysis

In This chapter the model as subjected to seismic loading at the base of the model. The seismic input is applied as shear stress history at the base of the model after modifying the boundary condition of the model as discussed earlier. The material properties of the liquefiable layer are converted to the Finn model from simplistic Mohr Coulomb's model. Damping properties of the material are also updated depending on the Modulus reduction and Damping curve. The changes in the pore pressure generation and liquefaction failure of the models are checked. We have cut vertical sections in the model and provided the pore pressure variation and Pore pressure ratio variation along the depth for each model.

4.2.1 Results of Dynamic Analysis for MOD-1

MOD-1 as mentioned in Table 13 the soil strata is subjected to a scaled 0.05g PGA of Loma Prieata. The pore pressure generation pattern is also not symmetric as the one in static analysis. This indicates a change in pore pressure which is evident from Fig 59. From Fig 60 the value of maximum excess pore pressure is 13.6 Kpa, it occurs at a depth of 8mtr from the surface. From Fig 61 the Maximum pore pressure ratio of the model is of 0.365 occurs at the depth of 1.5m from surface. The range of the excess pore pressure generation and Excess pore ratio contours confirms our consideration of top two layers as liquefiable layer of soil. In Fig 62 we have provided the plot of maximum excess pore pressure generation pattern. A section has been

cut through the centre of the model as shown in the schematic diagram (Fig 63) to generate the excess pore pressure variation and excess pore pressure ratio of the model with depth as shown in Fig 64 & 65. To determine whether the amplification or de-amplification of horizontal base acceleration had occurred or not we need to determine the acceleration-time history at the top of soil strata. Figure no 66 shows us the acceleration vs time graph for the top of crest. The maximum acceleration came out is 0.73m/sec2 and it is 1.64 times of maximum peak acceleration of input acceleration at base. So, we can say amplification of base acceleration had been occurred.

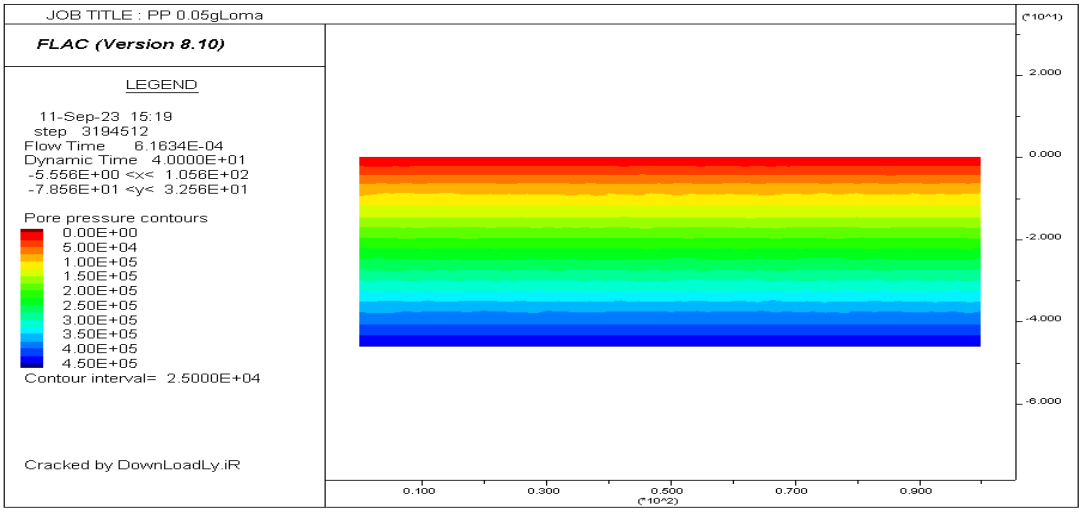

Fig 59: Pore pressure generation contour after seismic loading for MOD-1

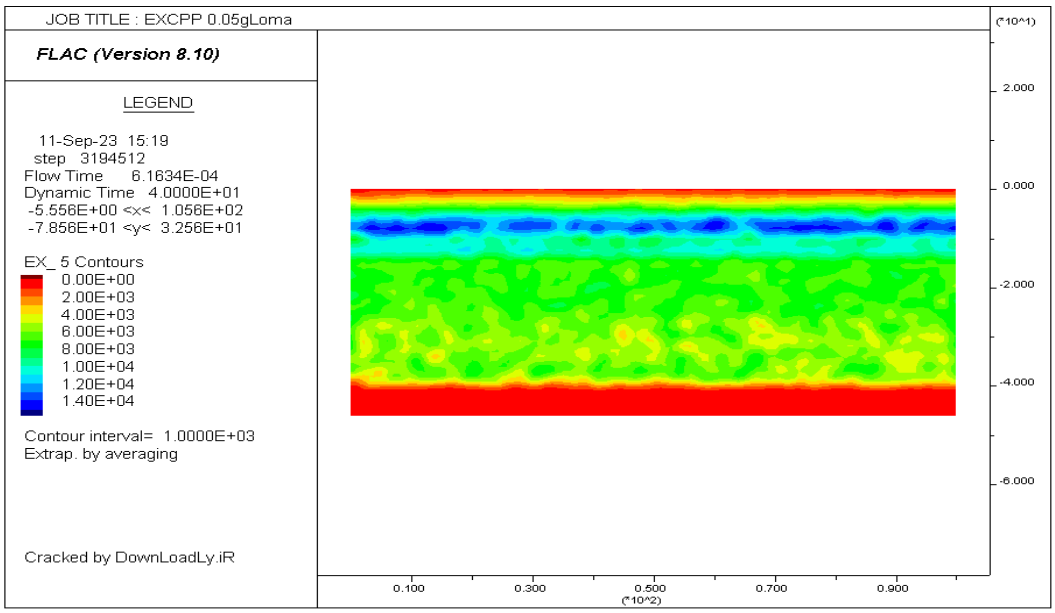

Fig 60: Excess Pore pressure generation contour after seismic loading for MOD-1

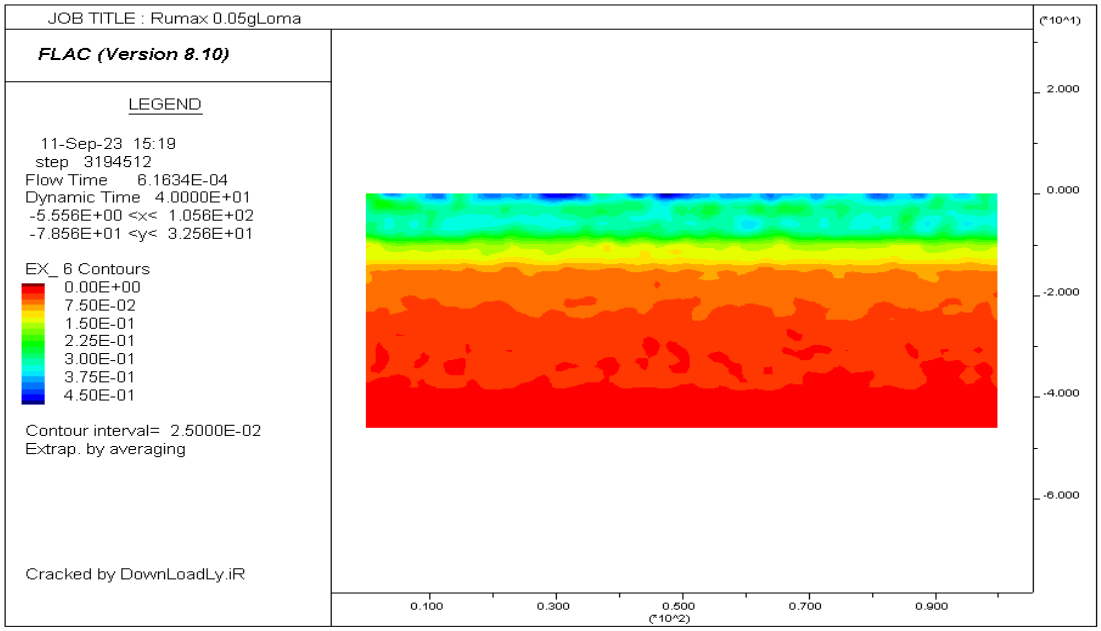

Fig 61: Maximum Pore pressure ratio contour after seismic loading for MOD-1

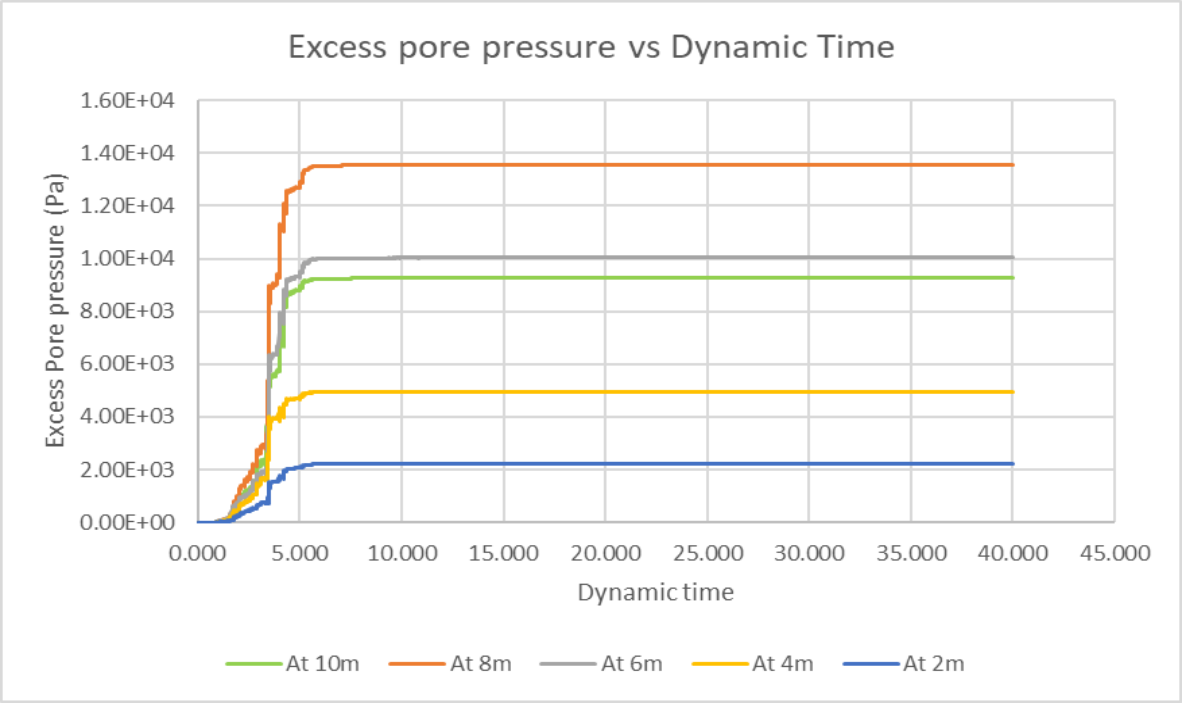

Fig 62: Excess Pore pressure generation for top 10m after seismic loading for MOD-1

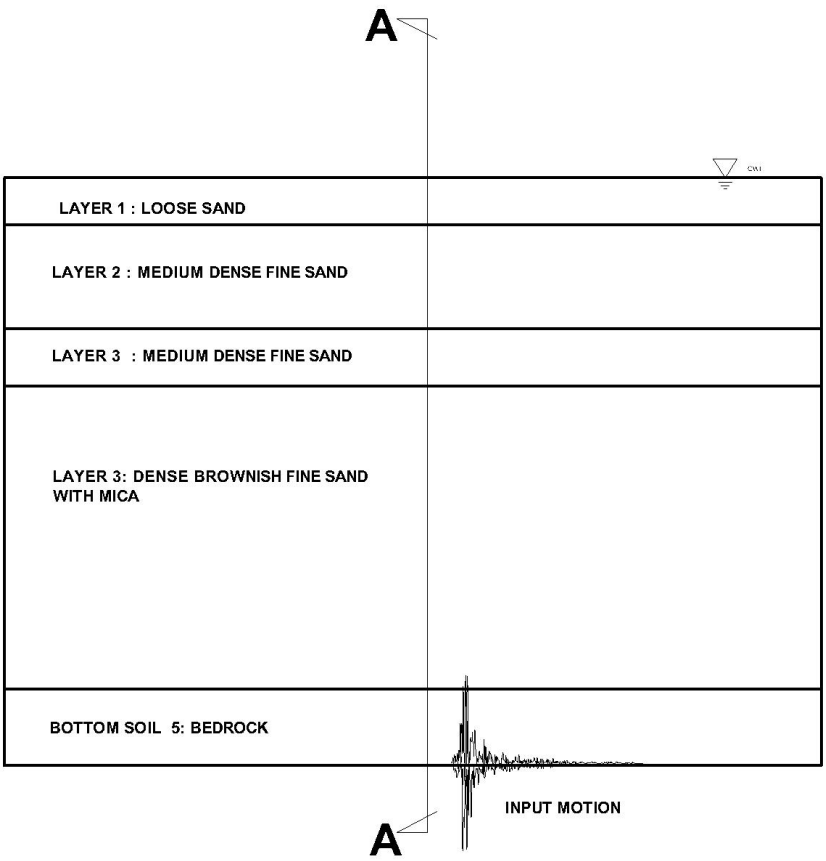

Fig 63: Schematic drawing of the model showing section A-A

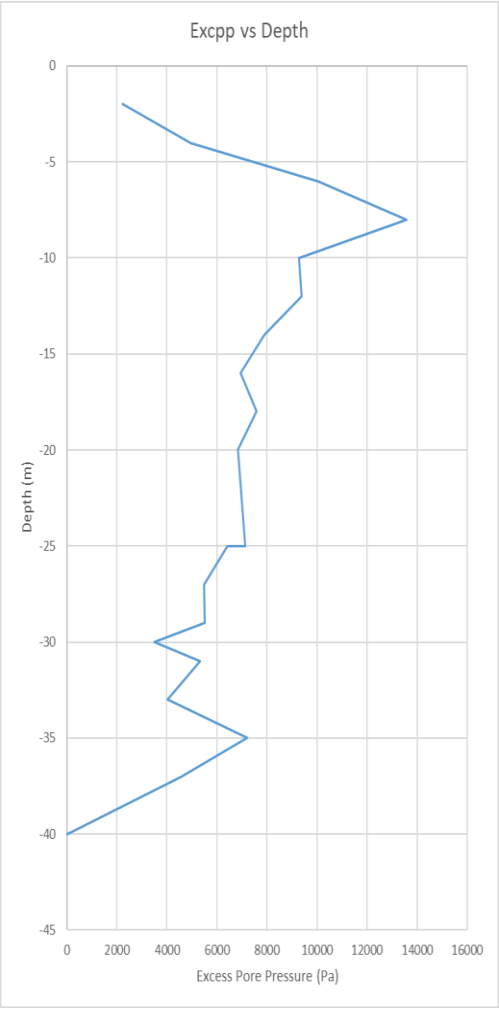

Fig 64: Excpp vs Depth at section A-A

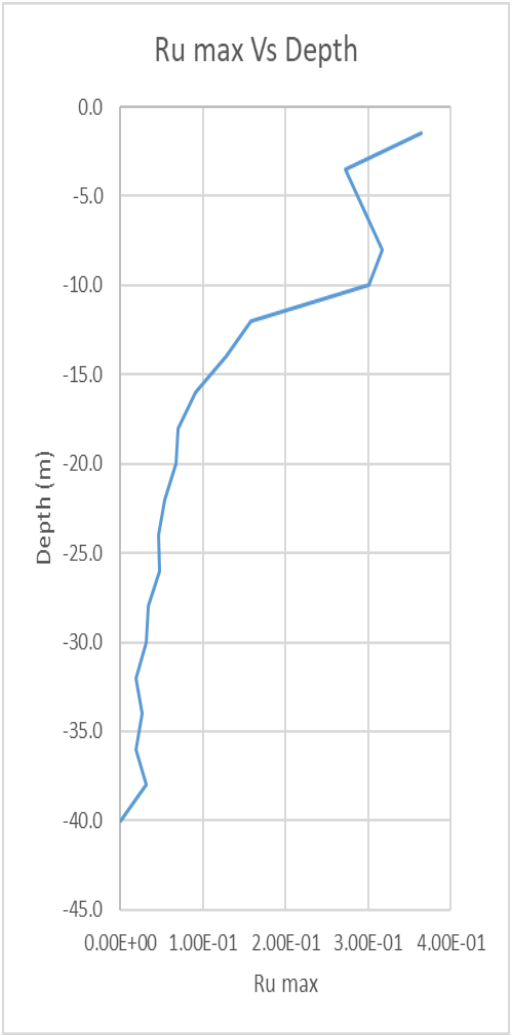

Fig 65: Ru max vs Depth at section A-A

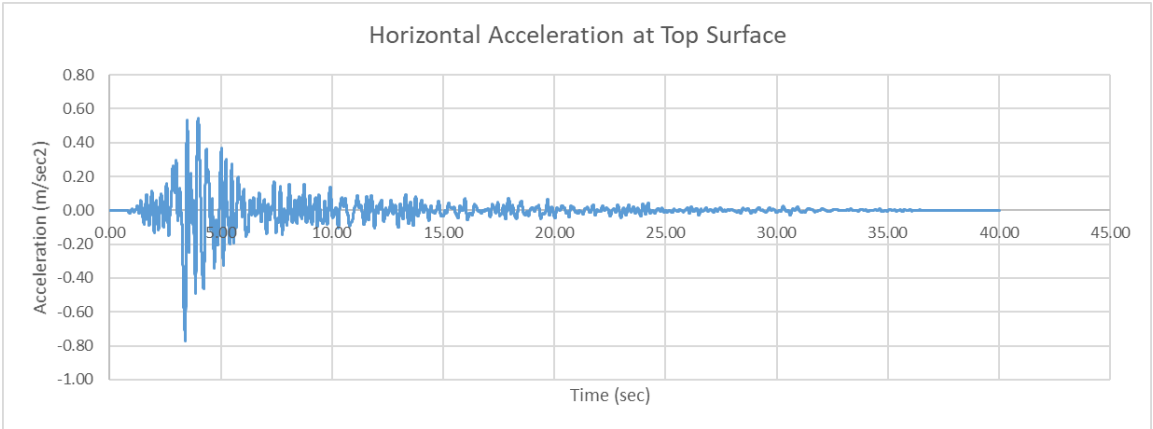

Fig 66: Horizontal acceleration at surface of model MOD-1

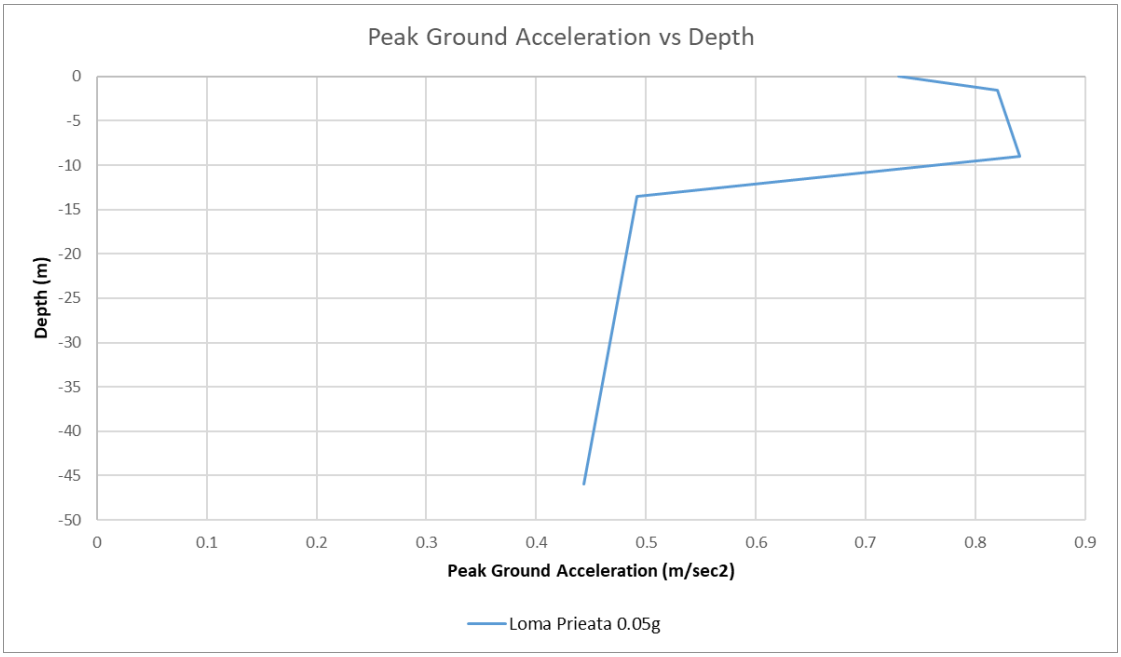

Fig 67: PGA vs Depth variation plot for model MOD-1

4.2.2 Results of Dynamic Analysis for MOD-2

MOD-2 as mentioned in Table 13 the soil strata is subjected to a scaled 0.1g PGA of Loma Prieta. From Fig 69 the value of maximum excess pore pressure is 36.2 Kpa, it occurs at a depth of 8mtr from the surface. From Fig 70 the Maximum pore pressure ratio of the model is of 1.0 (contour shows higher values) occurs at the depth of 1.5m from surface. In Fig 71 we have provided the plot of excess pore pressure generation pattern upto a depth of 10m. A section has been cut through the centre of the model as shown in the schematic diagram (Fig-65 to generate the excess pore pressure variation and excess pore pressure ratio of the model with depth as shown in Fig 72 & 73. To determine whether the amplification or de-amplification of horizontal base acceleration had occurred or not we need to determine the acceleration-time history at the top of soil strata. Fig 74 shows us the acceleration vs time graph for the top of crest. The maximum acceleration came out is 1.25m/sec2 and it is 1.4 times of maximum peak acceleration of input acceleration at base. So, we can say amplification of base acceleration had been occurred.

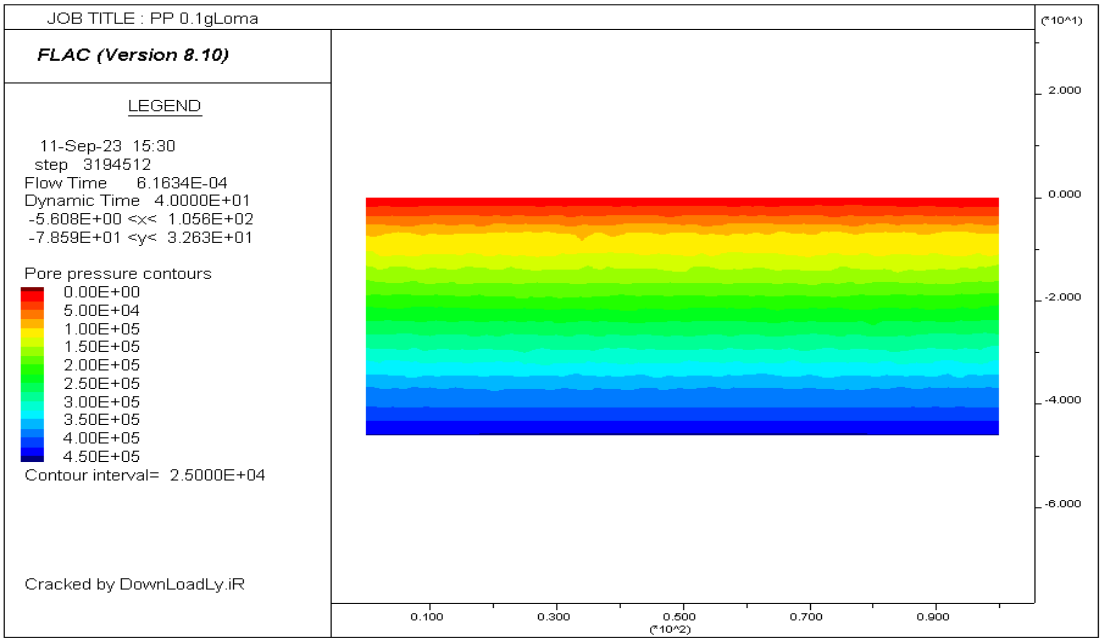

Fig 68: Pore pressure generation contour after seismic loading for MOD-2

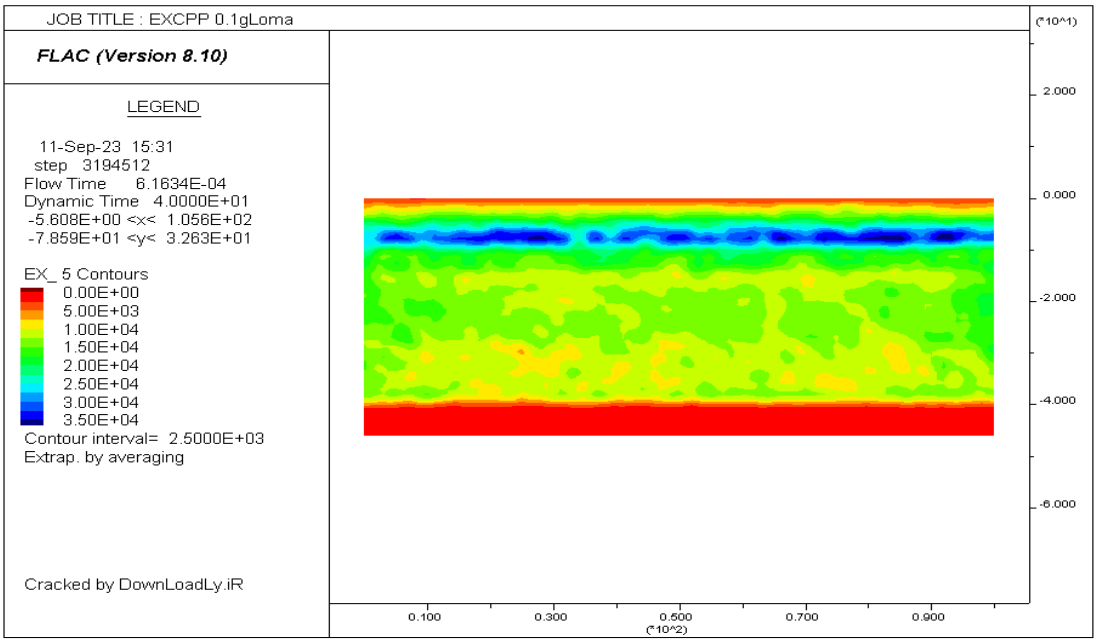

Fig 69: Excess Pore pressure generation contour after seismic loading for MOD-2

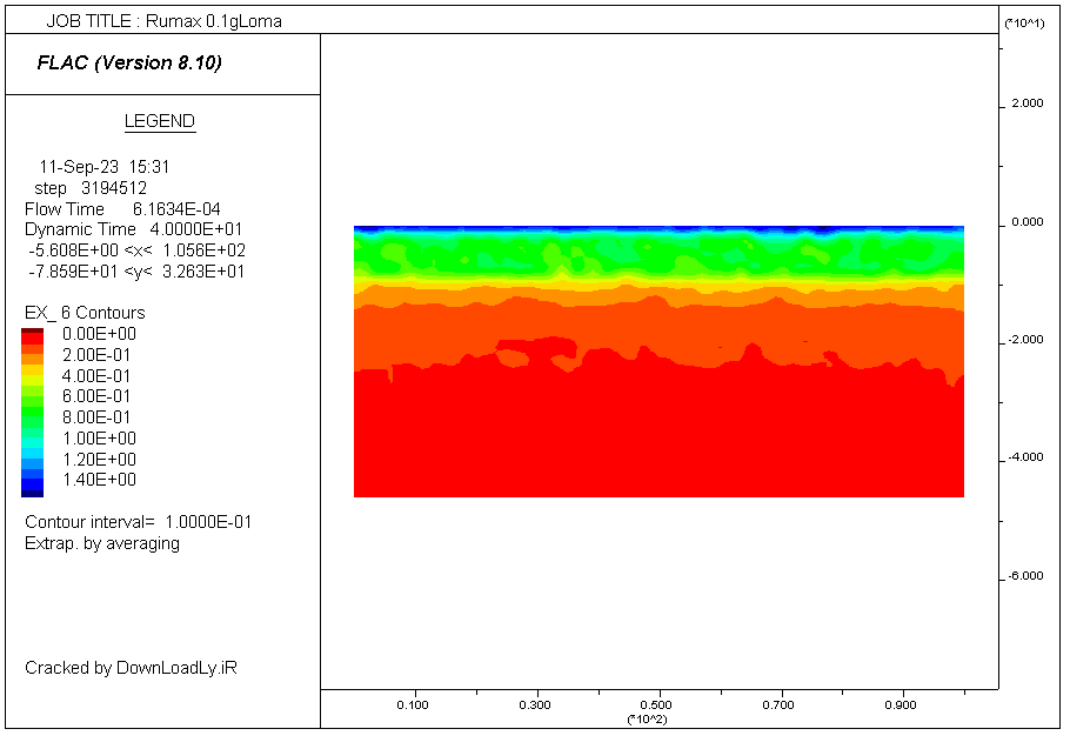

Fig 70: Pore pressure Ratio contour after seismic loading for MOD-2

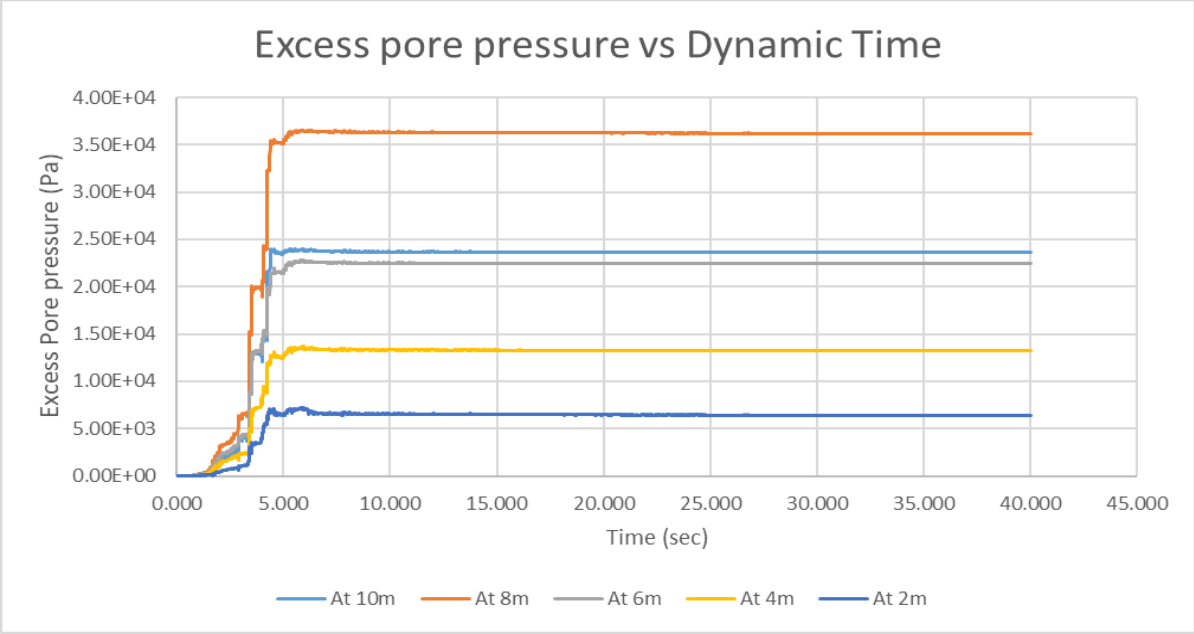

Fig 71: Excess Pore pressure generation for top 10m after seismic loading for MOD-1

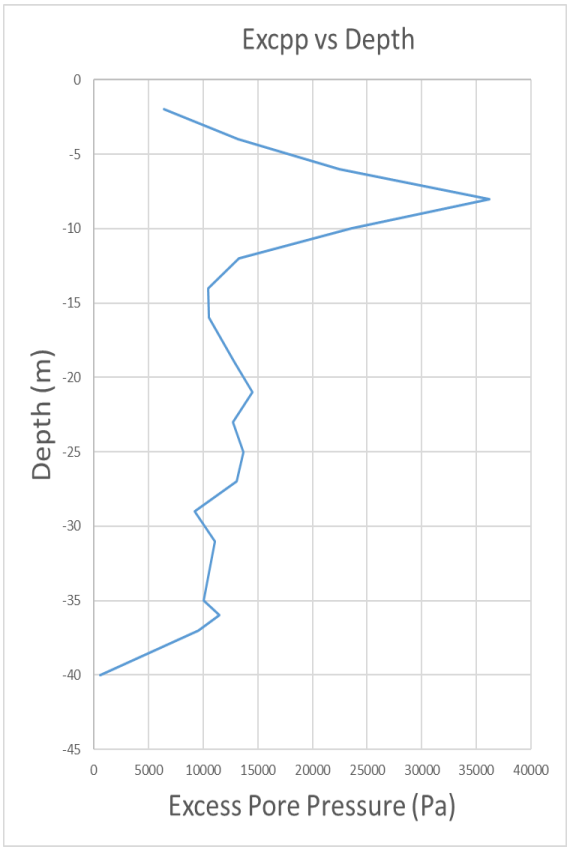

Fig 72: Excpp vs Depth at section A-A

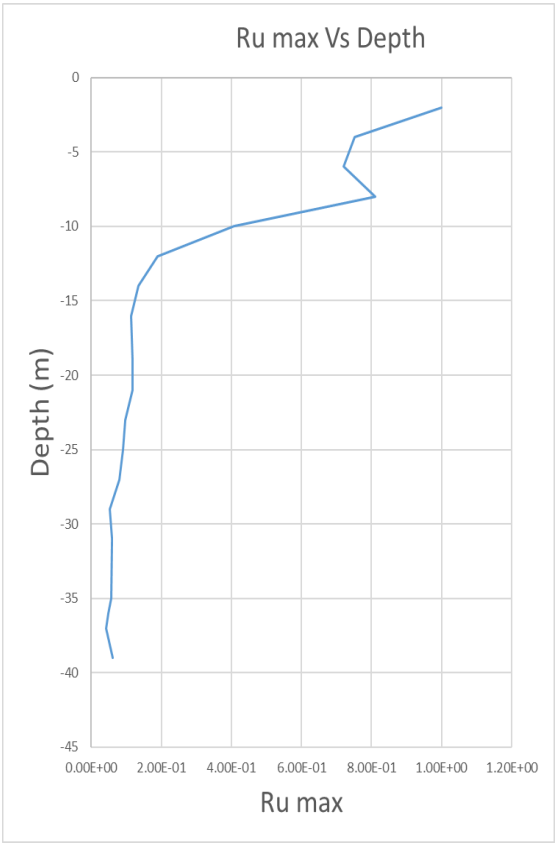

Fig 73: Ru max vs Depth at section A-A

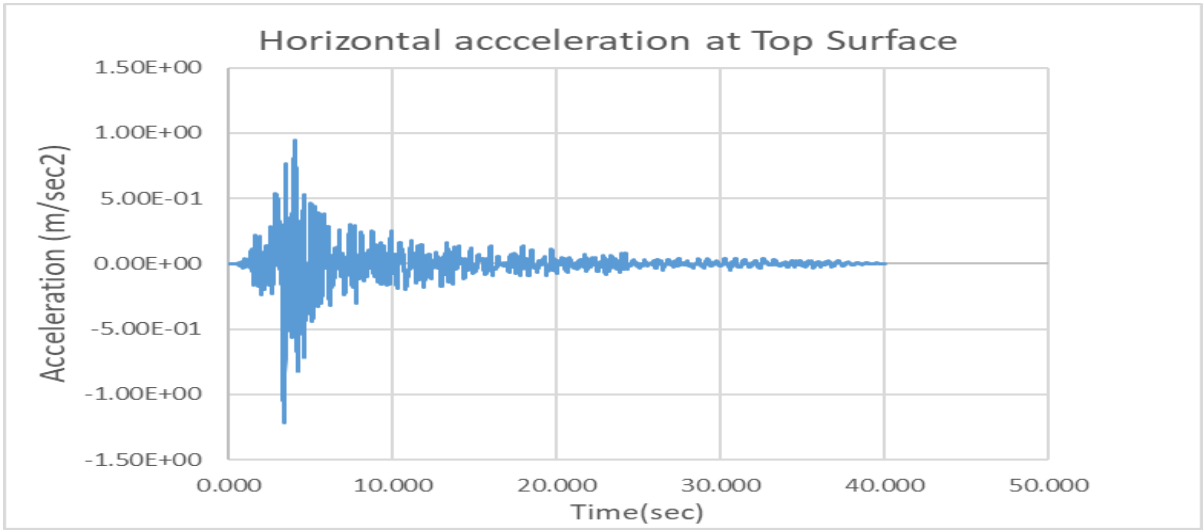

Fig 74: Horizontal acceleration at surface of model MOD-2

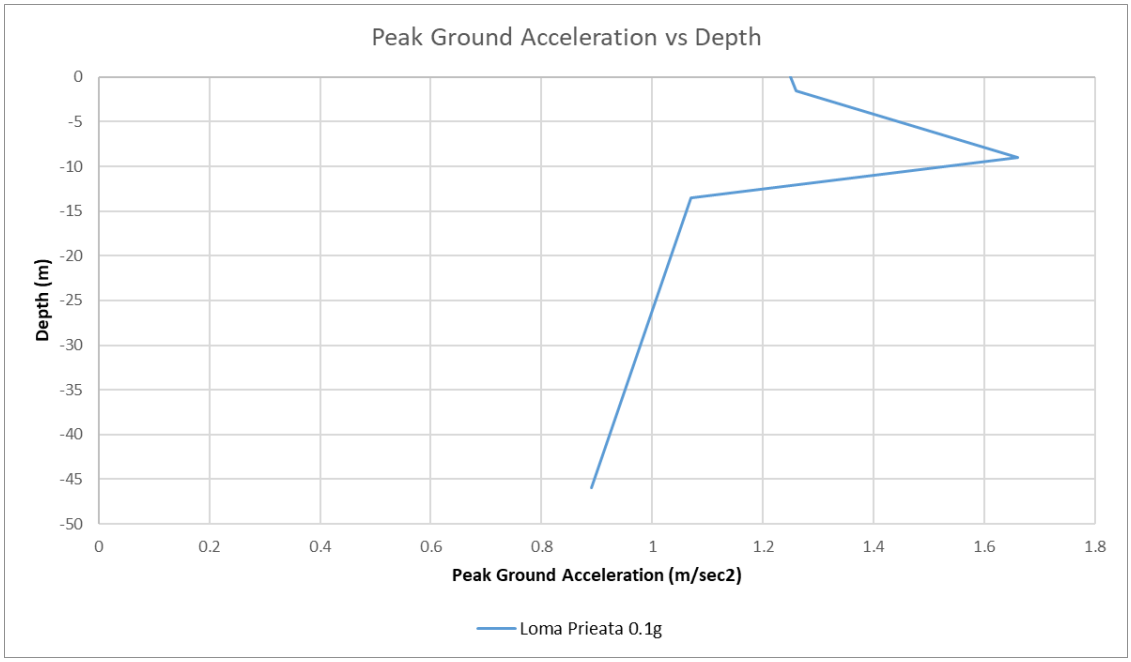

Fig 75: PGA vs Depth variation plot for model MOD-2

4.2.3 Results of Dynamic Analysis for MOD-3

MOD-3 as mentioned in Table 13 the soil strata is subjected to a scaled 0.2g PGA of Loma Prieata. From Fig 77 the value of maximum excess pore pressure is 66.4 Kpa, it occurs at a depth of 8mtr from the surface. From Fig 78 the Maximum pore pressure ratio of the model is of 1.0 and it starts at the depth of 1.5m from surface and continued till 8m depth. In Fig 79 we have provided the plot of maximum excess pore pressure generation pattern upto a depth of 10m. A section has been cut through the centre of the model as shown in the schematic diagram (Fig-65) to generate the excess pore pressure variation and excess pore pressure ratio of the model with depth as shown in Fig 80 & 81. To determine whether the amplification or de-amplification of horizontal base acceleration had occurred or not we need to determine the acceleration-time history at the top of soil strata. Fig 82 shows us the acceleration vs time graph for the top of crest. The maximum acceleration came out is 1.9m/sec2 and it is 1.067 times of maximum peak acceleration of input acceleration at base. So, we can say de-amplification of base acceleration had been occurred.

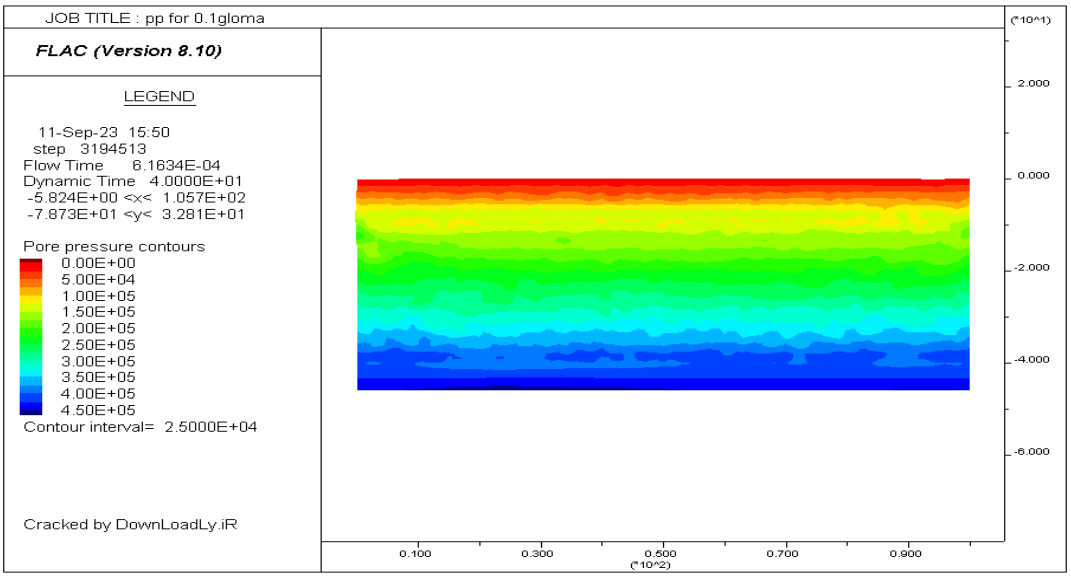

Fig 76: Pore pressure generation contour after seismic loading for MOD-3

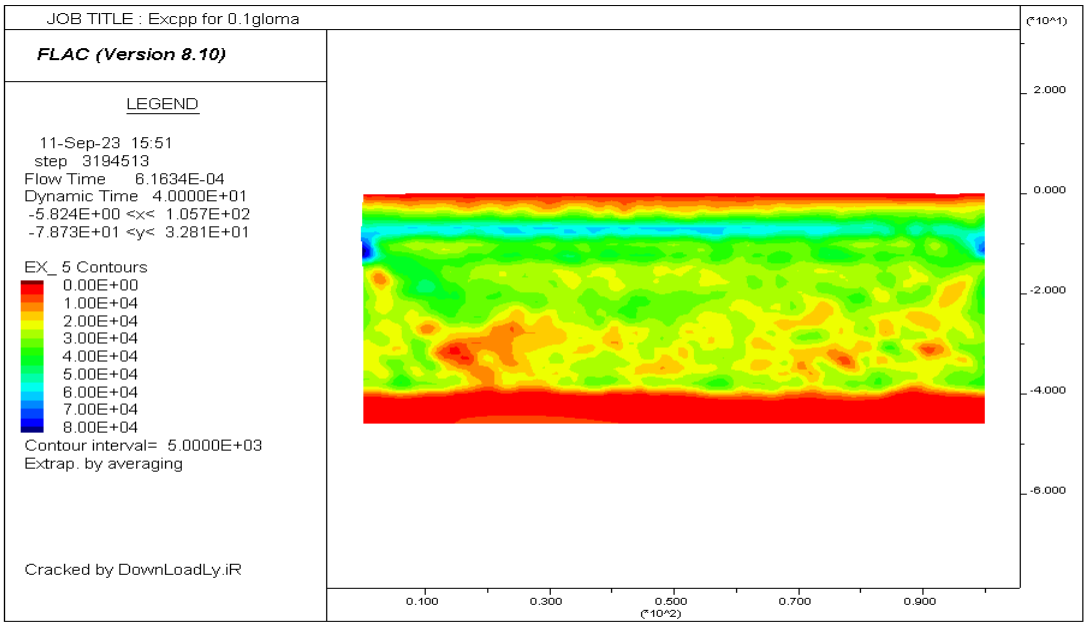

Fig 77: Excess Pore pressure generation contour after seismic loading for MOD-3

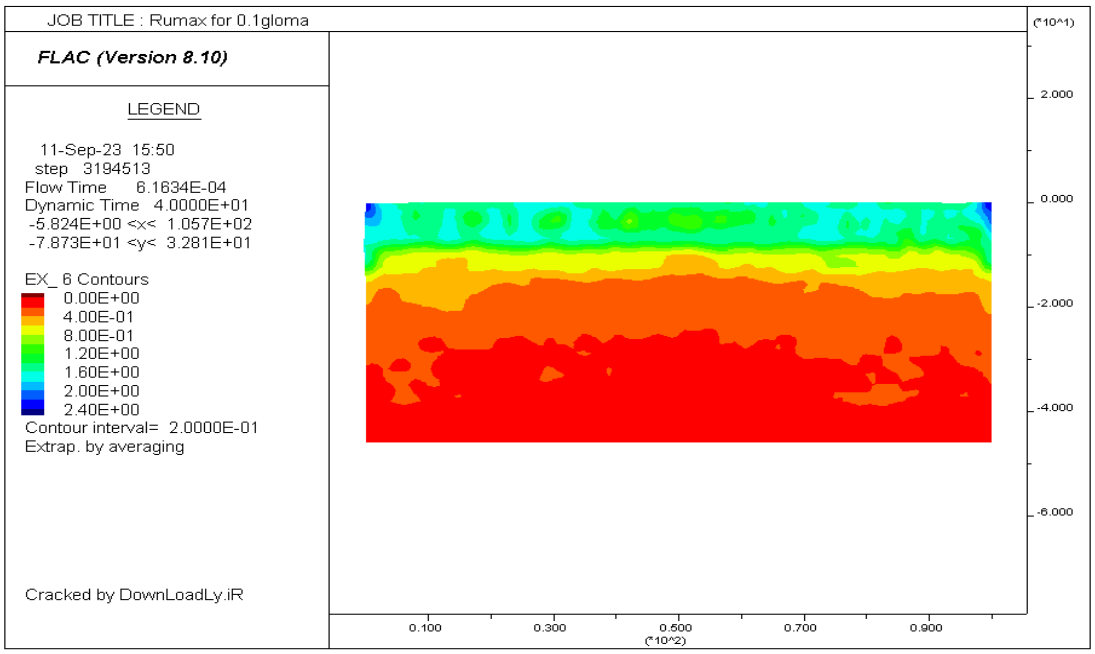

Fig 78: Pore pressure Ratio contour after seismic loading for MOD-3

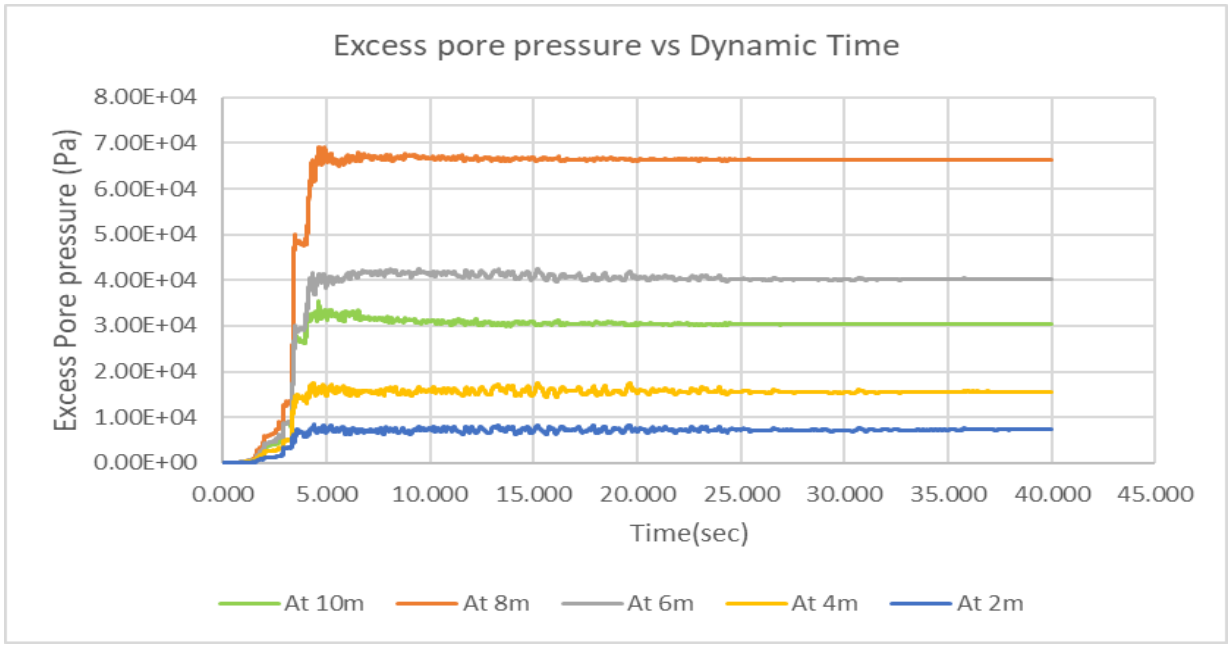

Fig 79: Excess Pore pressure generation for top 10m after seismic loading for MOD-3

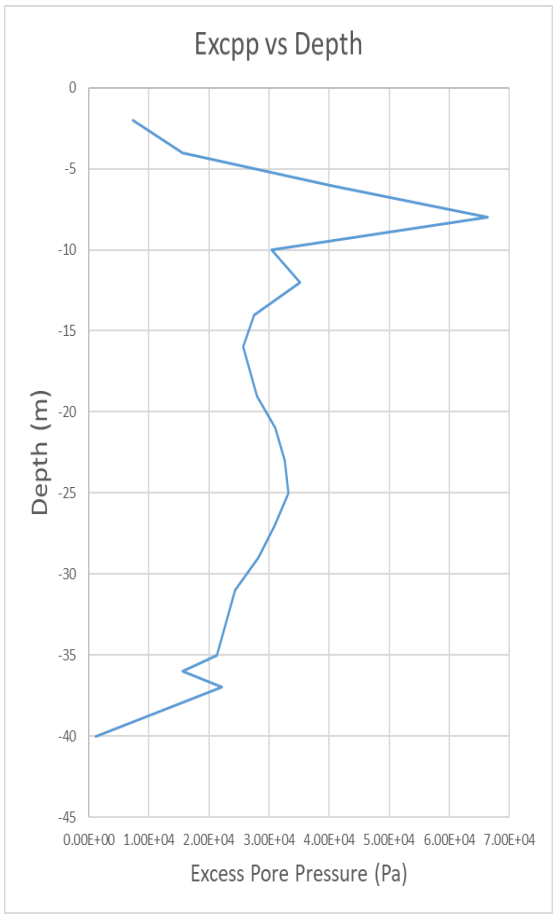

Fig 80: Excpp vs Depth at section A-A

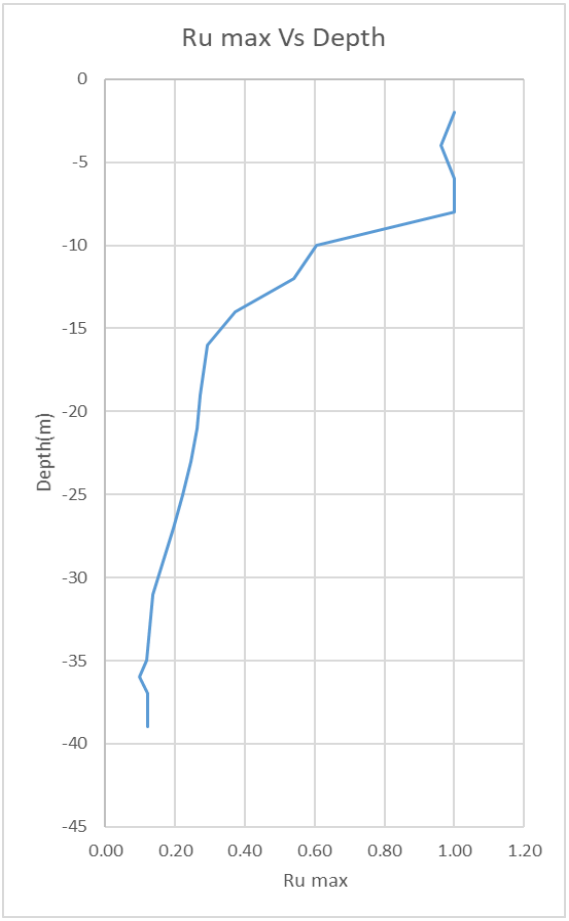

Fig 81: Ru max vs Depth at section A-A

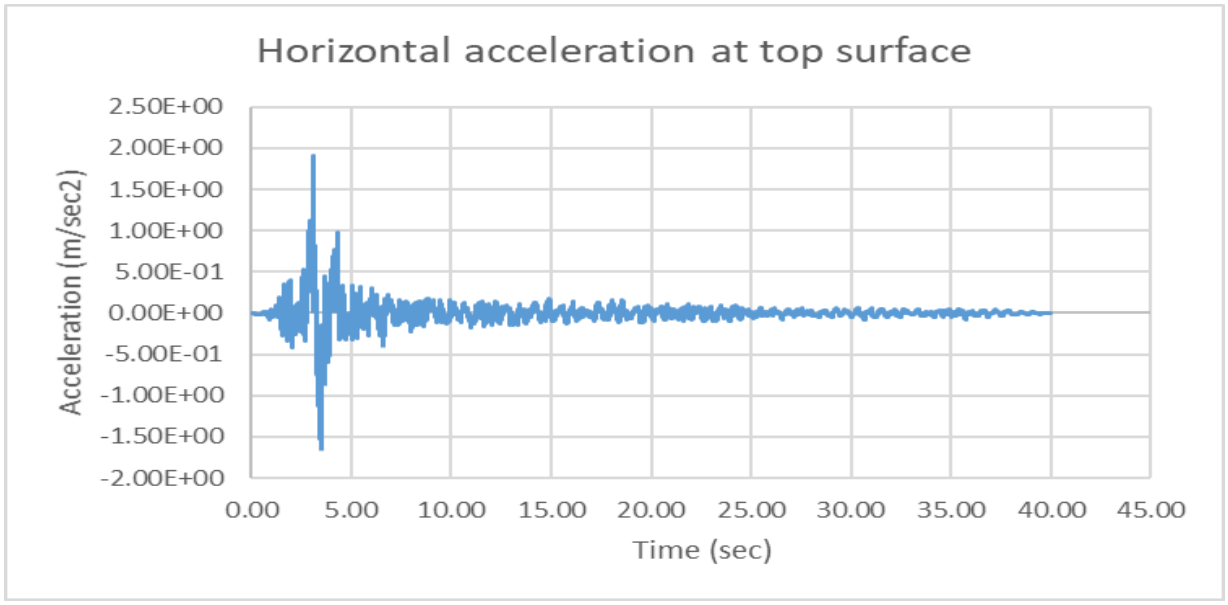

Fig 82: Horizontal acceleration at surface of model MOD-3

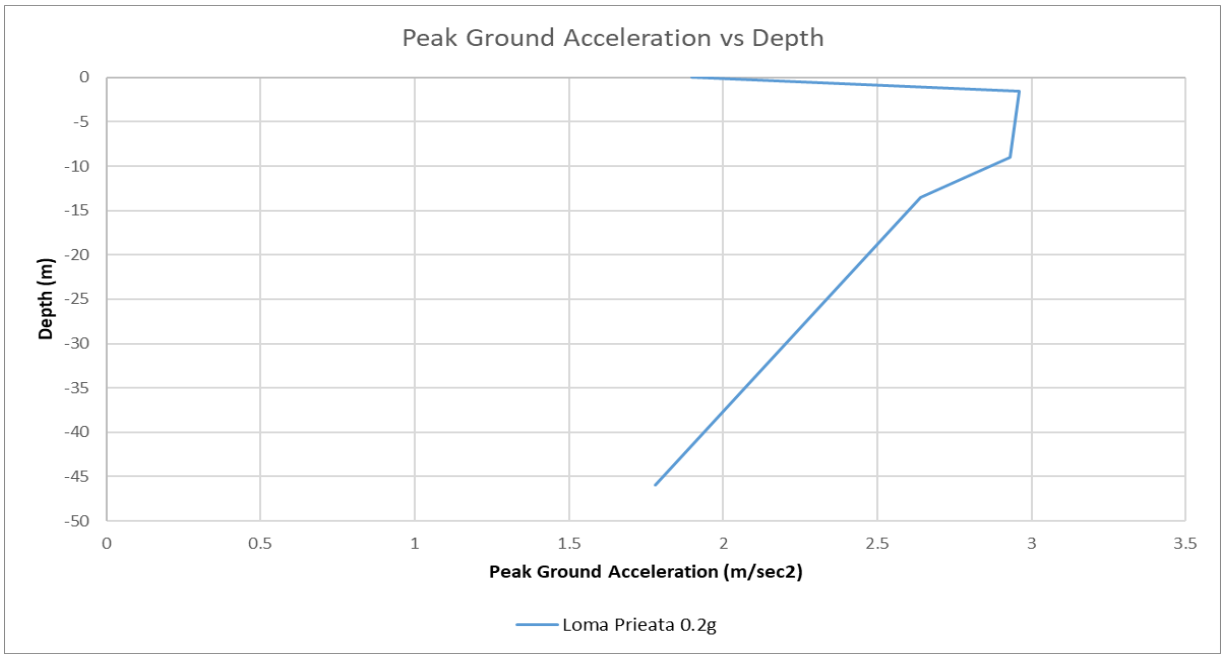

Fig 83: PGA vs Depth variation plot for model MOD-3

4.2.4 Results of Dynamic Analysis for MOD-4

MOD-4 as mentioned in Table 13 the soil strata is subjected to a scaled 0.357g PGA of Loma Prieata. From Fig 85 the value of maximum excess pore pressure is 107 Kpa, it occurs at a depth of 12mtr from the surface. From Fig 86 the Maximum pore pressure ratio of the model is of 1.0 and it starts at the depth of 1.5m from surface and extend till 12m depth. In Fig 87 we have provided the plot of maximum excess pore pressure generation pattern upto a depth of 34m. A section has been cut through the centre of the model as shown in the schematic diagram (Fig-65) to generate the excess pore pressure variation and excess pore pressure ratio of the model with depth as shown in Fig 88 & 89. To determine whether the amplification or de-amplification of horizontal base acceleration had occurred or not we need to determine the acceleration-time history at the top of soil strata. Fig 90 shows us the acceleration vs time graph for the top of crest. The maximum acceleration came out is 2.17m/sec2 and it is 0.66 times of maximum peak acceleration of input acceleration at base. So, we can say de-amplification of base acceleration had been occurred

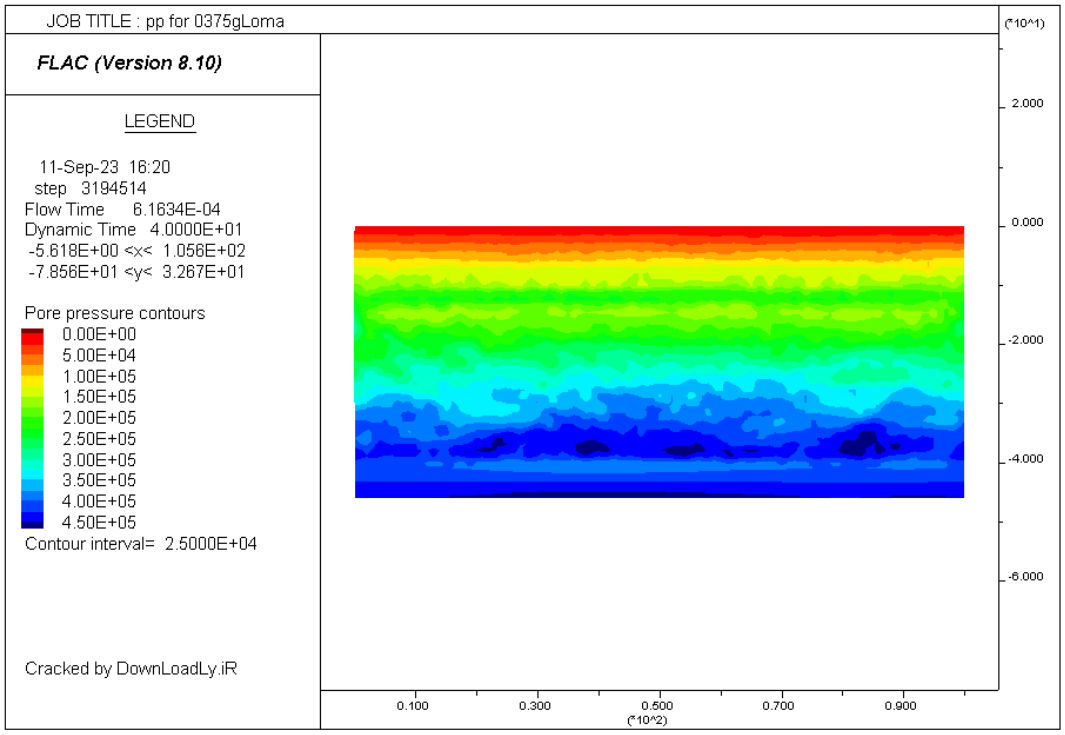

Fig 84: Pore pressure generation contour after seismic loading for MOD-4

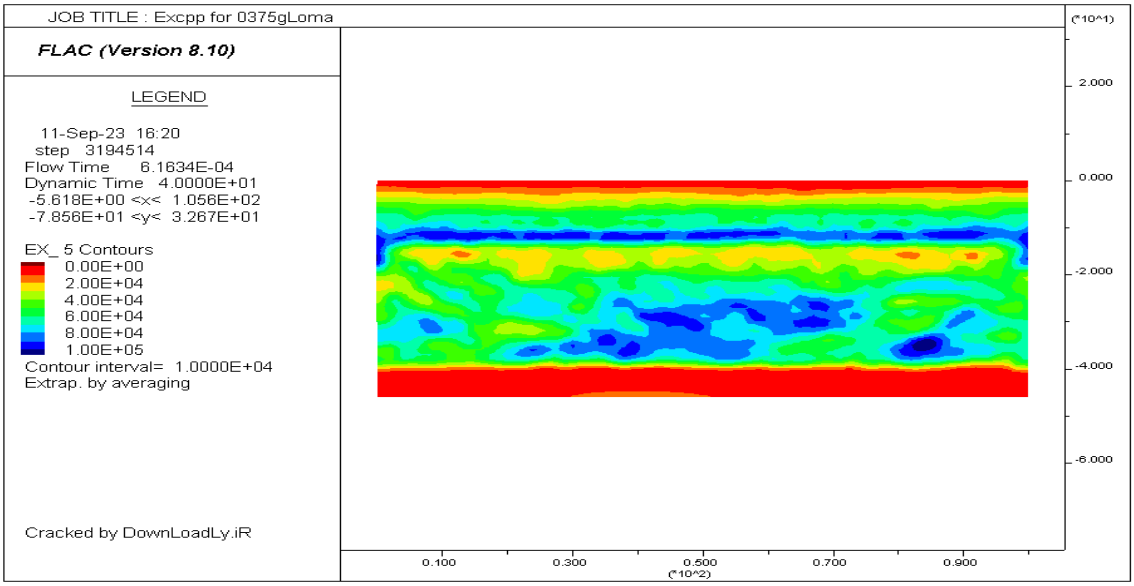

Fig 85: Excess Pore pressure generation contour after seismic loading for MOD-4

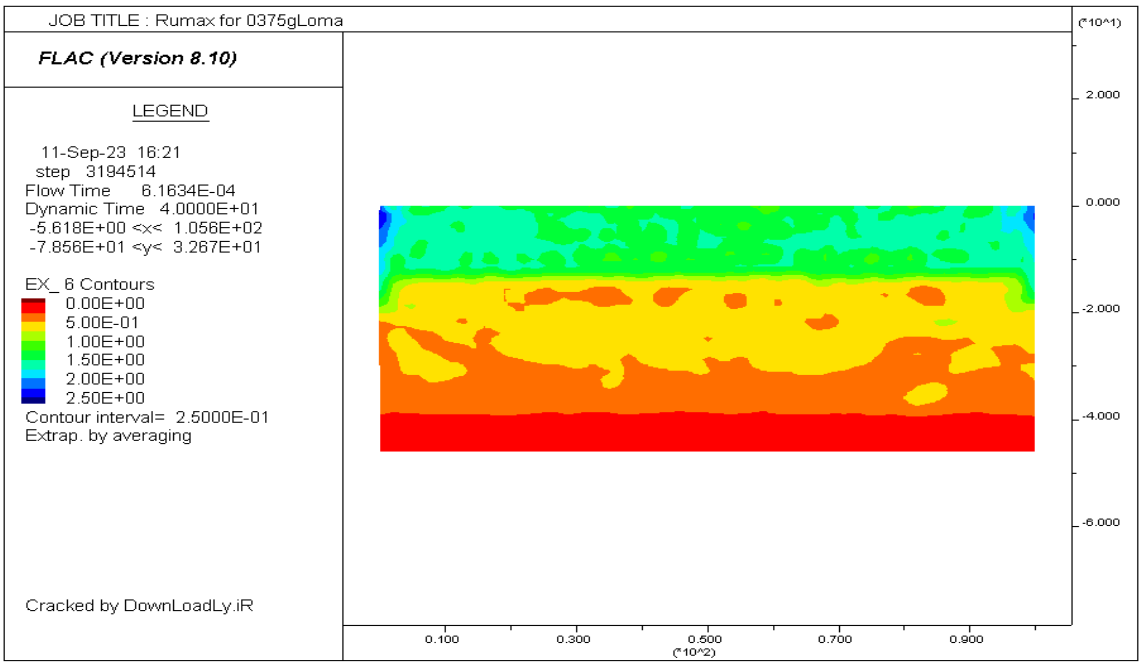

Fig 86: Pore pressure Ratio contour after seismic loading for MOD-4

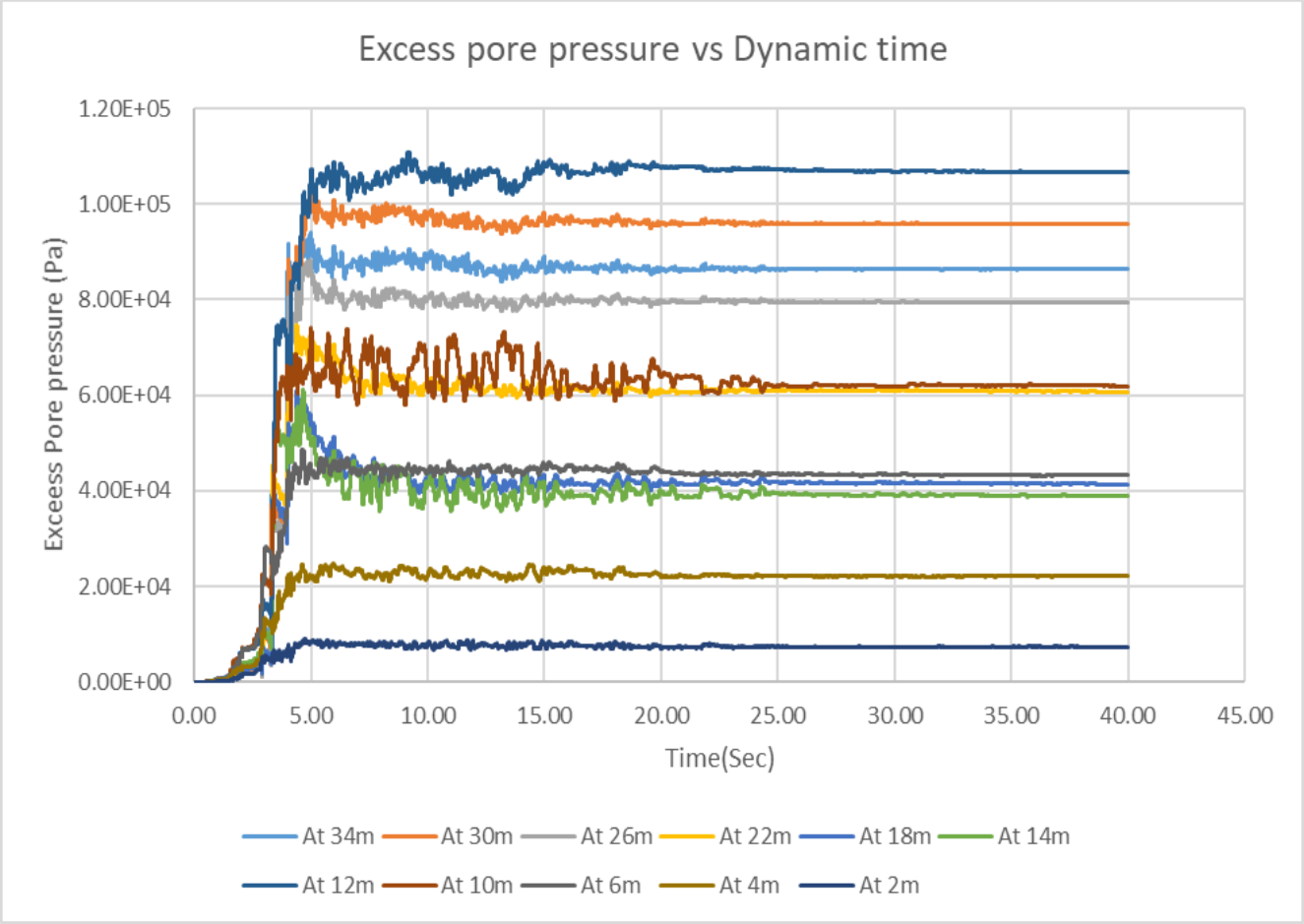

Fig 87: Excess Pore pressure generation for top 34m after seismic loading for MOD-4

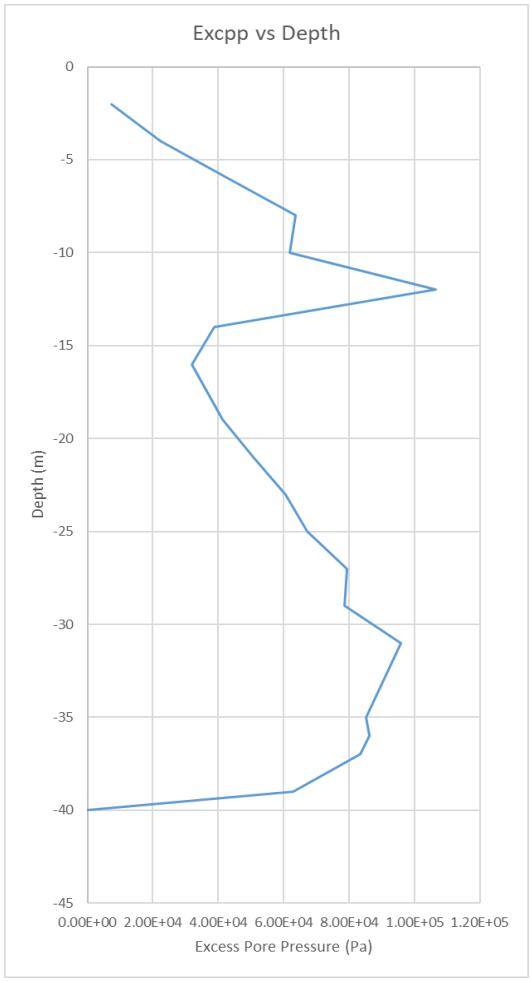

Fig 88: Excpp vs Depth at section A-A

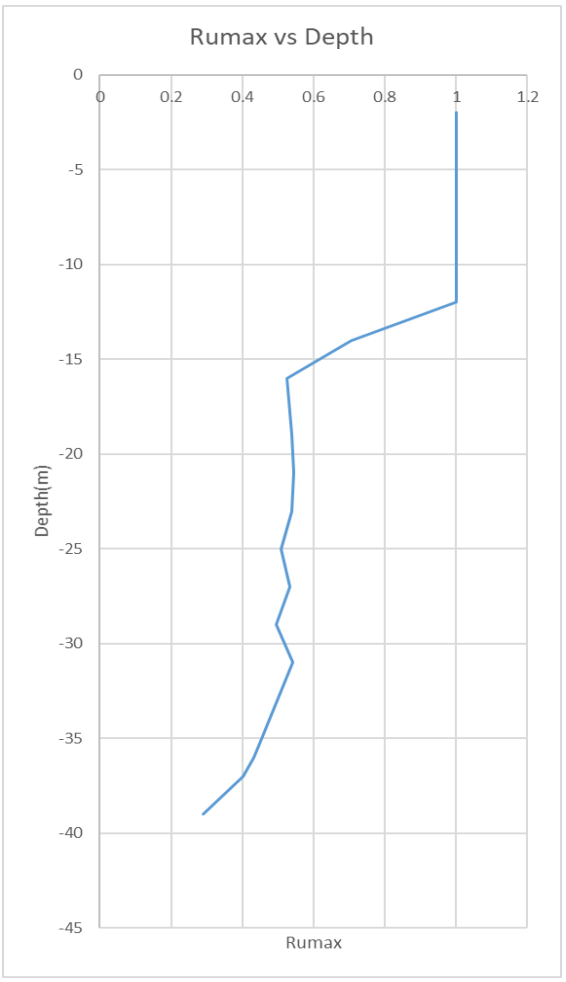

Fig 89: Ru max vs Depth at section A-A

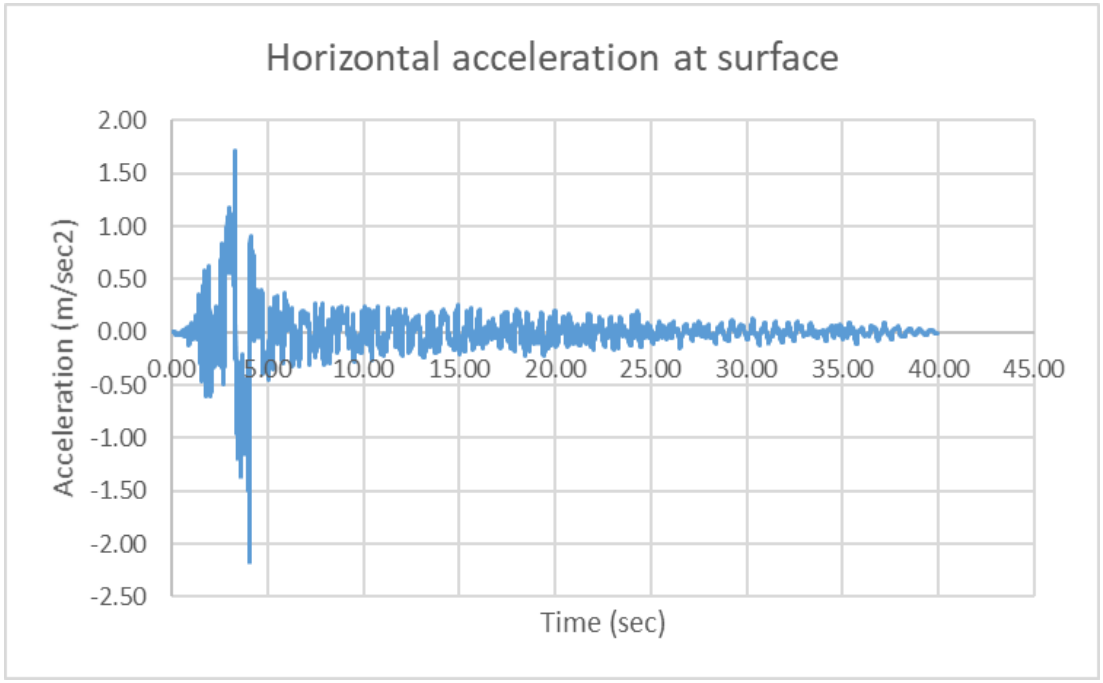

Fig90: Horizontal acceleration at surface of model MOD-4

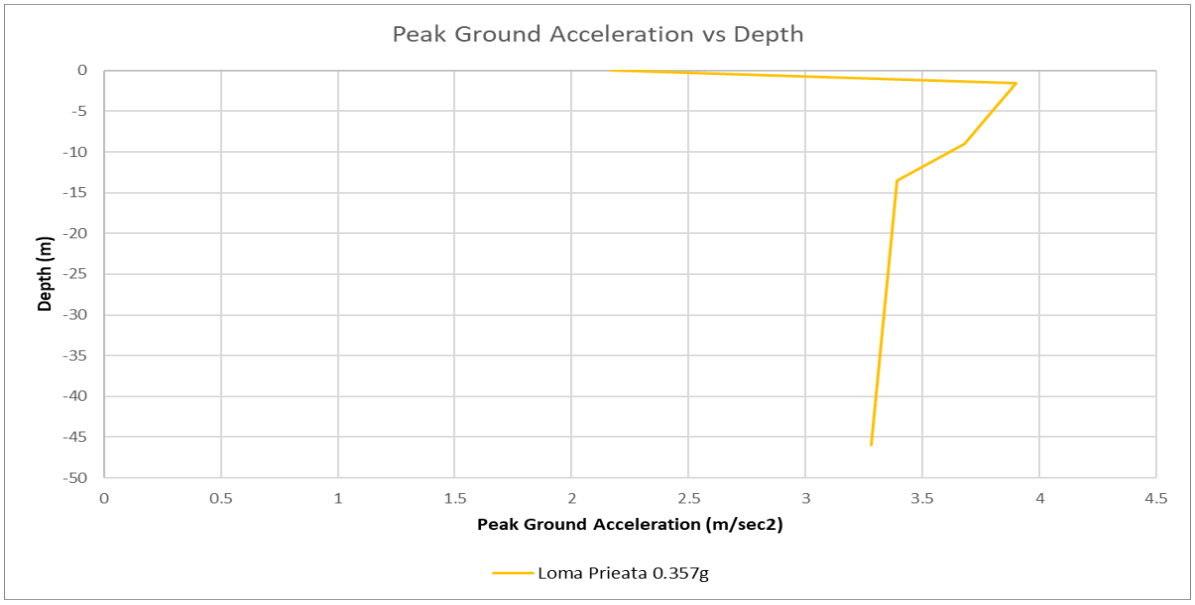

Fig 91: PGA vs Depth variation plot for model MOD-4

4.2.5 Results of Dynamic Analysis for MOD-5

MOD-5 as mentioned in Table 13 the soil strata is subjected to a scaled 0.2g PGA of Mammoth Lake. From Fig 93 the value of maximum excess pore pressure is 58 Kpa, it occurs at a depth of 8mtr from the surface. From Fig 94 the Maximum pore pressure ratio of the model is of 1.0 and it starts at the depth of 1.5m from surface and extend upto 8m depth. In Fig 95 we have provided the plot of maximum excess pore pressure generation pattern upto a depth of 18m. A section has been cut through the centre of the model as shown in the schematic diagram (Fig-65) to generate the excess pore pressure variation and excess pore pressure ratio of the model with depth as shown in Fig 96 & 97. To determine whether the amplification or de-amplification of horizontal base acceleration had occurred or not we need to determine the acceleration-time history at the top of soil strata. Fig 98 shows us the acceleration vs time graph for the top of crest. The maximum acceleration came out is 1.56m/sec2 and it is 1.11 times of maximum peak acceleration of input acceleration at base. So, we can say amplification of base acceleration had been occurred

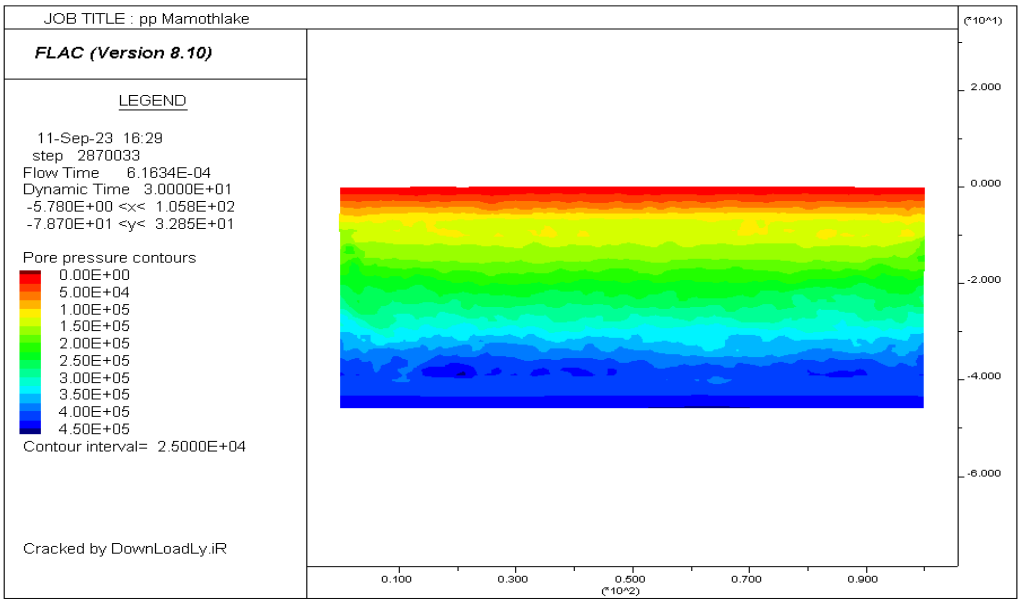

Fig 92: Pore pressure generation contour after seismic loading for MOD-5

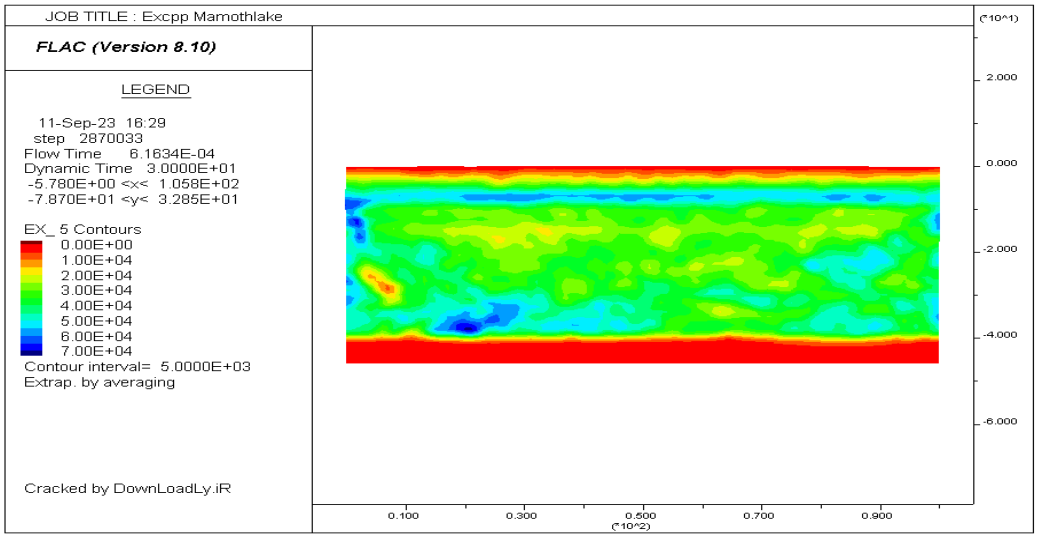

Fig 93: Excess Pore pressure generation contour after seismic loading for MOD-5

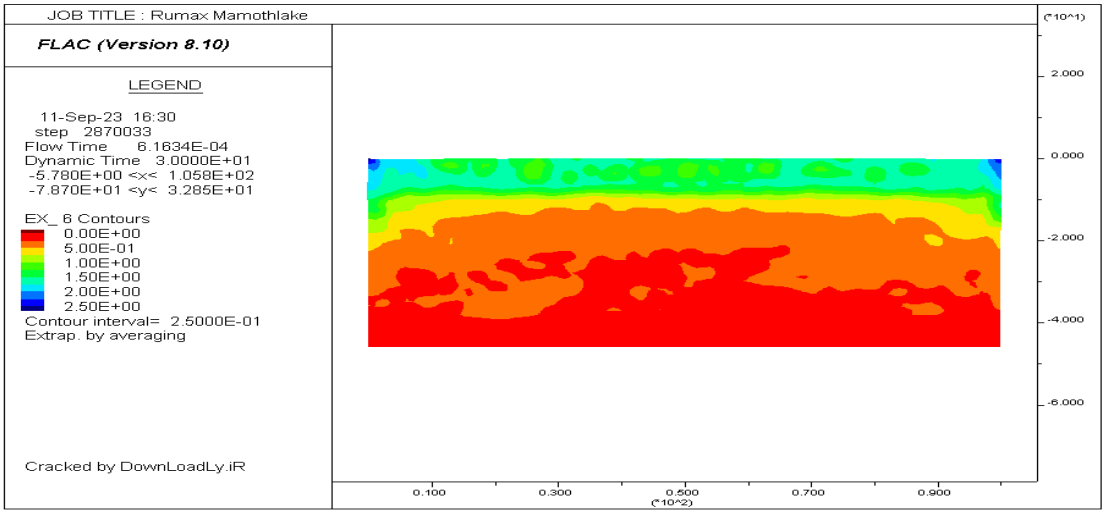

Fig 94: Pore pressure Ratio contour after seismic loading for MOD-5

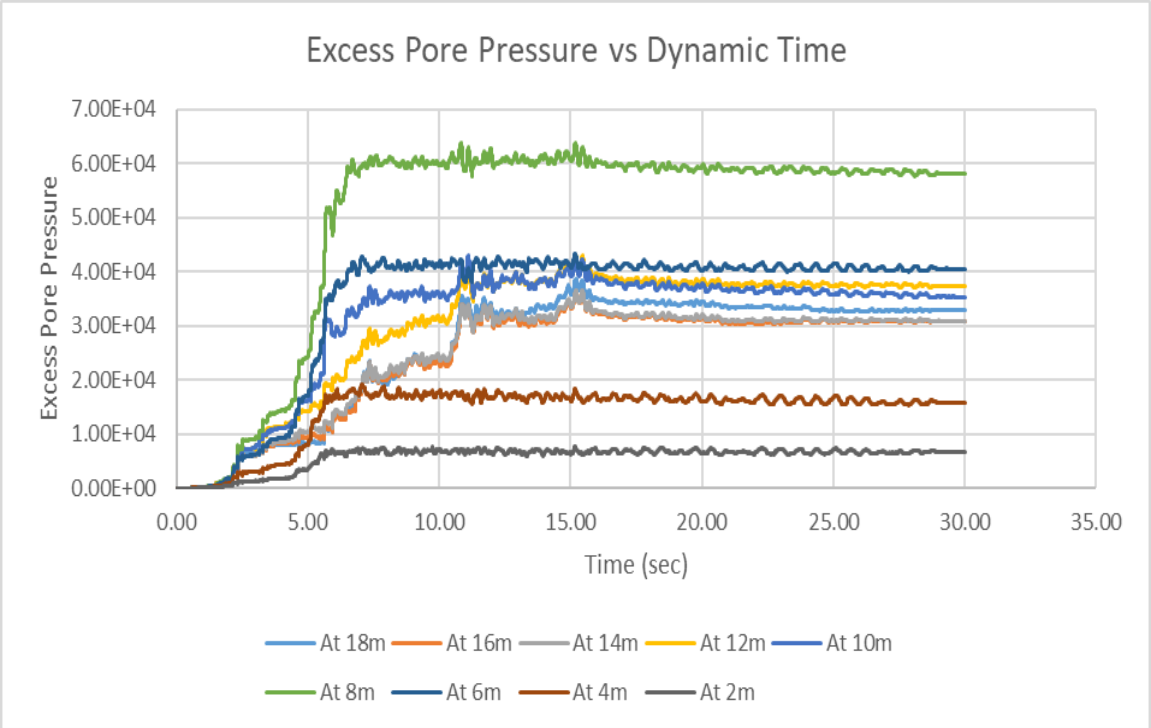

Fig 95: Excess Pore pressure generation for top 18m after seismic loading for MOD-5

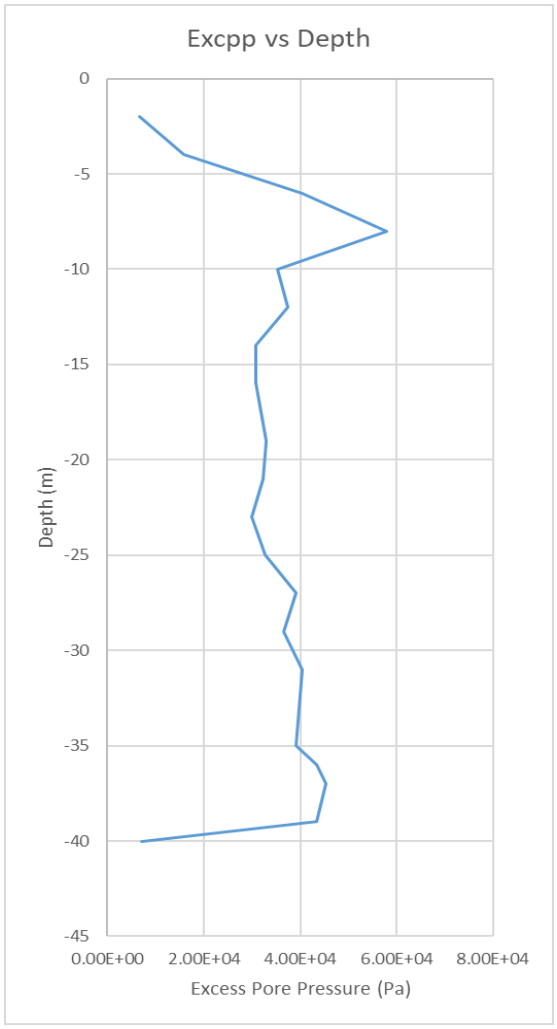

Fig 96: Excpp vs Depth at section A-A

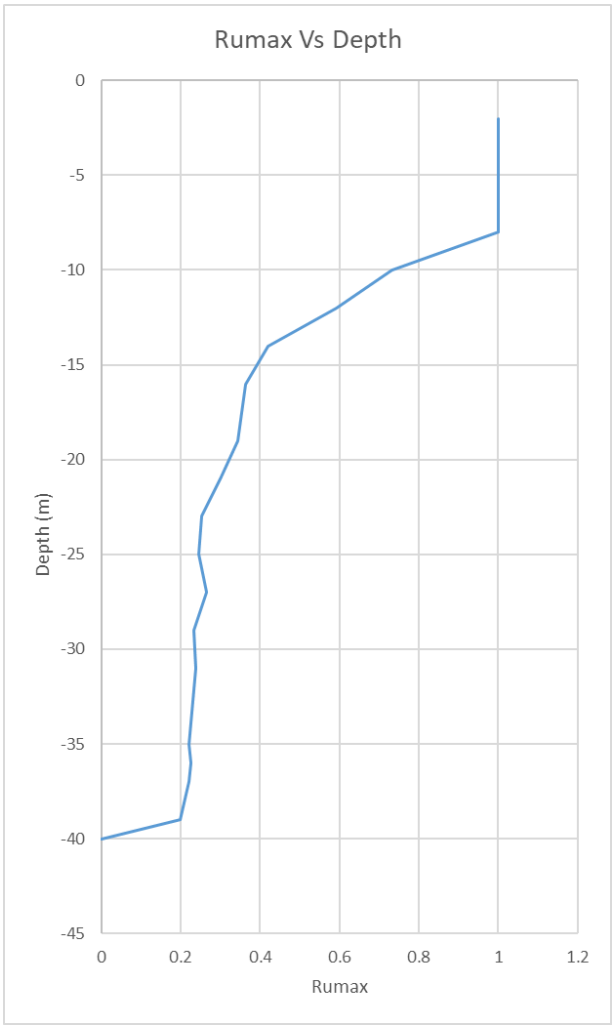

Fig 97: Ru max vs Depth at section A-A

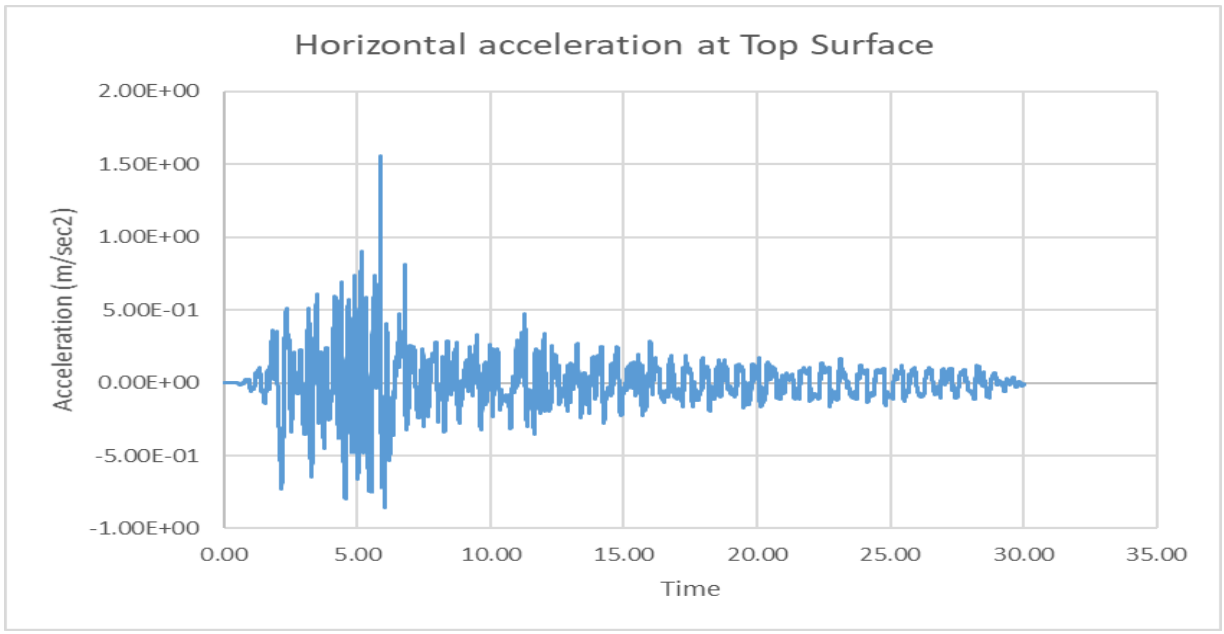

Fig 98: Horizontal acceleration at surface of model MOD-5

4.2.6 Results of Dynamic Analysis for MOD-6

MOD-6 as mentioned in Table 13 the soil strata is subjected to a scaled 0.2g PGA of North ridge From Fig 100 the value of maximum excess pore pressure is 62.7 Kpa, it occurs at a depth of 8mtr from the surface. From Fig 101 the Maximum pore pressure ratio of the model is of 1.0 and it starts at the depth of 1.5m from surface and continued till 8m depth. In Fig 102 we have provided the plot of maximum excess pore pressure generation pattern upto a depth of 12m. A section has been cut through the centre of the model as shown in the schematic diagram (Fig-65) to generate the excess pore pressure variation and excess pore pressure ratio of the model with depth as shown in Fig 103 & 104. To determine whether the amplification or de-amplification of horizontal base acceleration had occurred or not we need to determine the acceleration-time history at the top of soil strata. Fig 105 shows us the acceleration vs time graph for the top of crest. The maximum acceleration came out is 1.04m/sec2 and it is 0.5 times of maximum peak acceleration of input acceleration at base. So, we can say de-amplification of base acceleration had been occurred.

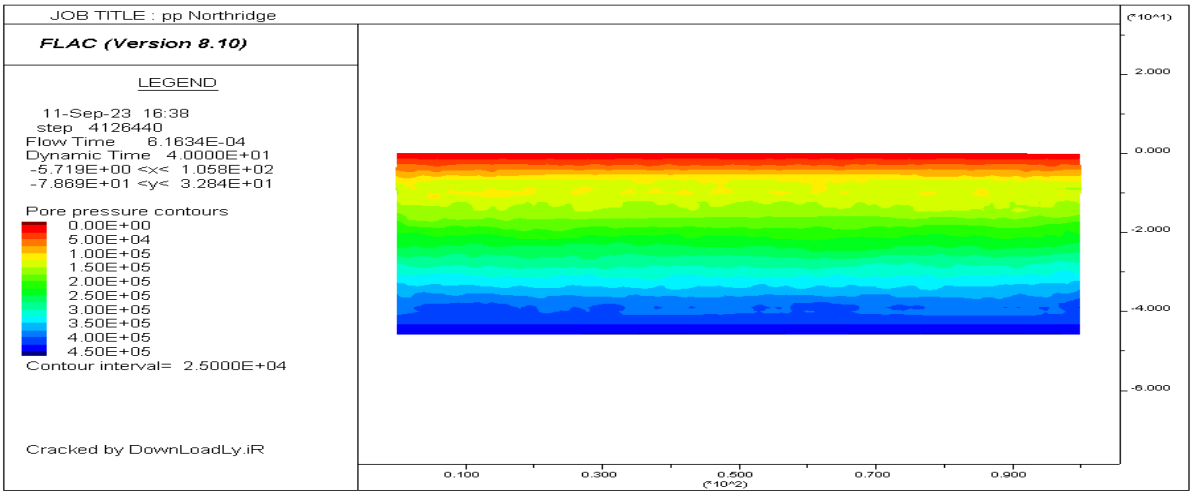

Fig 99: Pore pressure generation contour after seismic loading for MOD-6

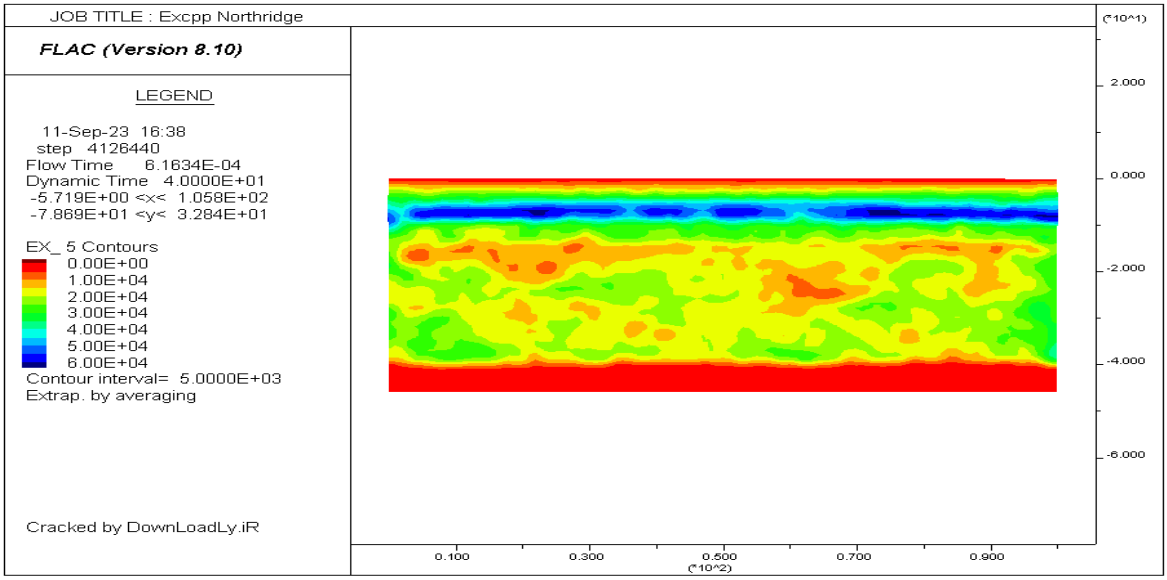

Fig 100: Excess Pore pressure generation contour after seismic loading for MOD-6

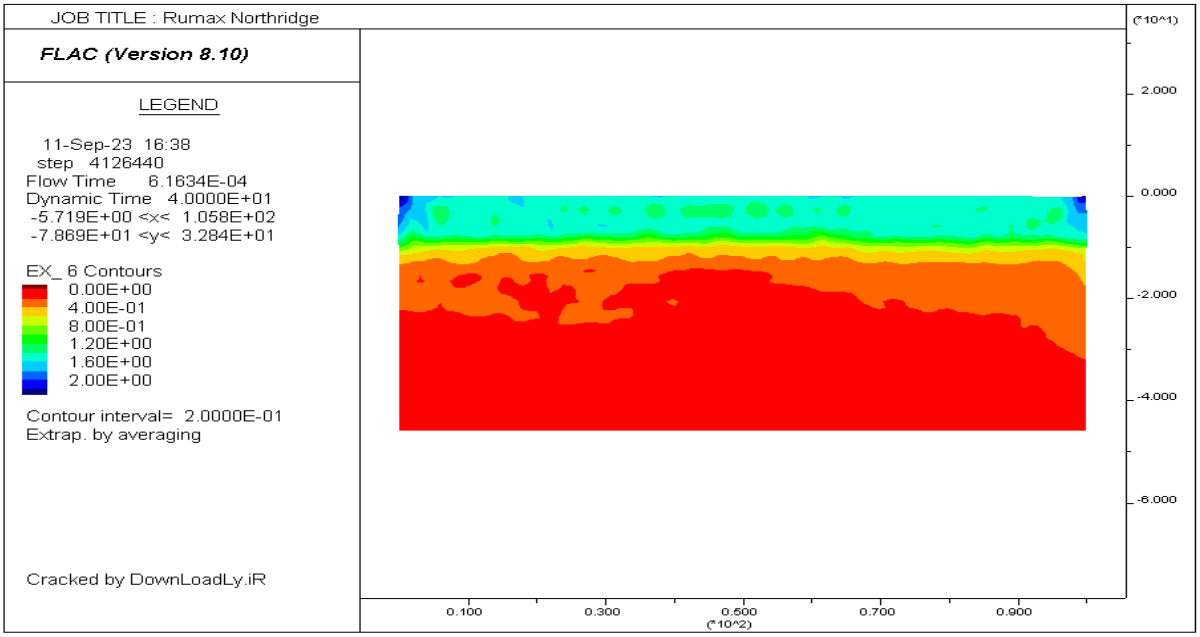

Fig 101: Pore pressure Ratio contour after seismic loading for MOD-6

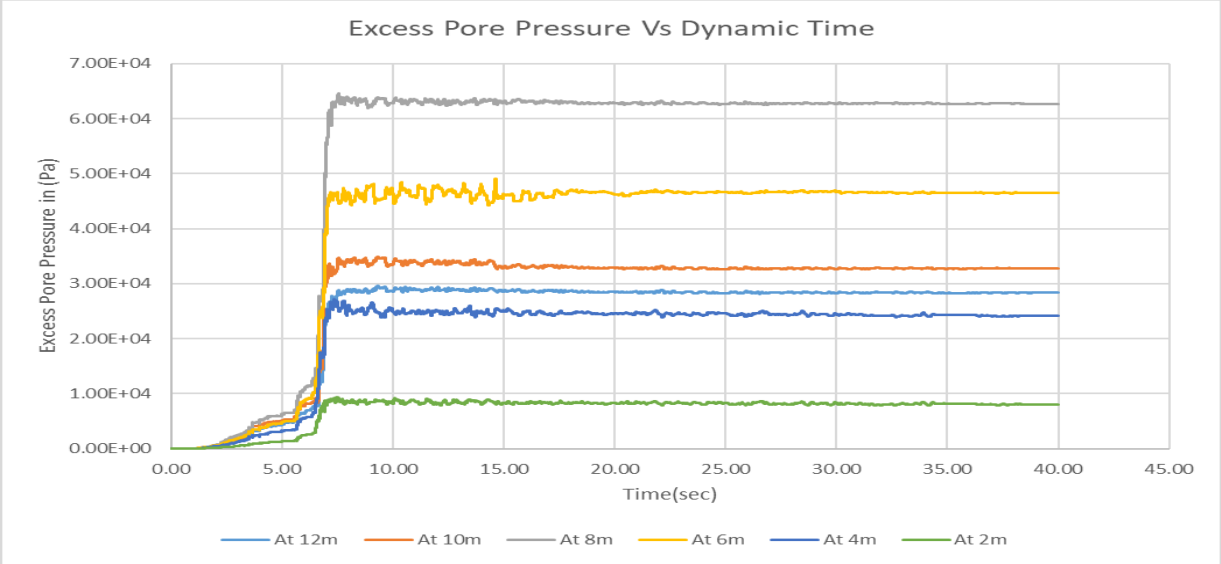

Fig 102: Excess Pore pressure generation for top 18m after seismic loading for MOD-6

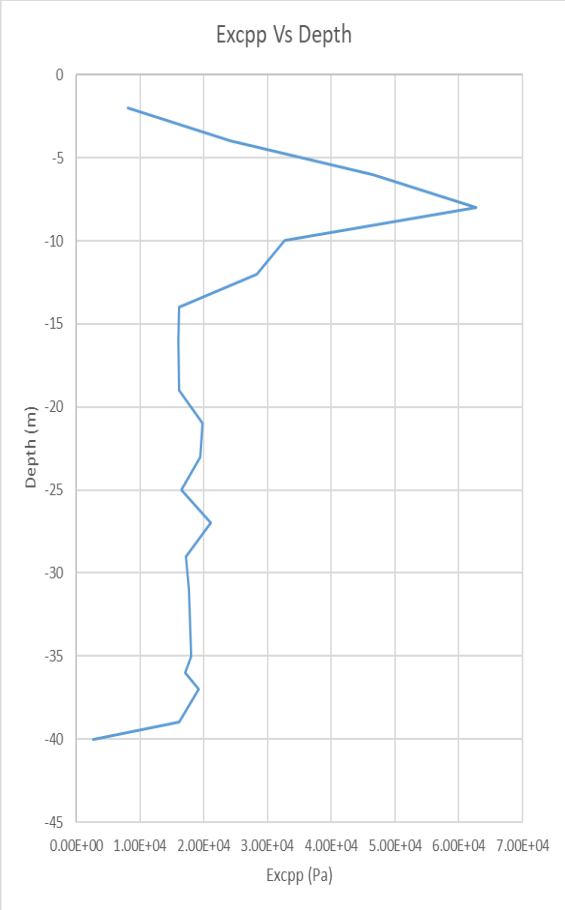

Fig 103: Excpp vs Depth at section A-A

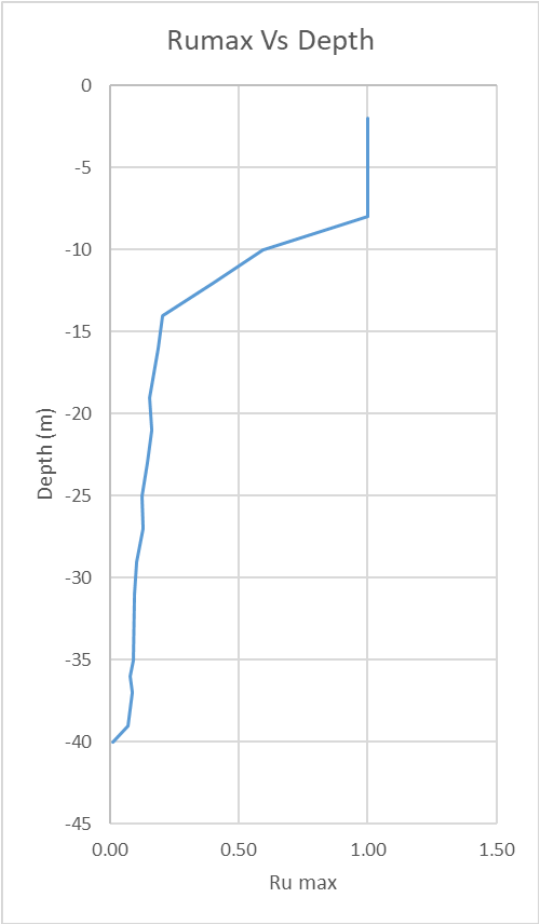

Fig 104: Ru max vs Depth at section A-A

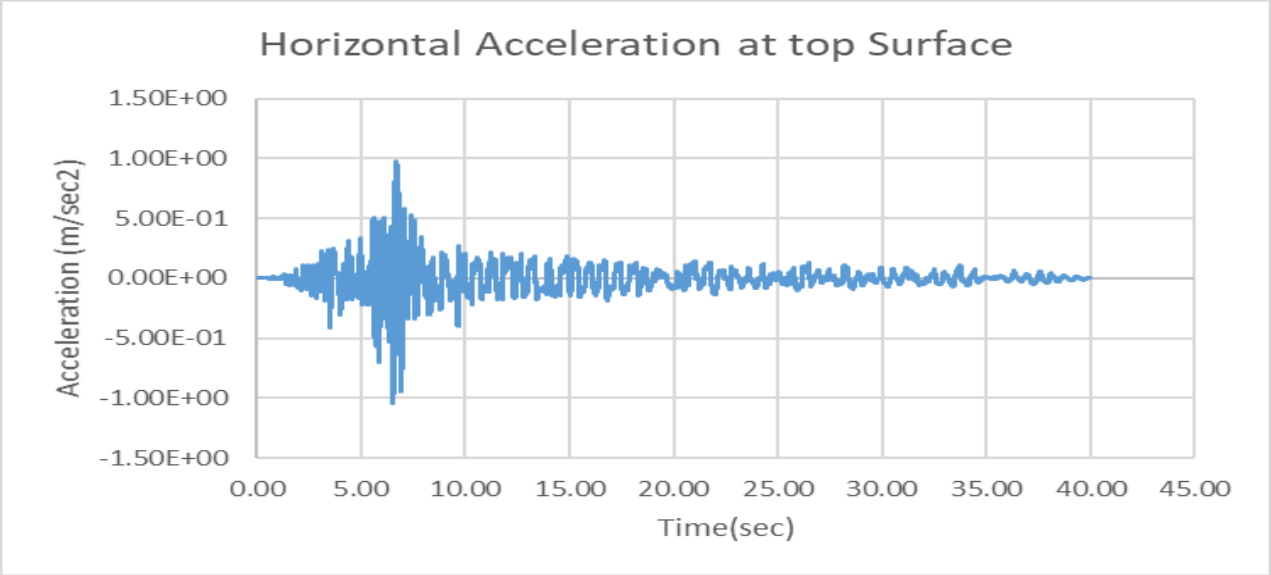

Fig 105: Horizontal acceleration at surface of model MOD-6

4.2.7 Results of Dynamic Analysis for MOD-7

MOD-7 as mentioned in Table 13 the soil strata with Embankment of 10m top width is subjected to a scaled 0.2g PGA of Loma Prieata. From Fig 106 the maximum vertical displacement can be seen in crest of value 150mm. Fig 107 and 108 provides us the pattern of pore pressure generation and excess pore pressure generation in foundation soil respectively. From Fig 109 it is evident that pore pressure ratio is lesser immediately below the embankment than at the free field edges. So we have decided to divide the model in three sections as shown in schematic drawing Fig 110 to enhance our observations. The plot of variation of Excess Pore pressure generation and Pore pressure ratio along the depth for those 3 section have been shown in Fig 111 and 112. Below the embankment the pore pressure ratio barely reaches to 1, whereas the free field location liquefaction reaches to a value of 1 at depth of 1.5m and extend to 8m depth. This is due to the fact of increase in effective stress due to embankment. Fig 113 provides the horizontal acceleration at crest of embankment. The peak value of acceleration is 1.9m/sec2, so an amplification of 1.06 times of input peak can be observed.

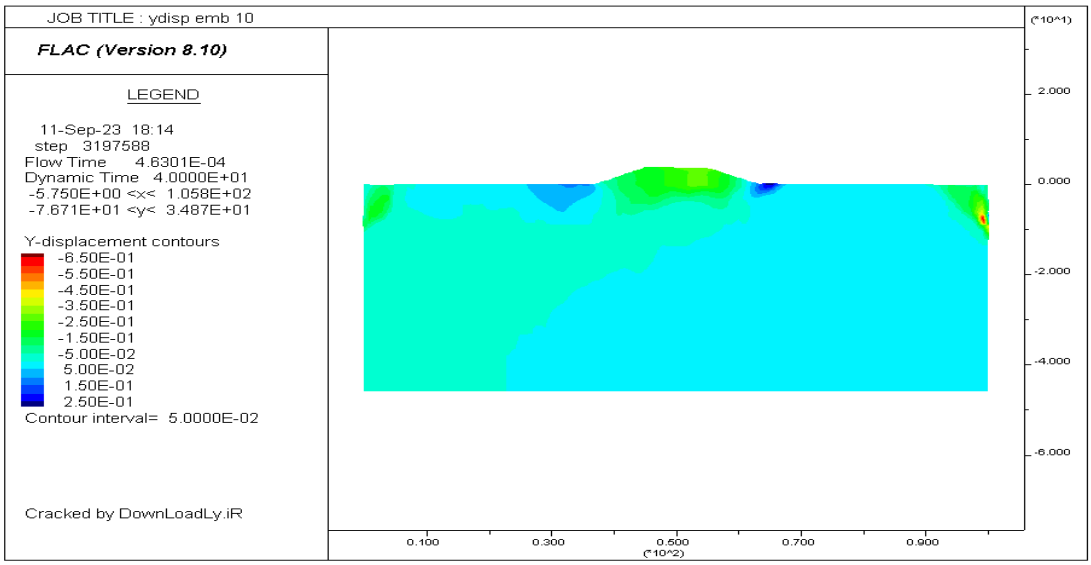

Fig 106: Y displacement contour for model MOD-7

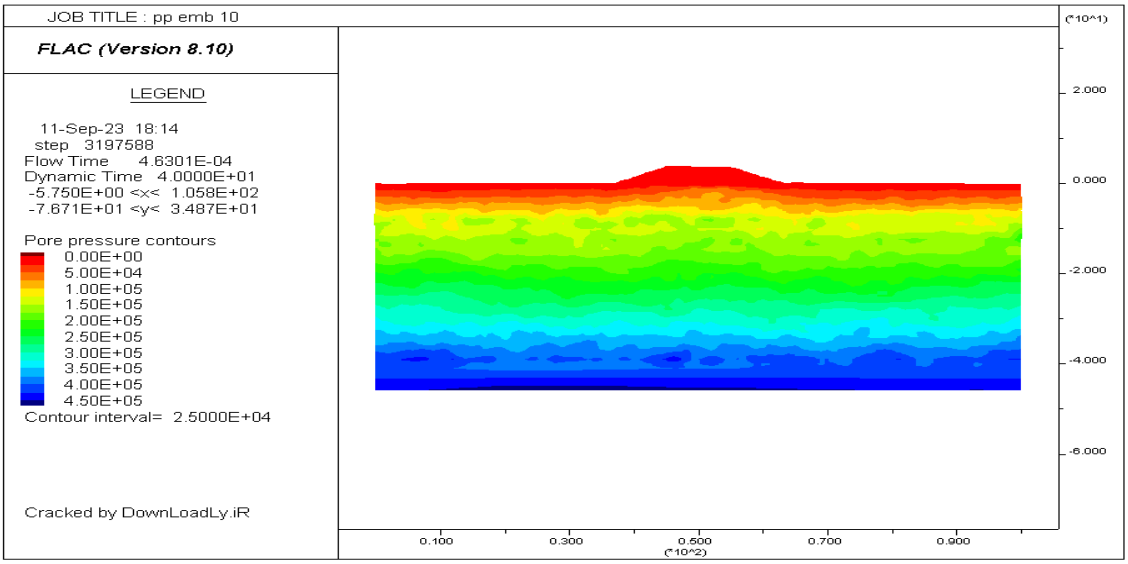

Fig 107: Pore pressure generation contour after seismic loading for MOD-7

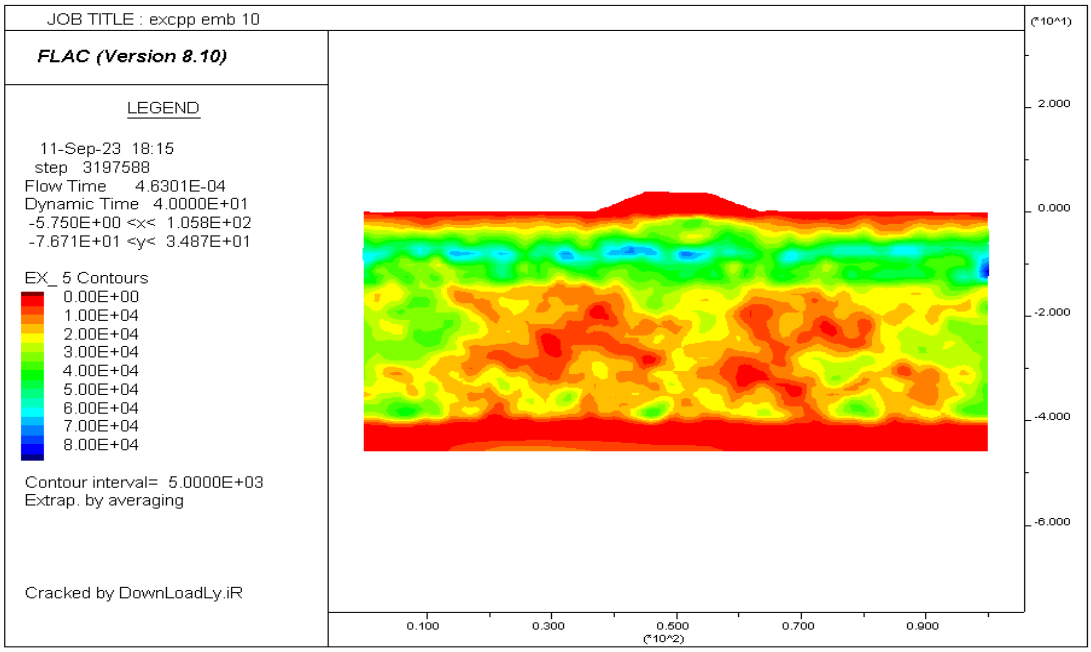

Fig 108: Excess Pore pressure generation contour after seismic loading for MOD-7

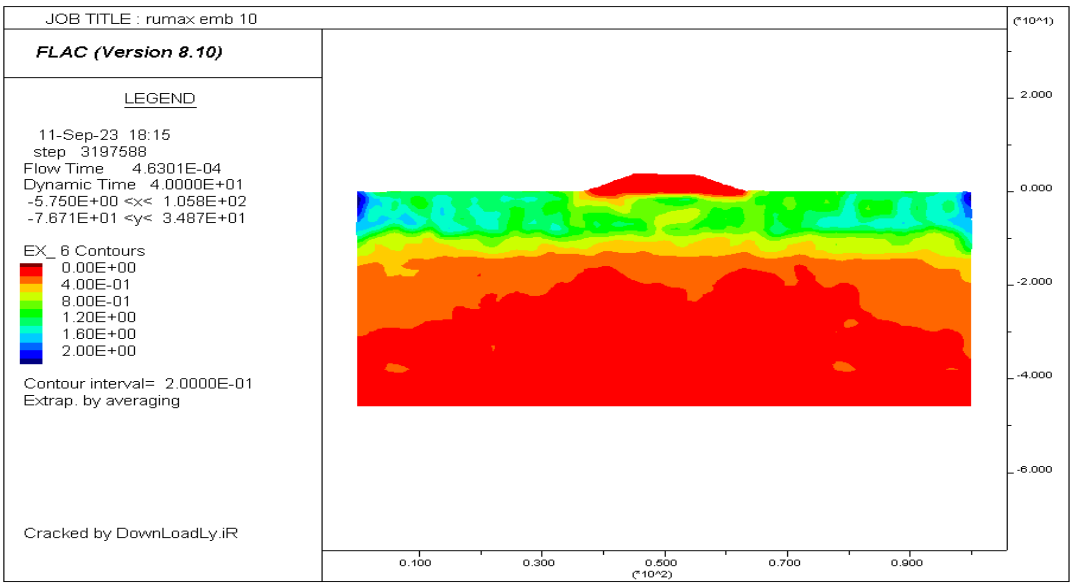

Fig 109: Pore pressure Ratio contour after seismic loading for MOD-7

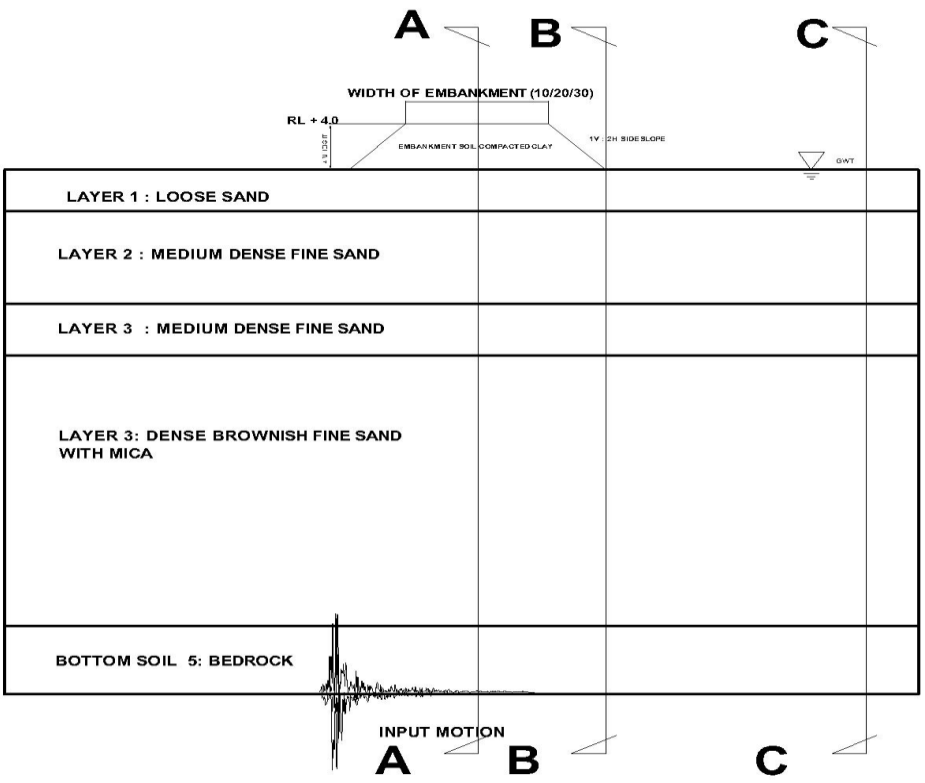

Fig 110: Schematic drawing of the model showing section A-A, section B-B and C-C

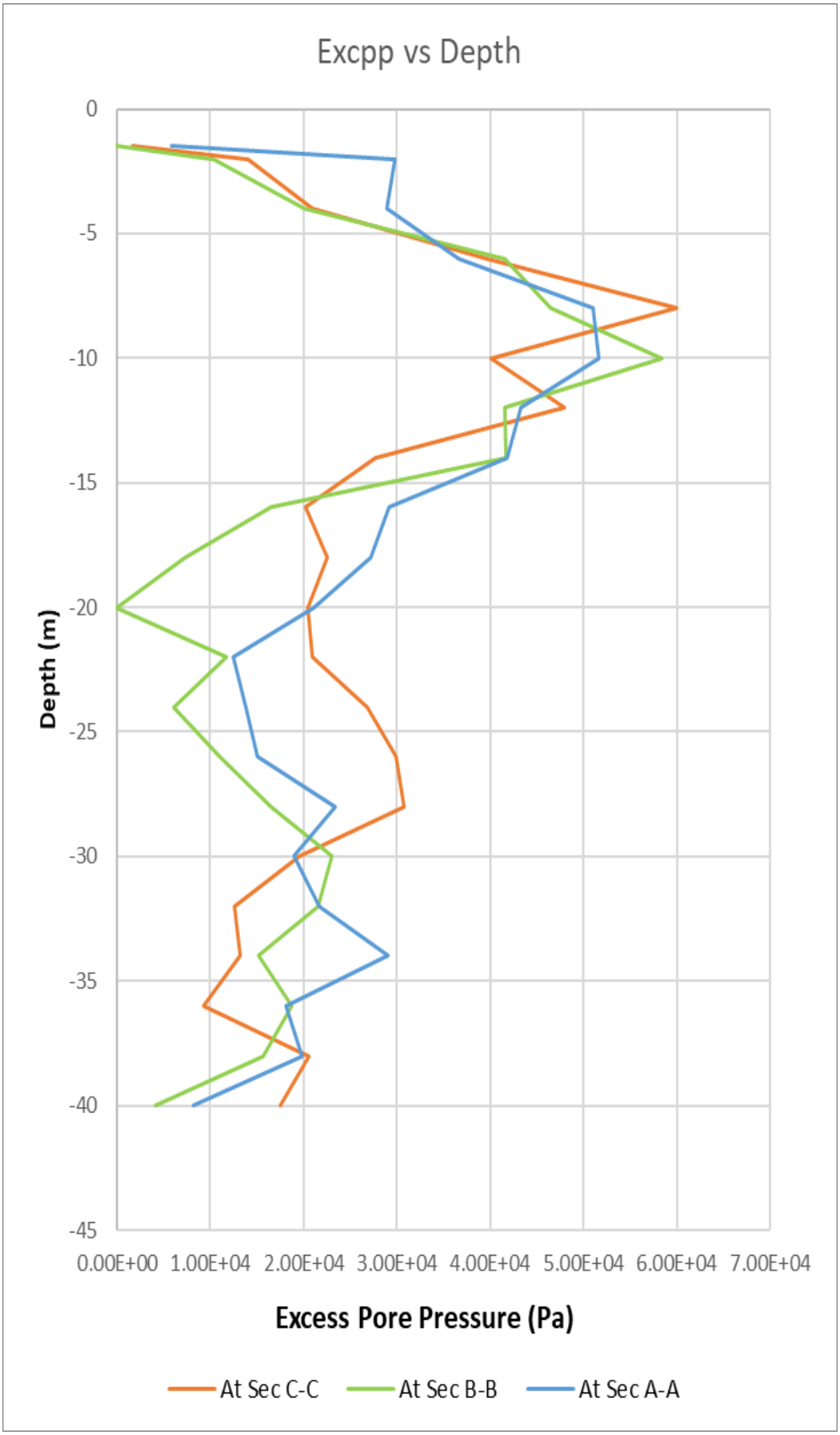

Fig 111: Excpp vs Depth at section A-A, B-B and C-C

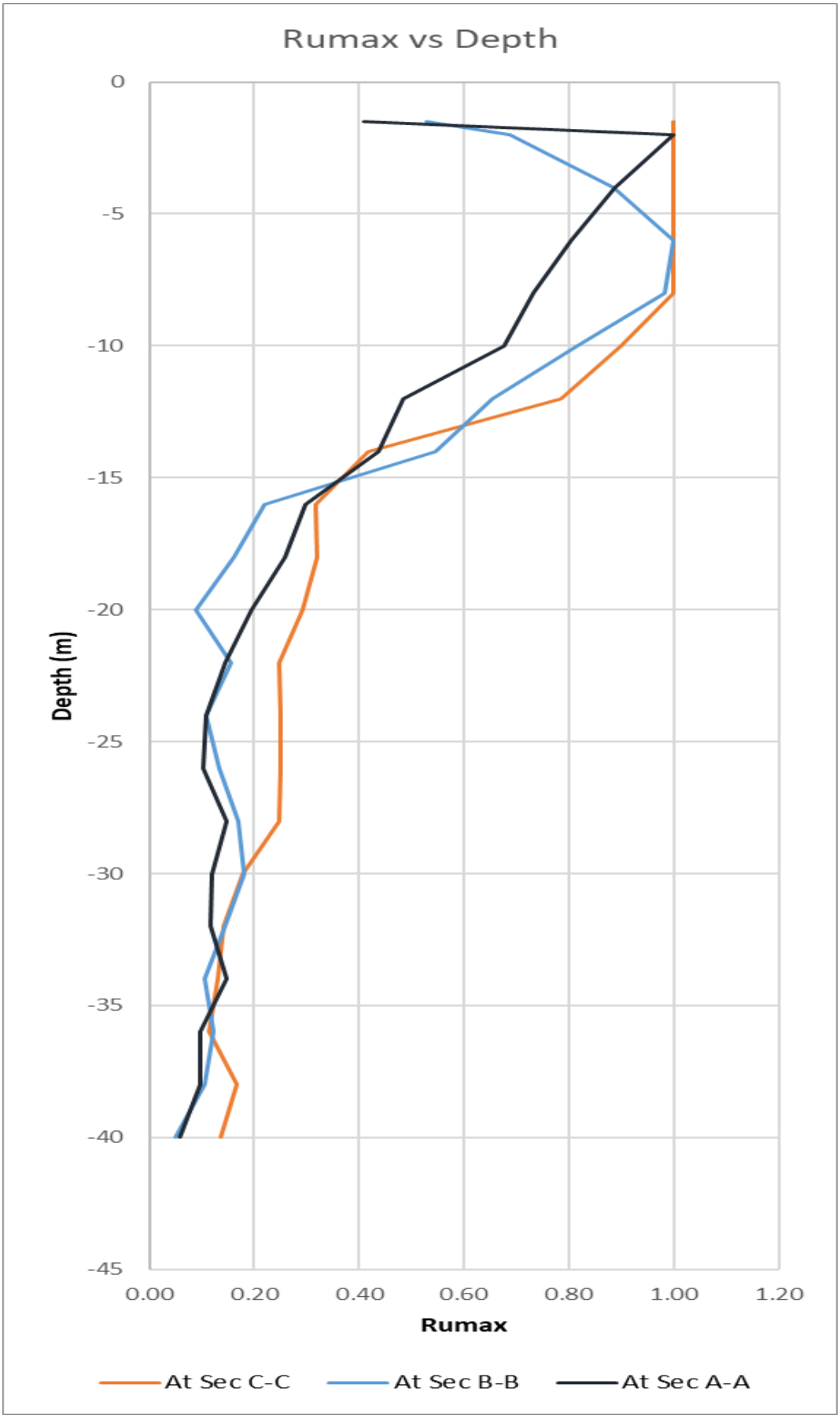

Fig 112: Ru max vs Depth at section A-A, B-B and C-C

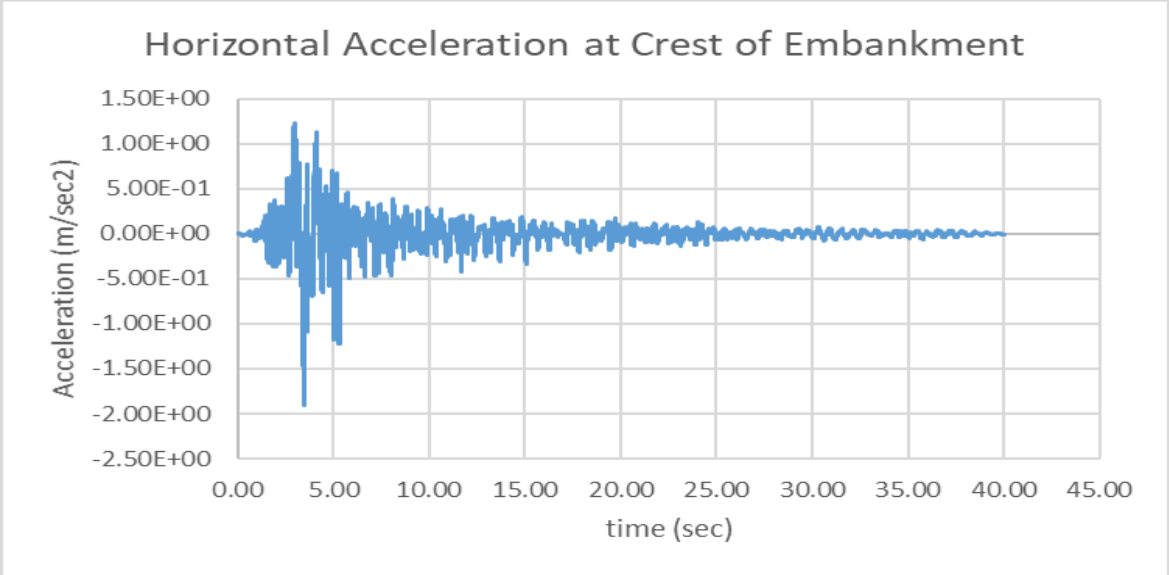

Fig 113: Horizontal acceleration at crest of Embankment of model MOD-7

4.2.8 Results of Dynamic Analysis for MOD-8

MOD-8 as mentioned in Table 13 the soil strata with Embankment of 20m top width is subjected to a scaled 0.2g PGA of Loma Prieata. From Fig 114 the maximum vertical displacement can be seen in crest of value 250mm. Fig 115 and 116 provides us the pattern of pore pressure generation and excess pore pressure generation in foundation soil respectively. From Fig 118 it is evident that pore pressure ratio is lesser immediately below the embankment than at the free field edges. From Fig 119 it is seen that the depth of liquefied layer is smaller the depth of liquefied layer at free field condition. This is due to the fact of increase in effective stress due to embankment. With the increase in the width of the embankment an increase in excess pore pressure generation below the embankment is also observed in Fig 118 (from 51Kpa in Fig 111 to 67Kpa in Fig 118), than the previous model. Fig 120 provides the horizontal acceleration at crest. The peak acceleration value at crest is 2.09 m/sec2. Thus an amplification of 1.17 times the input motion is observed.

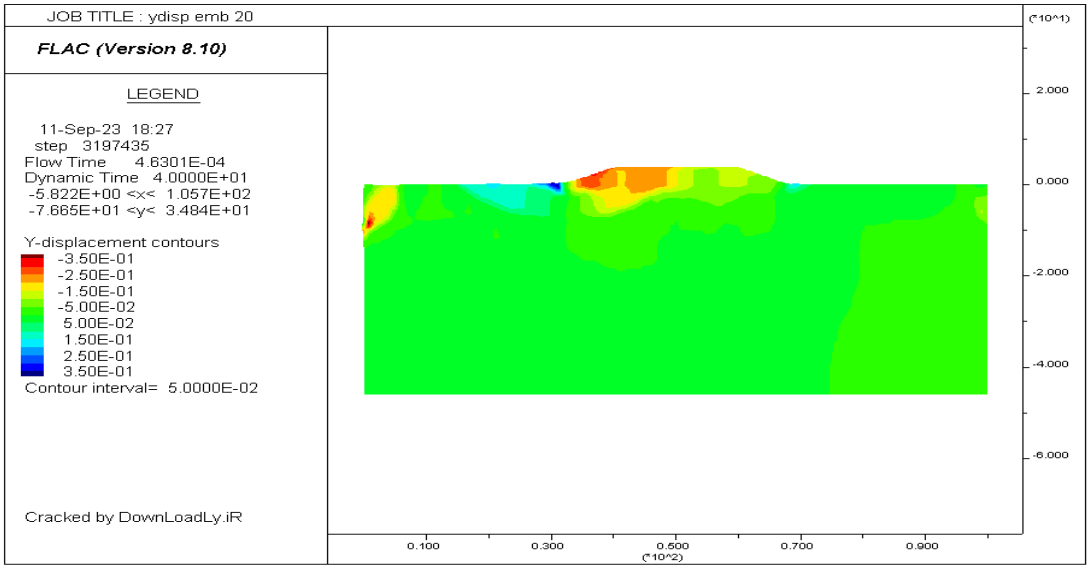

Fig 114: Y displacement contour for model MOD-8

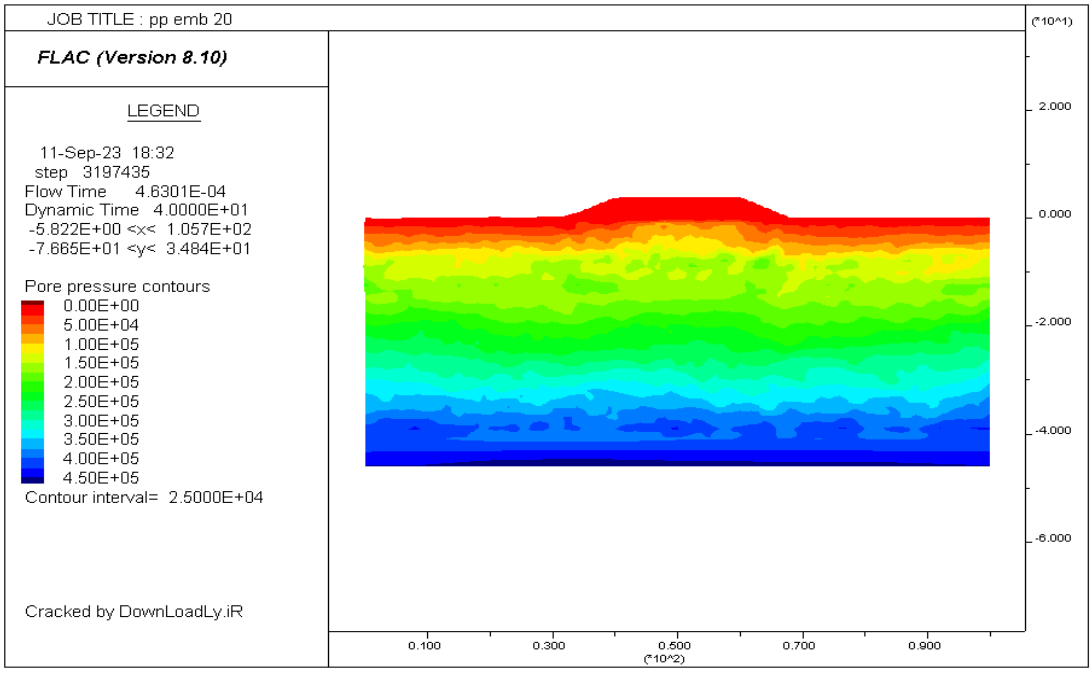

Fig 115: Pore pressure generation contour after seismic loading for MOD-8

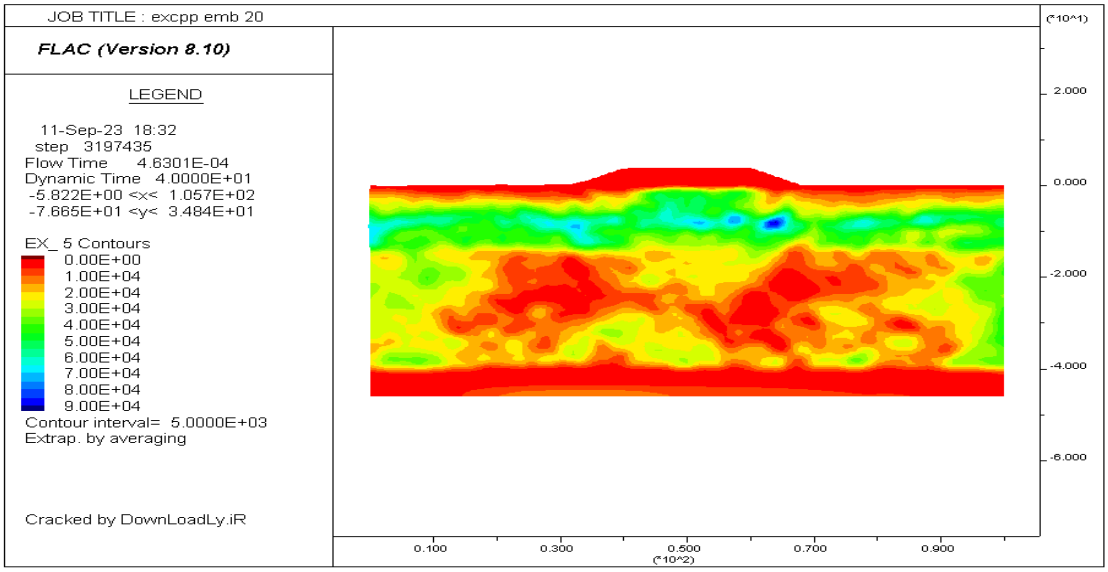

Fig 116: Excess Pore pressure generation contour after seismic loading for MOD-8

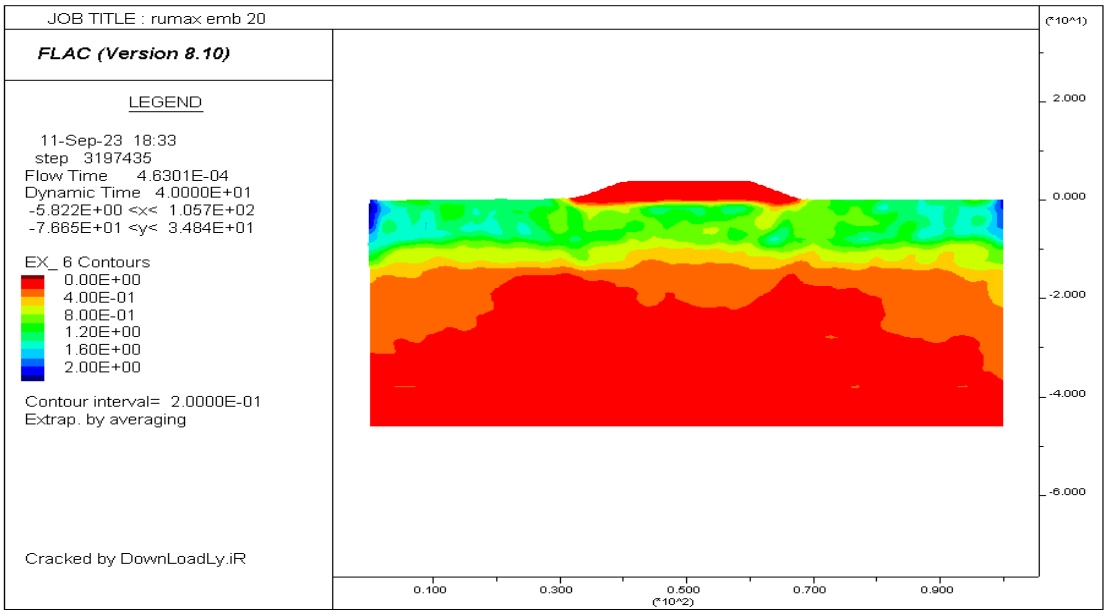

Fig 117: Pore pressure Ratio contour after seismic loading for MOD-8

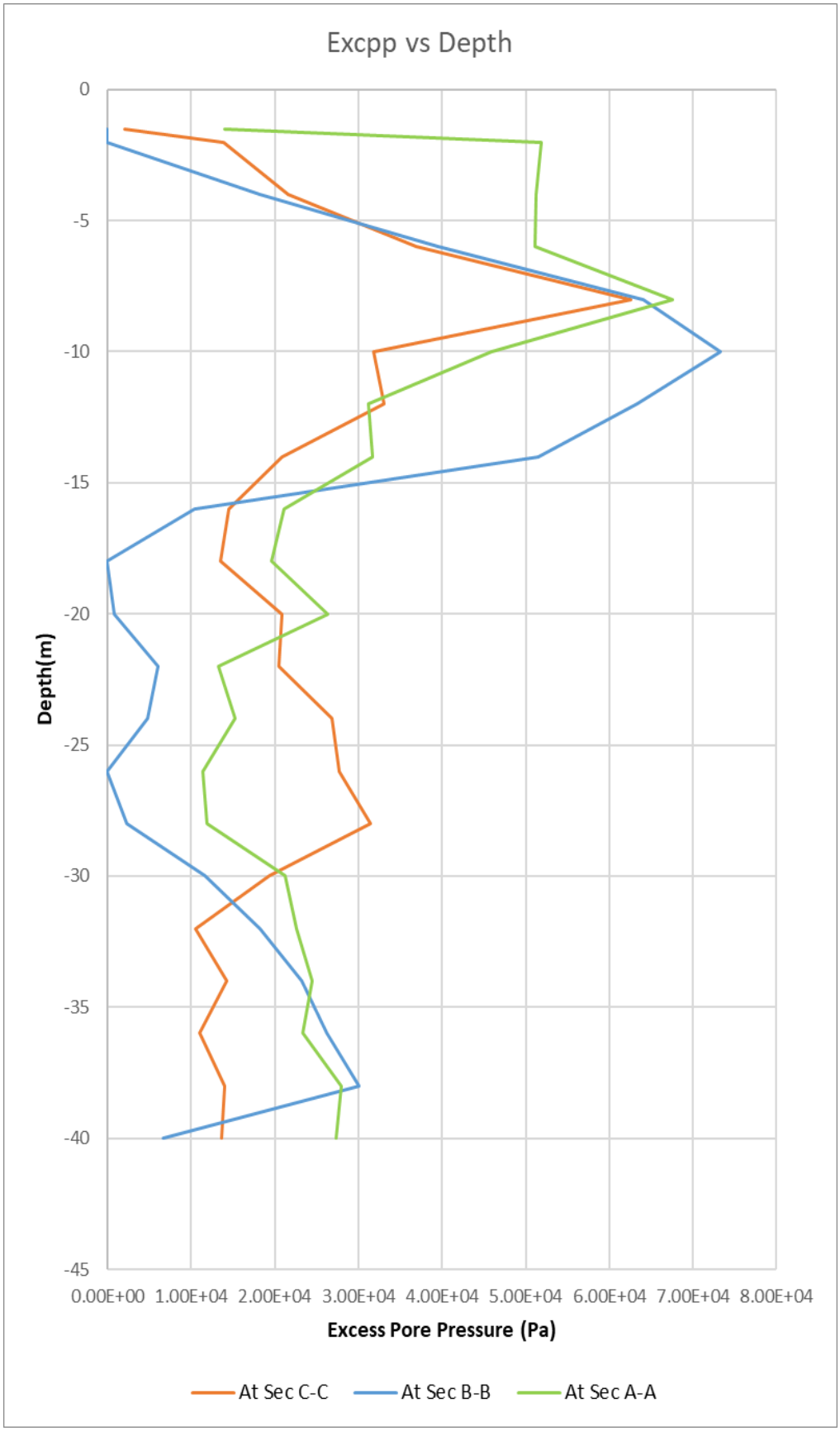

Fig 118: Excpp vs Depth at section A-A, B-B and C-C

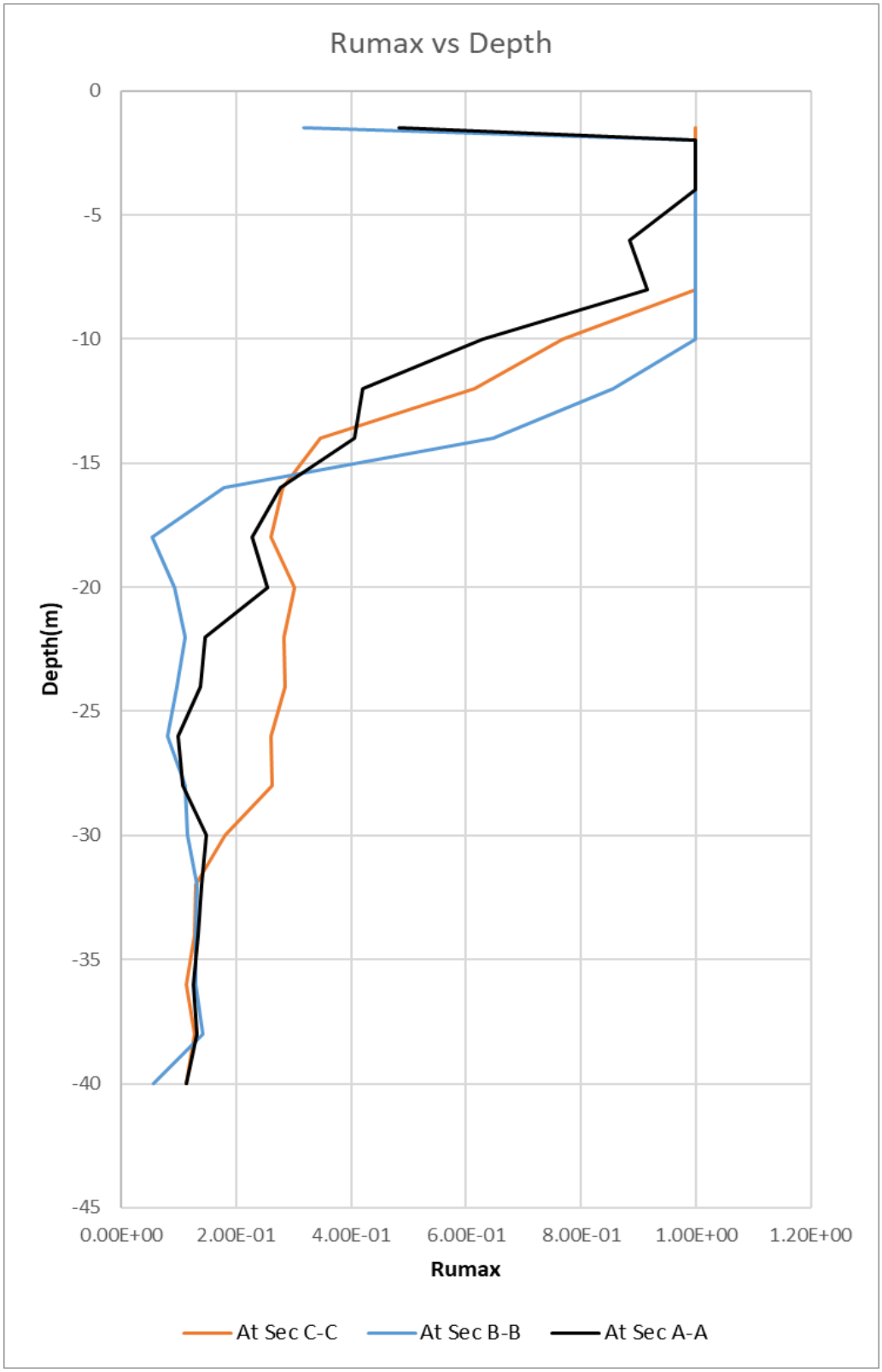

Fig 119: Ru max vs Depth at section A-A, B-B and C-C

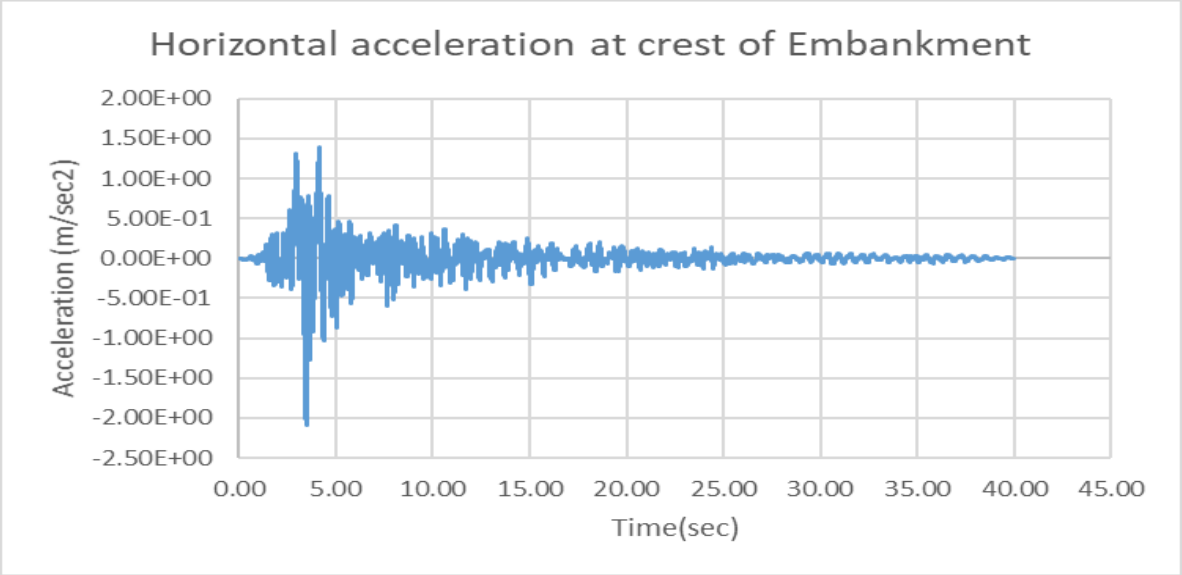

Fig 120: Horizontal acceleration at crest of Embankment of model MOD-8

4.2.9 Results of Dynamic Analysis for MOD-9

MOD-9 as mentioned in Table 13 the soil strata with Embankment of 30m top width is subjected to a scaled 0.2g PGA of Loma Prieata. From Fig 121 the maximum vertical displacement can be seen in crest of value 500mm. Fig 122 and 123 provides us the pattern of pore pressure generation and excess pore pressure generation in foundation soil respectively. From Fig 124 the liquefied soil layer depth below embankment has increased to 4m. With the increase in the width of the embankment an increase in excess pore pressure generation below the embankment is also observed in Fig 125 (from 67Kpa in Fig 118 to 78Kpa in Fig 125), than the previous model. Fig 127 provides the horizontal acceleration at crest. The peak acceleration value at crest is 1.84 m/sec2. Thus an amplification of 1.03 times the input motion is observed.

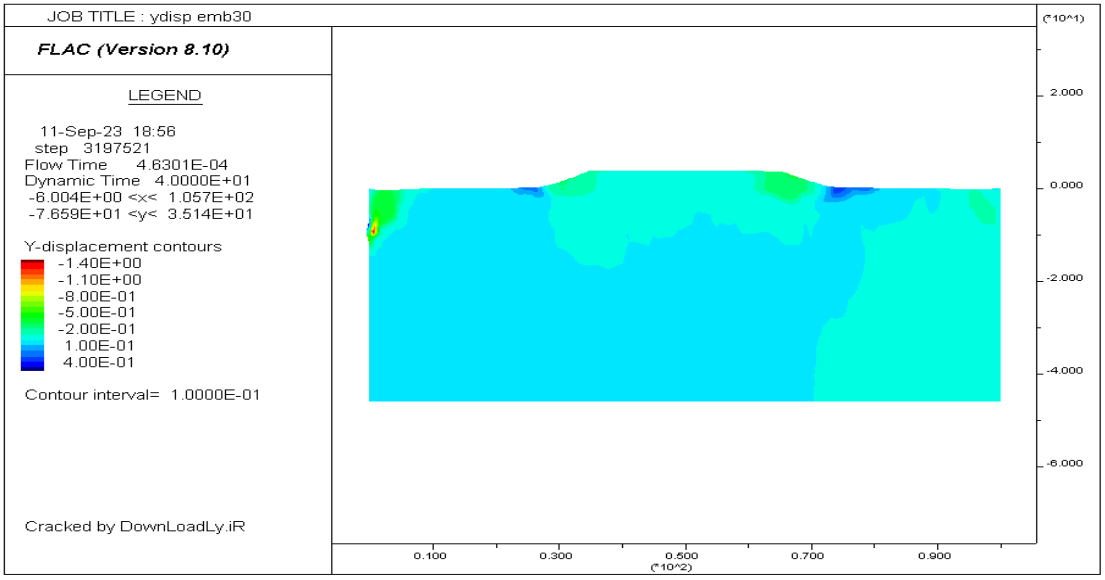

Fig 121: Y displacement contour for model MOD-9

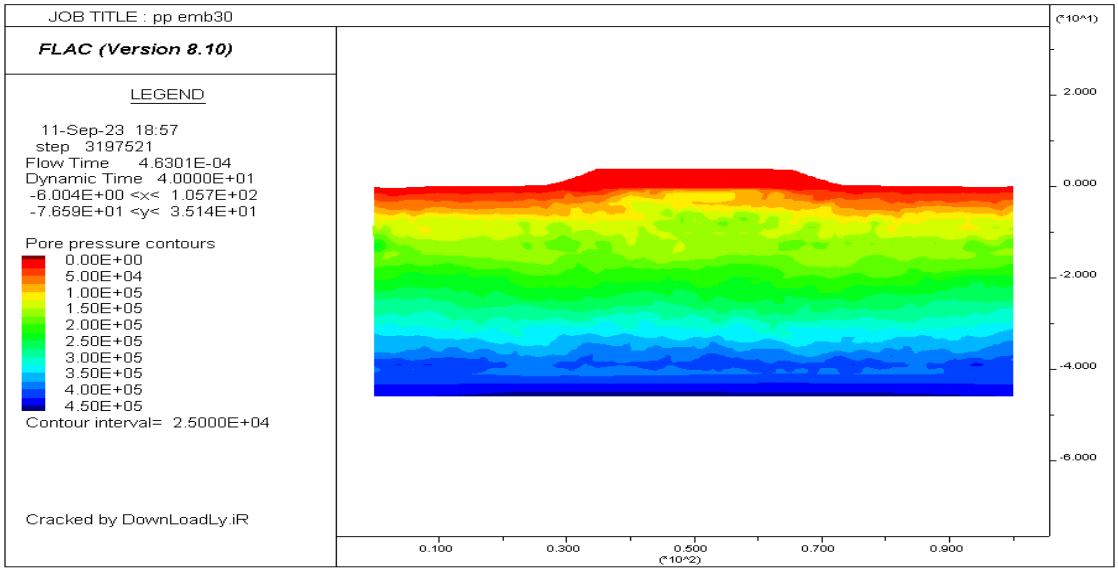

Fig 122: Pore pressure generation contour after seismic loading for MOD-9

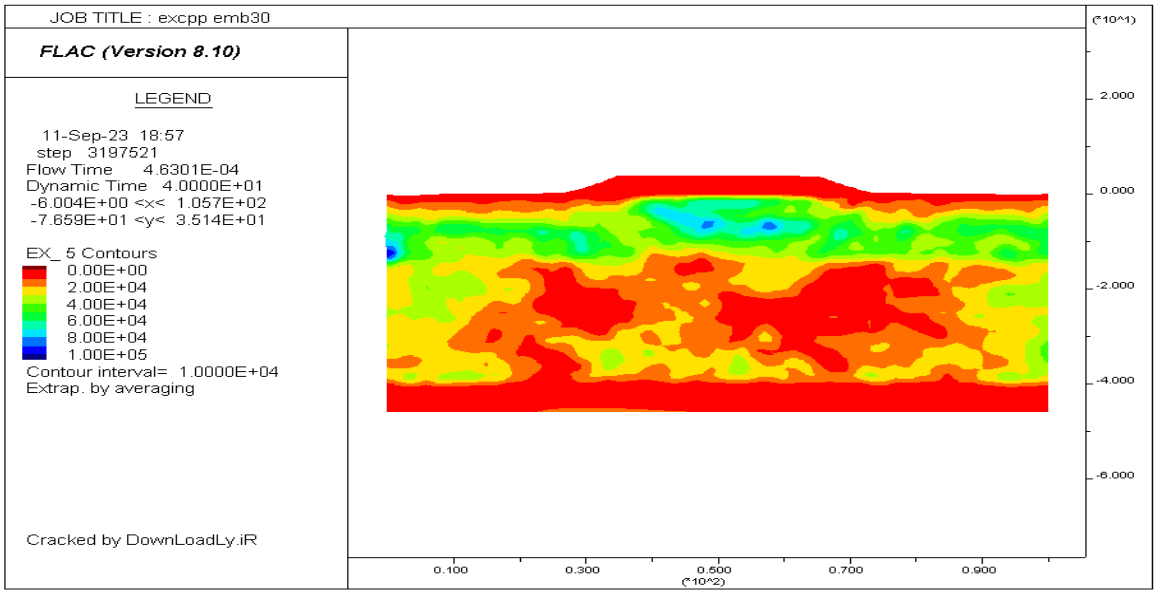

Fig 123: Excess Pore pressure generation contour after seismic loading for MOD-9

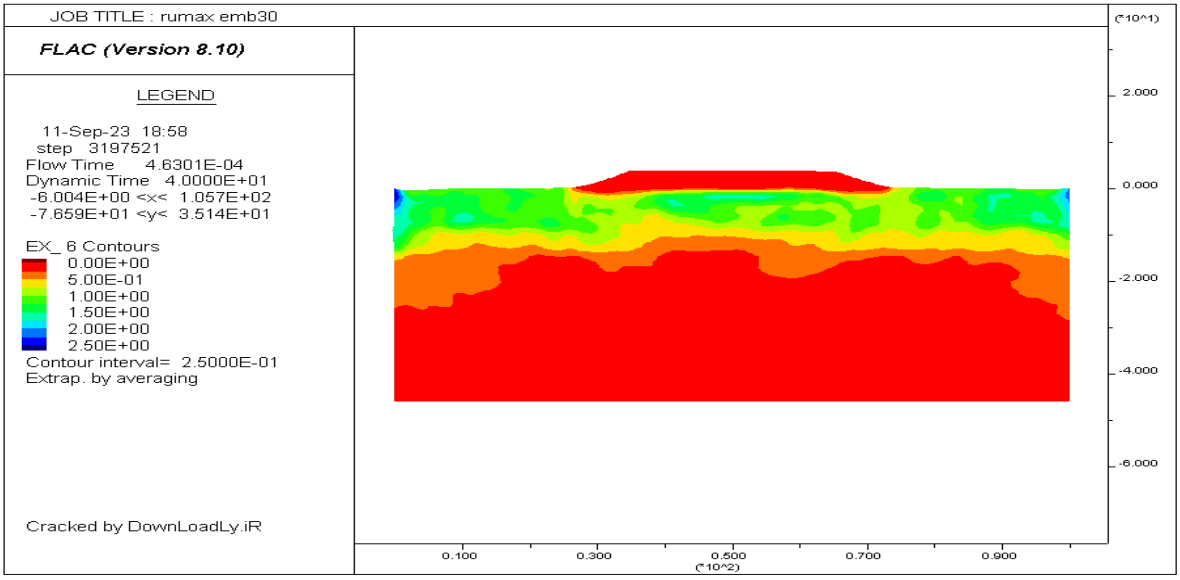

Fig 124: Pore pressure Ratio contour after seismic loading for MOD-9

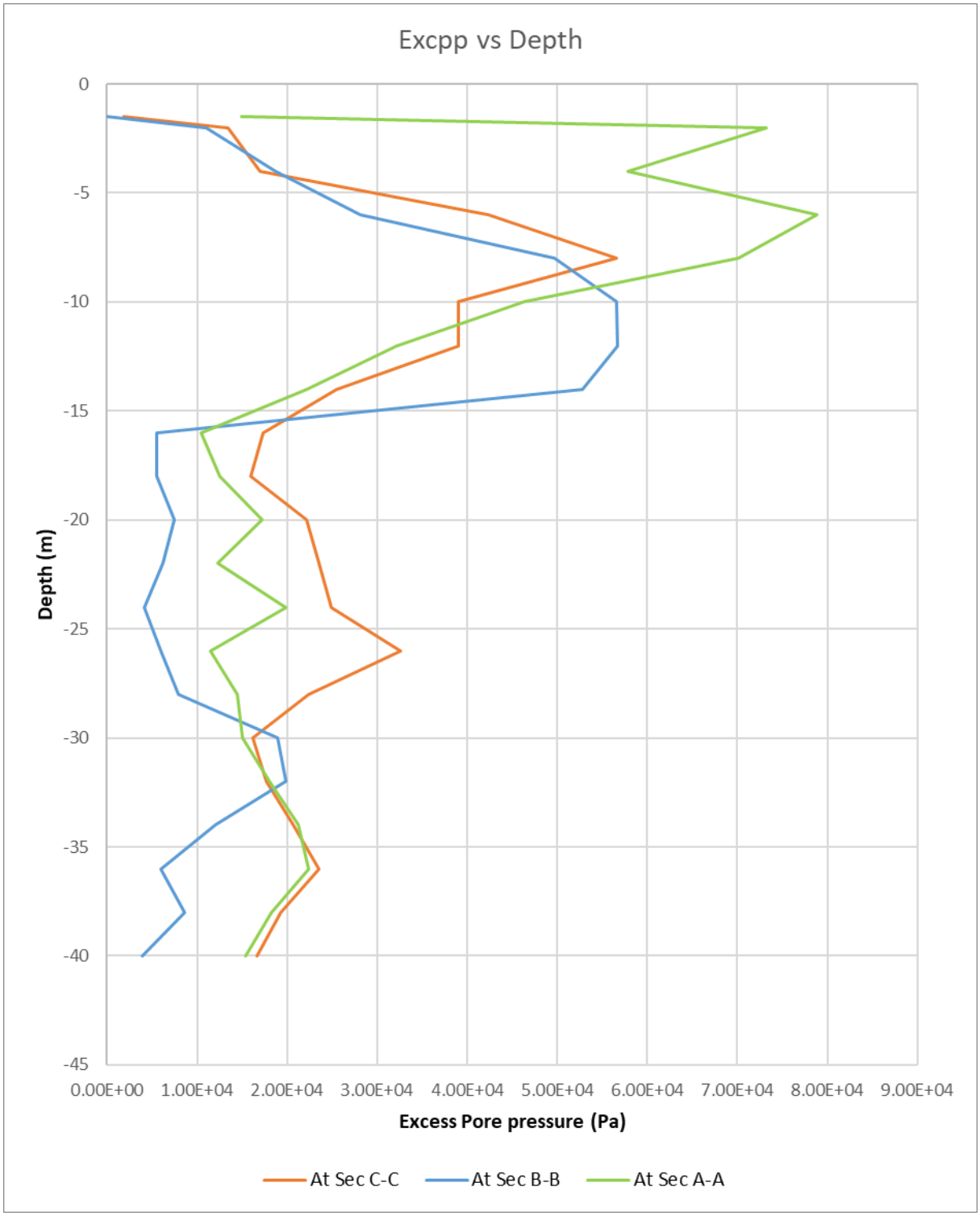

Fig 125: Excpp vs Depth at section A-A, B-B and C-C

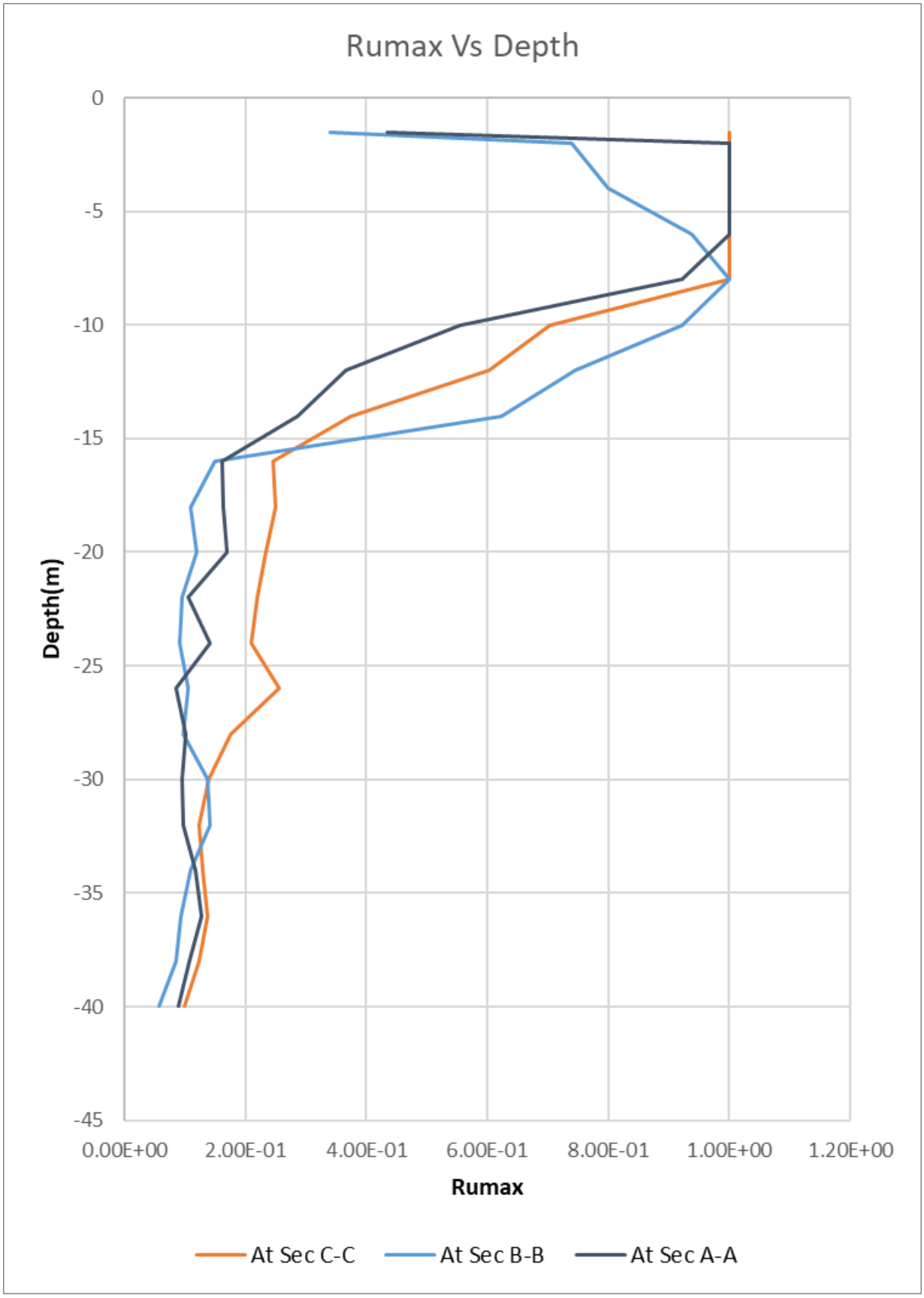

Fig 126: Ru max vs Depth at section A-A, B-B and C-C

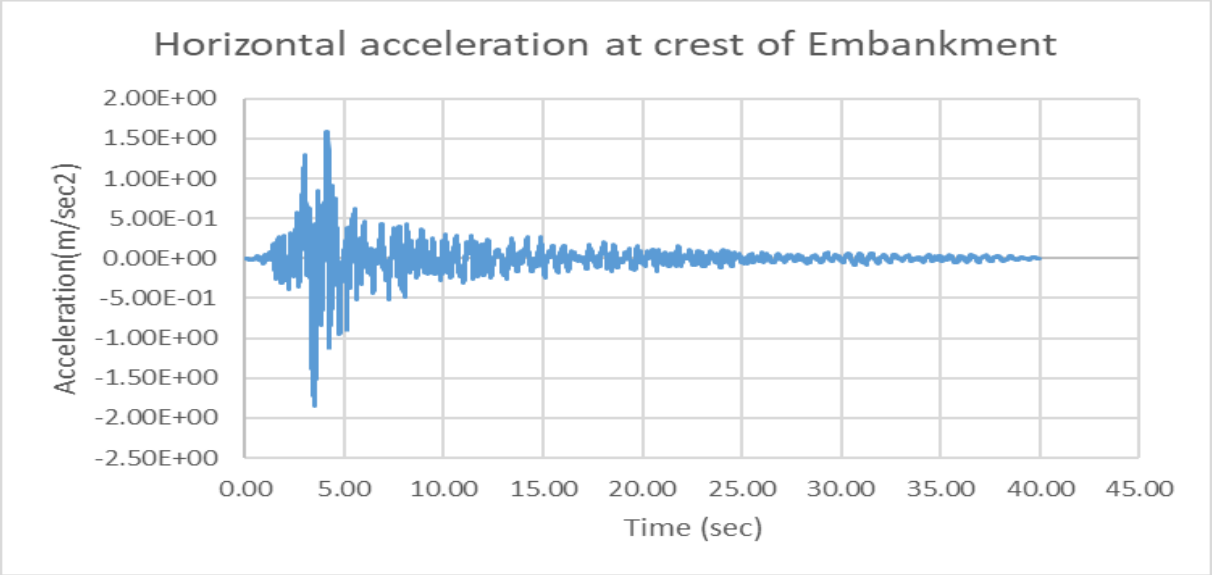

Fig 127: Horizontal acceleration at crest of Embankment of model MOD-9

4.2.10 Results of Dynamic Analysis for MOD-10

MOD-10 as mentioned in Table 13 the soil strata with modified liquefiable layer depth 5m keeping the overall soil strata of same thickness & subjected to a scaled 0.2g PGA of Loma Prieata. A schematic diagram of the model is shown below in Fig 131. From Fig 129 and 132 the maximum excess pore pressure generated in the model is of 33.8Kpa and at a depth of 39m from surface. The maximum pore pressure ratio of the model reached to 1.0 for top 5m layer indicating the liquefaction had occurred in this layer. The peak surface acceleration in Fig 134 is 1.69m/sec2. So the acceleration has been de-amplified by 0.95 times the input acceleration.

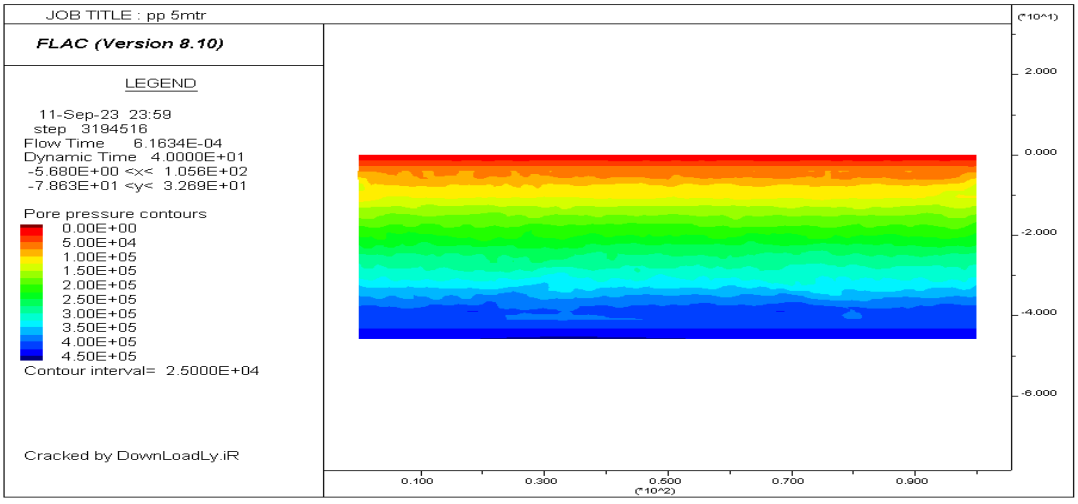

Fig 128: Pore pressure generation contour after seismic loading for MOD-10

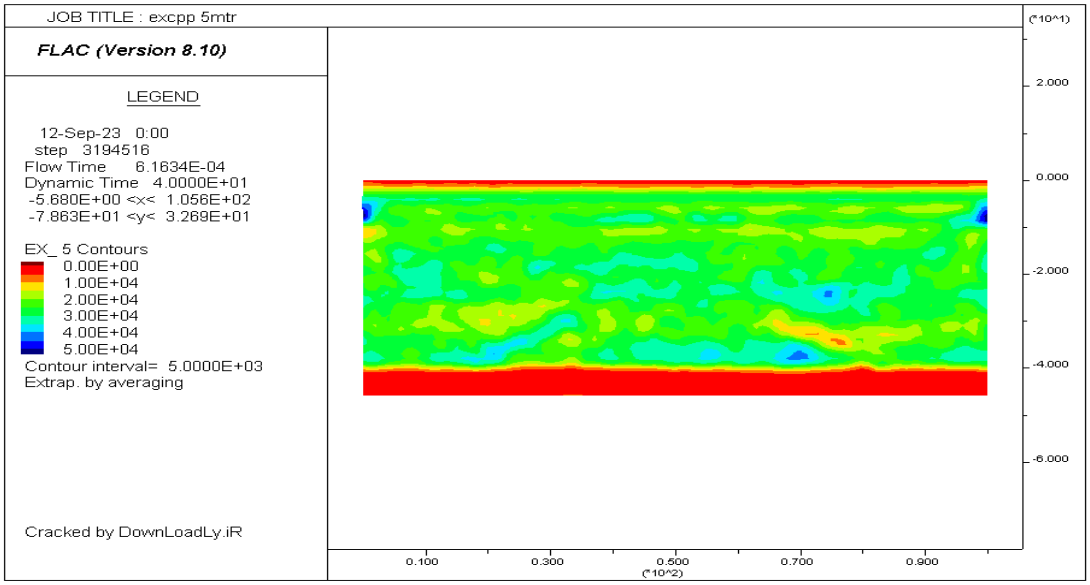

Fig 129: Excess Pore pressure generation contour after seismic loading for MOD-10

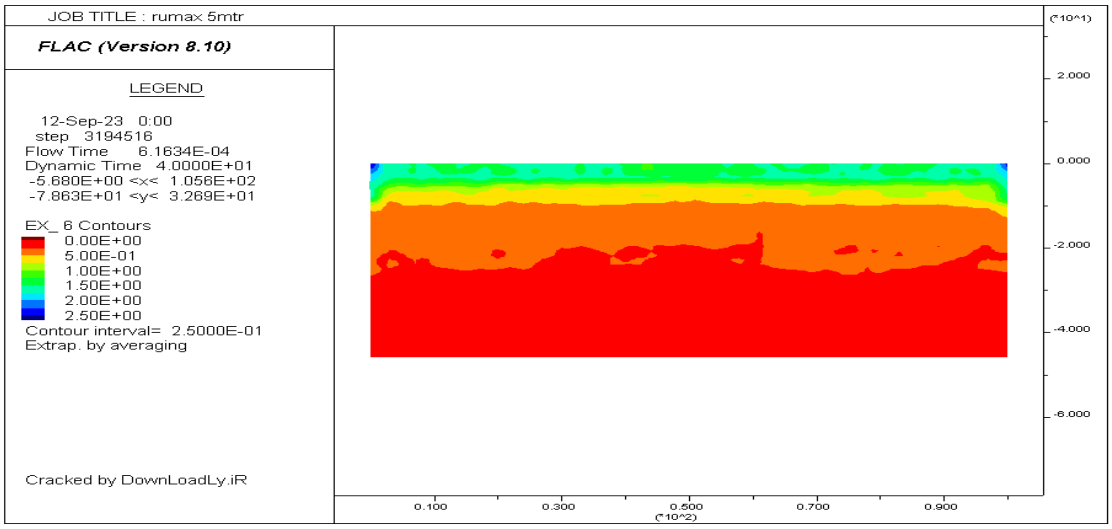

Fig 130: Pore pressure Ratio contour after seismic loading for MOD-10

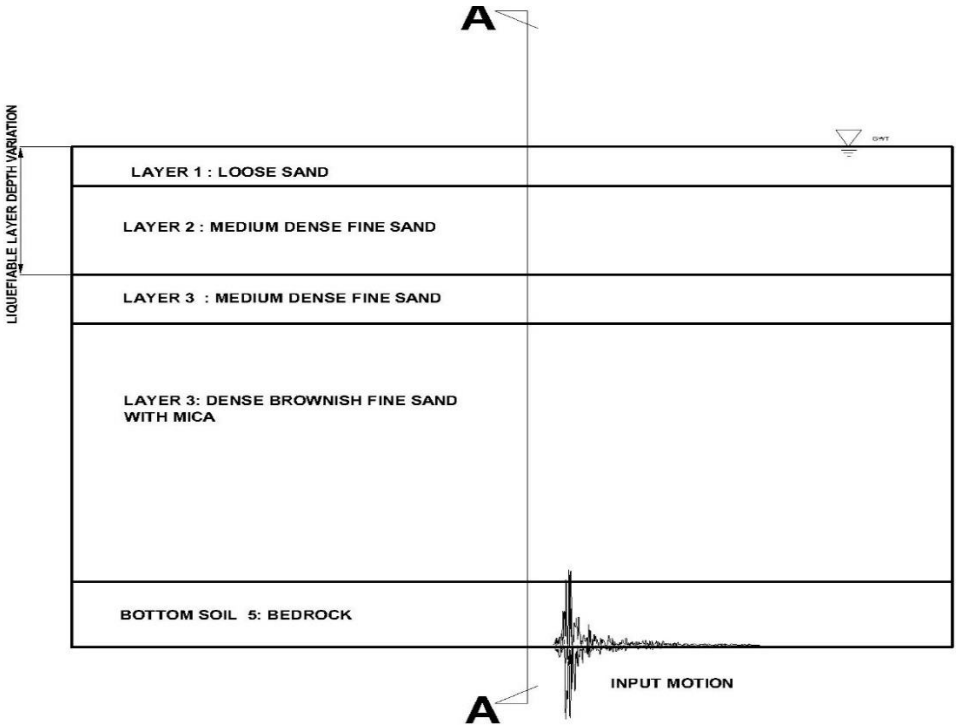

Fig 131: Schematic drawing of the model showing section A-A

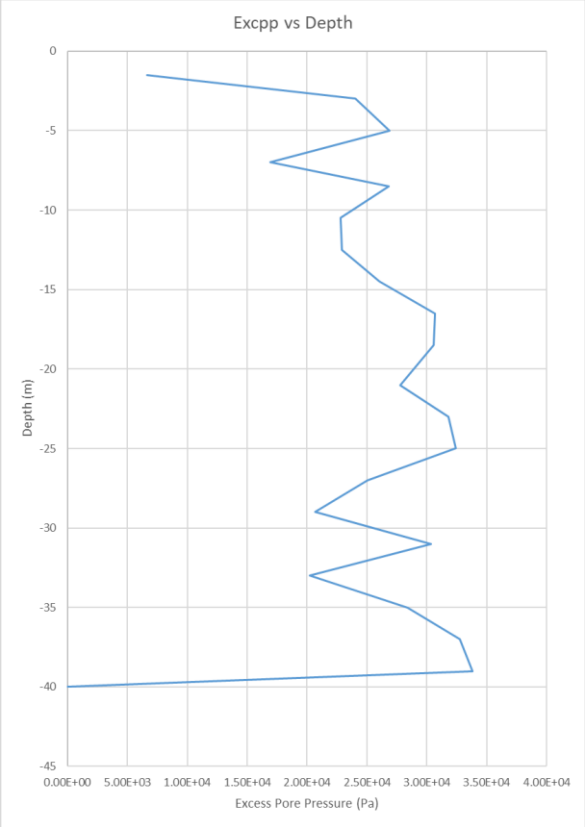

Fig 132: Excpp vs Depth at section A-A,

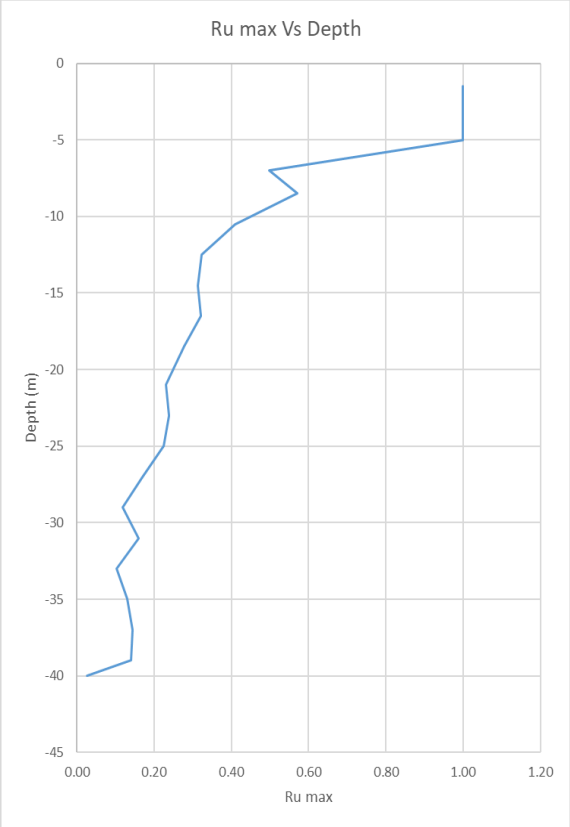

Fig 133: Ru max vs Depth at section A-A

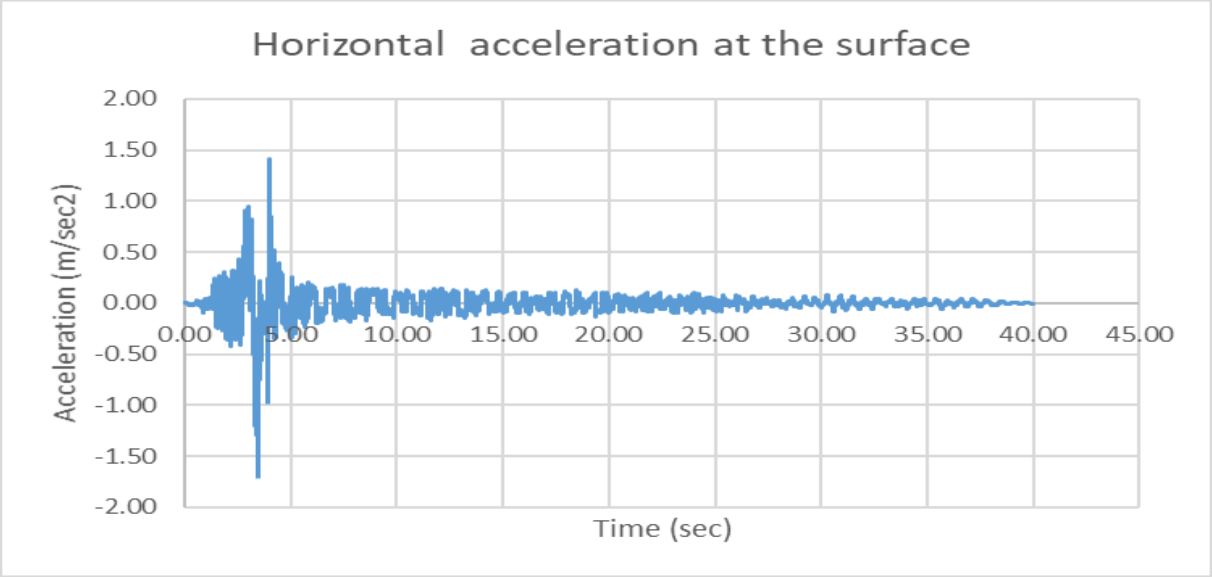

Fig 134: Horizontal acceleration at crest of Embankment of model MOD-10

4.2.11 Results of Dynamic Analysis for MOD-11

MOD-11 as mentioned in Table 13 the soil strata with modified liquefiable layer depth 15m keeping the overall soil strata of same thickness & subjected to a scaled 0.2g PGA of Loma Prieata. From Fig 136 and 138 the maximum excess pore pressure generated in the model is of 86.4Kpa. The maximum pore pressure ratio of the model reached to 1 starting at the depth of 1.5m from top and extending to 12.5m. The peak surface acceleration in Fig 140 is 1.52m/sec2. So the acceleration has been de-amplified by 0.85 times the input acceleration

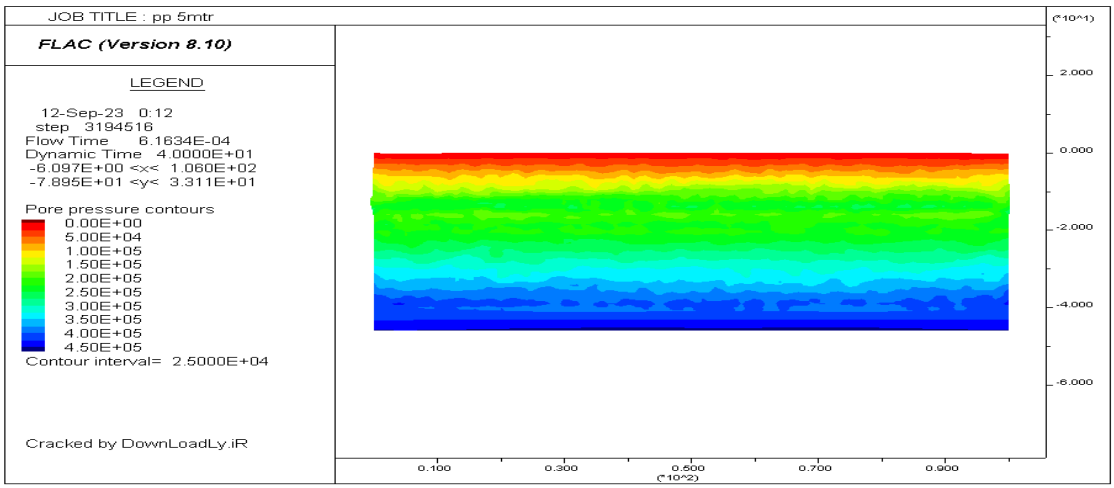

Fig 135: Pore pressure generation contour after seismic loading for MOD-11

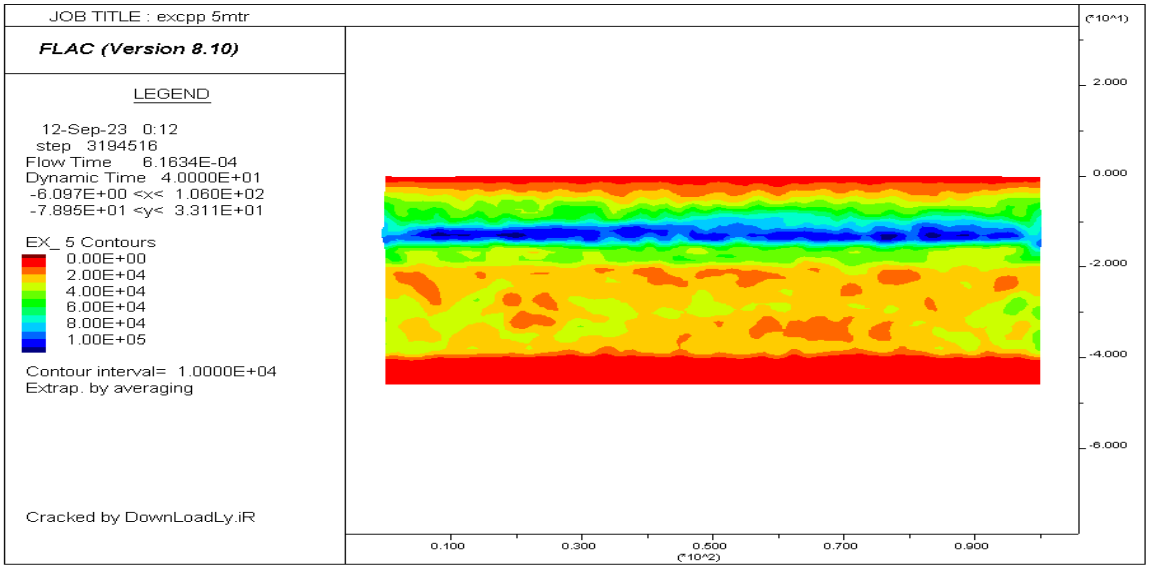

Fig 136: Excess Pore pressure generation contour after seismic loading for MOD-11

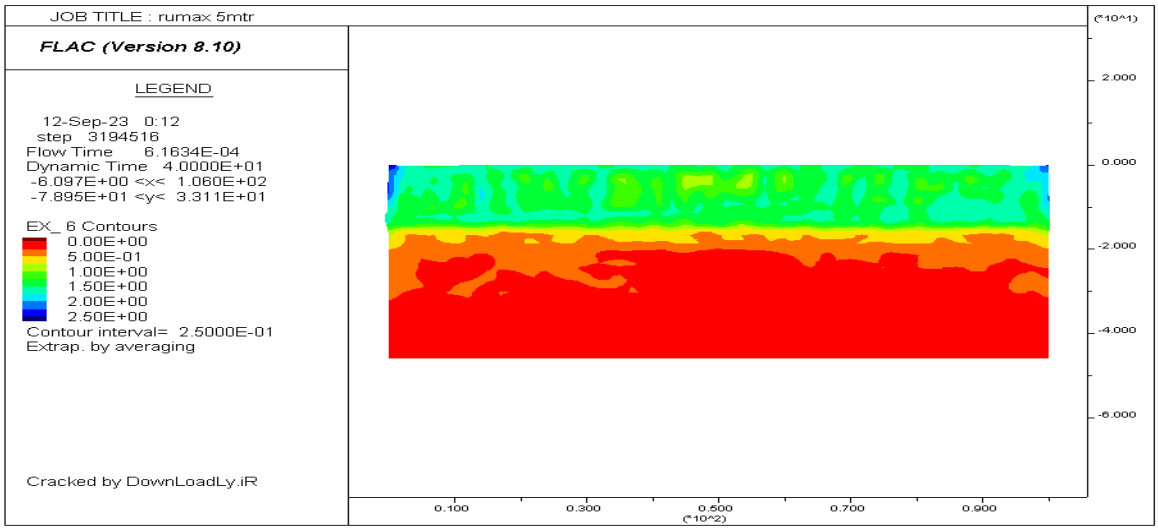

Fig 137: Pore pressure Ratio contour after seismic loading for MOD-11

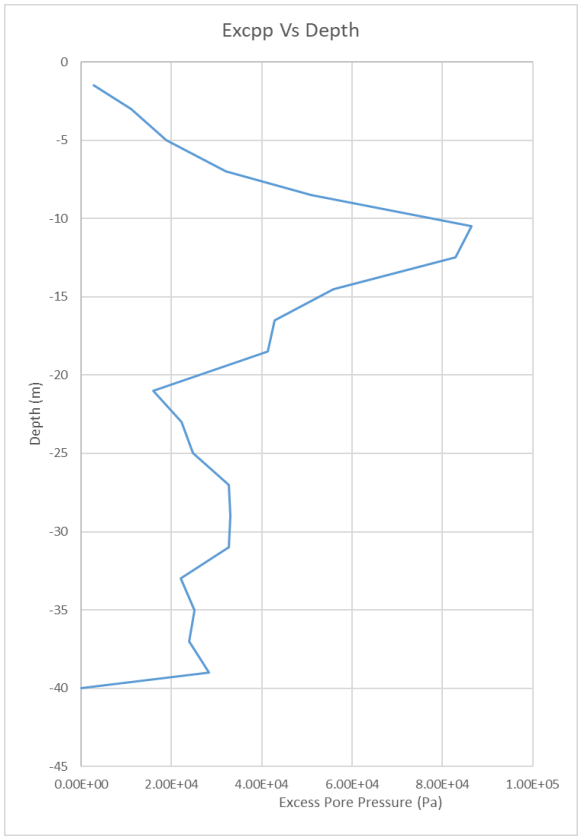

Fig 138: Excpp vs Depth at section A-A,

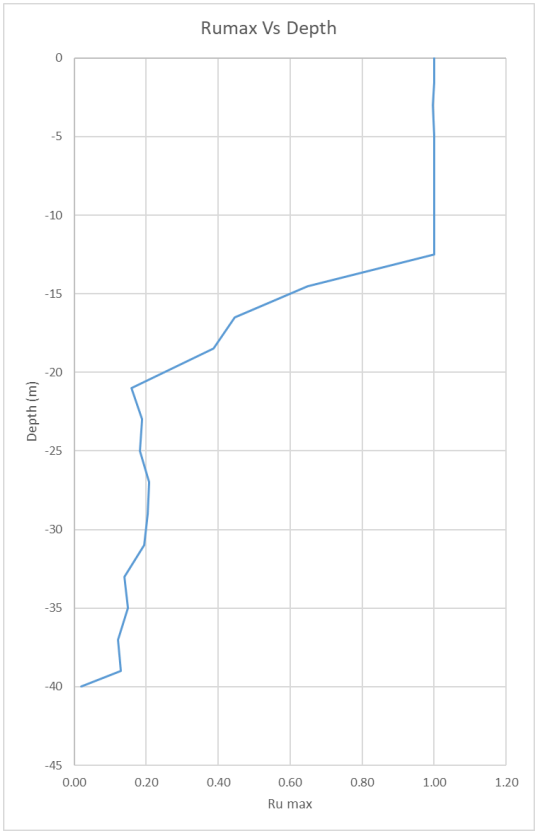

Fig 139: Ru max vs Depth at section A-A

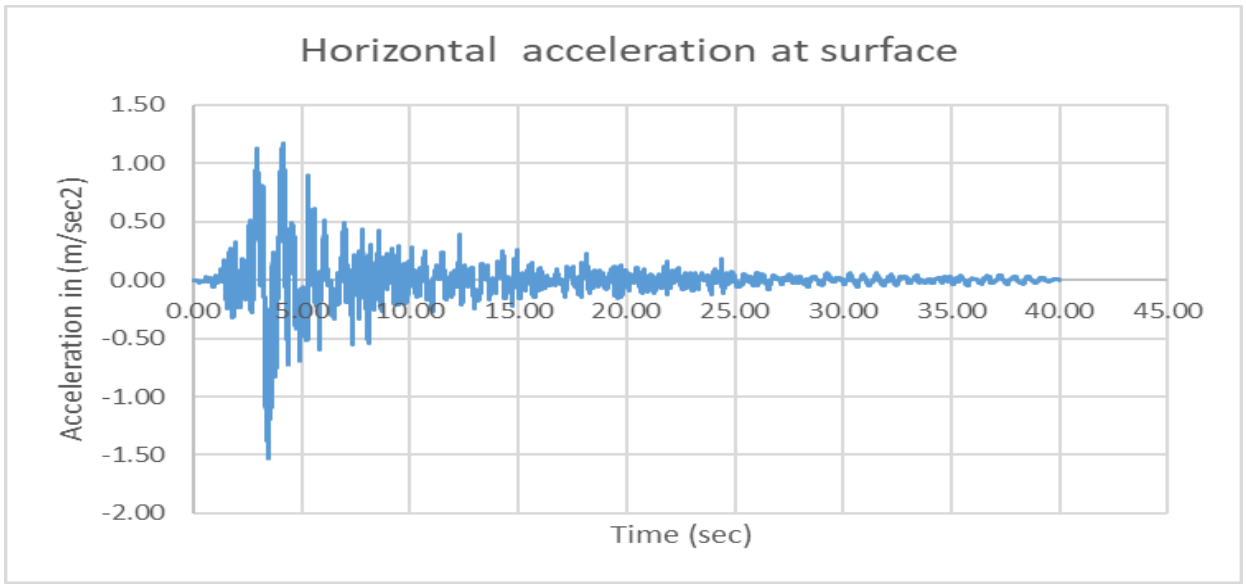

Fig 140: Horizontal acceleration at crest of Embankment of model MOD-11

4.2.12 Results of Dynamic Analysis for MOD-12

MOD-12 as mentioned in Table 13 the soil strata with modified liquefiable layer depth 20m keeping the overall soil strata of same thickness & subjected to a scaled 0.2g PGA of Loma Prieta. From Fig 142 and 144 the maximum excess pore pressure generated in the model is of 102Kpa. The maximum pore pressure ratio of the model reached to 1 at 1.5m from surface and extend to the depth of 12.5m. The peak surface acceleration in Fig 146 is 1.22m/sec2. So the acceleration has been amplified by 0.68 times the input acceleration

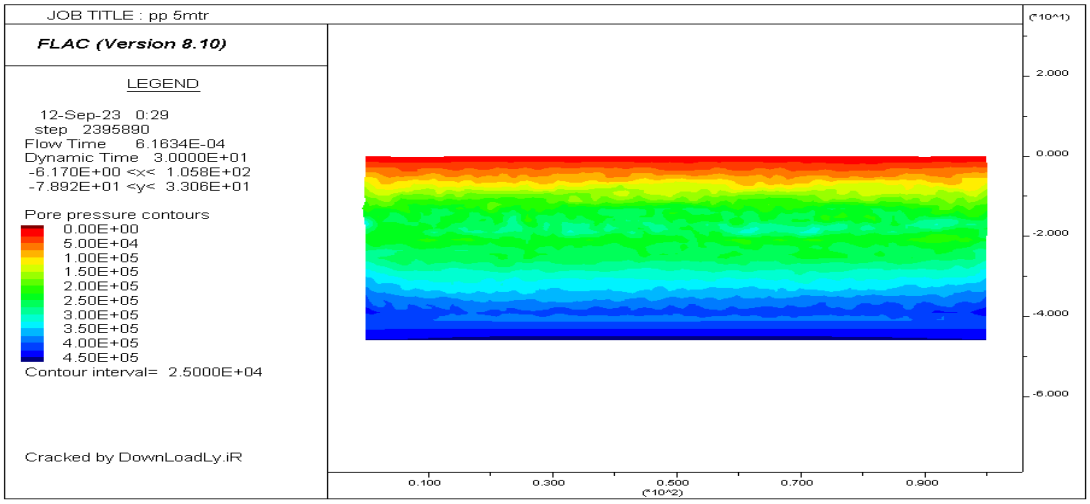

Fig 141: Pore pressure generation contour after seismic loading for MOD-12

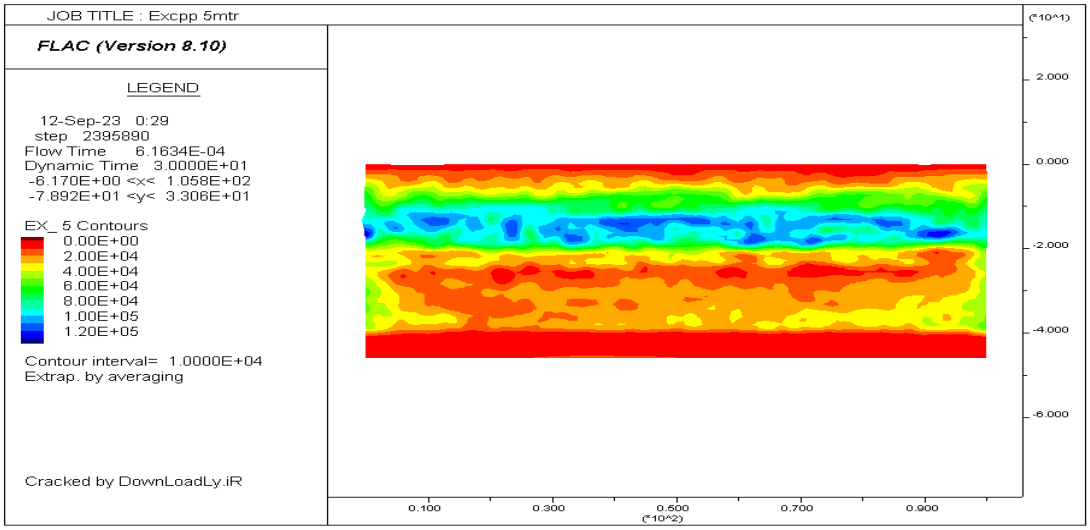

Fig 142: Excess Pore pressure generation contour after seismic loading for MOD-12

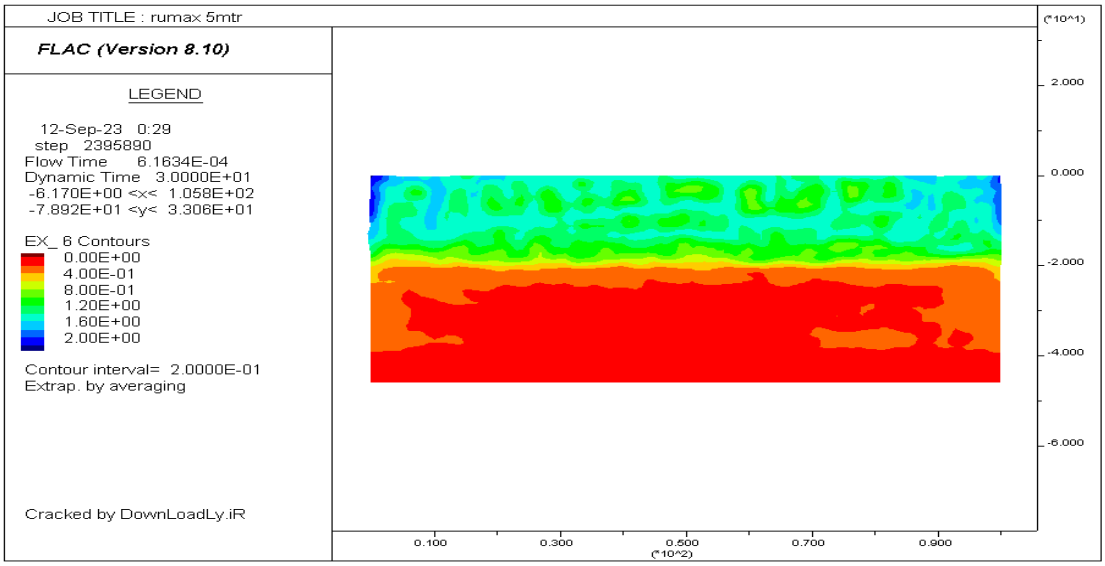

Fig 143: Pore pressure Ratio contour after seismic loading for MOD-12

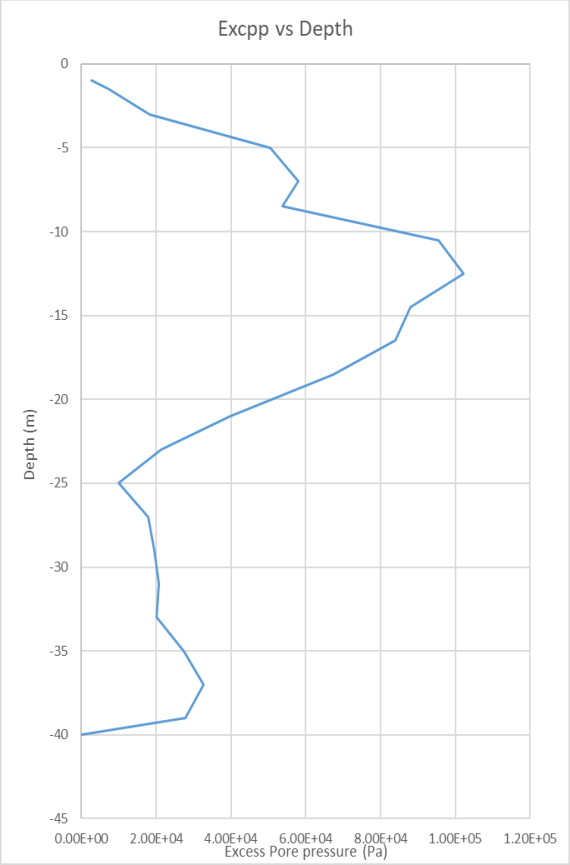

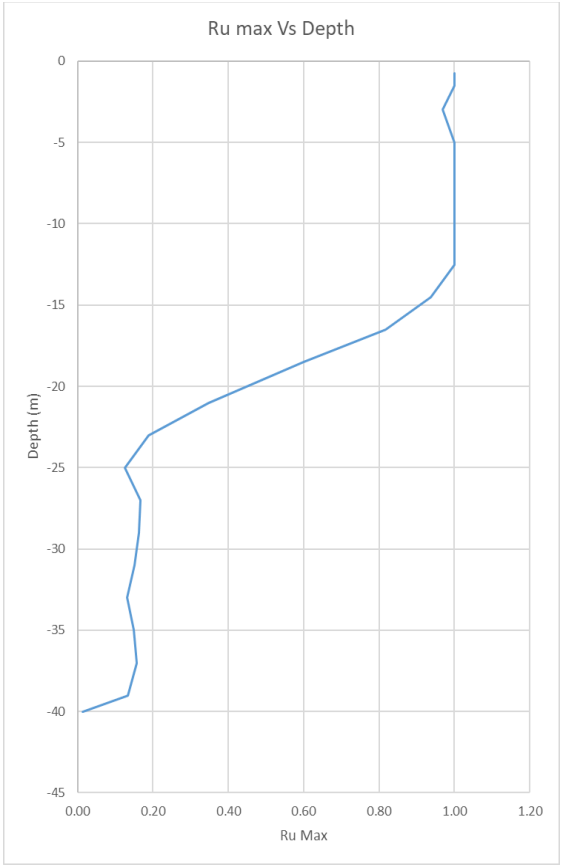

Fig 144: Excpp vs Depth at section A-A,

Fig 145: Ru max vs Depth at section A-A

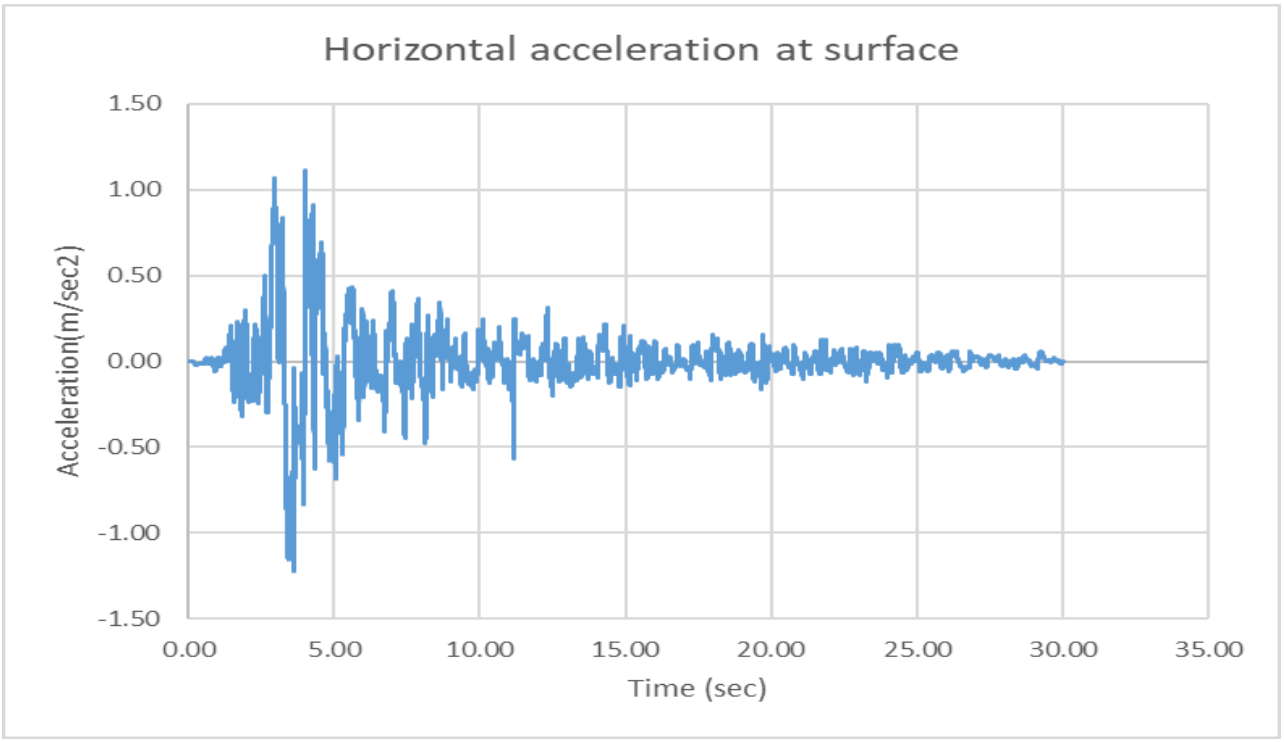

Fig 146: Horizontal acceleration at crest of Embankment of model MOD-12

4.3Discussion on Results

Effect of intensity of motion.

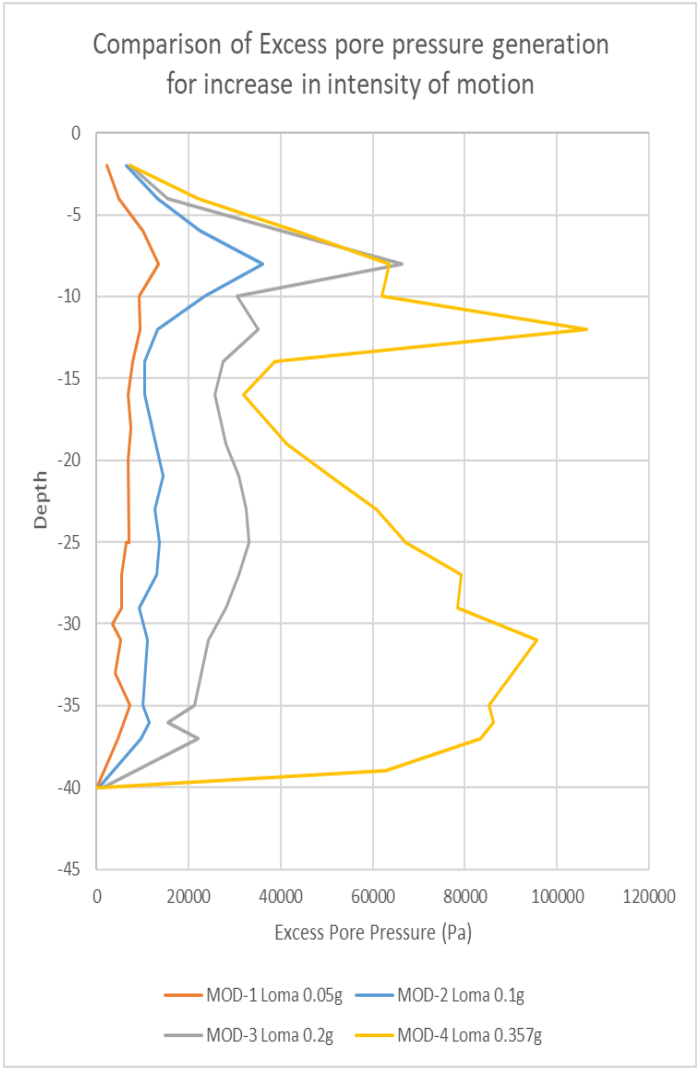

Fig 147: Comparison of Excess pore pressure in MOD-1, 2, 3 &4 for increase in intensity effect

Comparing the results of Model MOD-1, 2, 3 and 4 it has been observed that with the increase in intensity of earthquake the excess pore pressure generation and pore pressure ratio of the soil increases. Pore pressure generation increased in model increase by a multiple of 2 when the input acceleration is increased by 2.

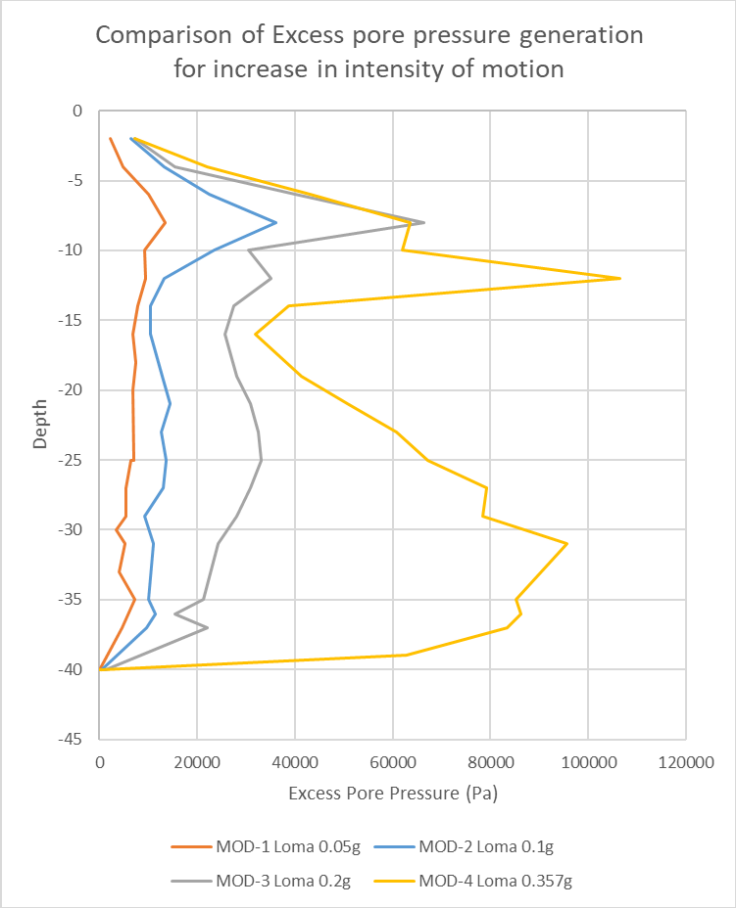

Fig 148: Comparison of Excess pore pressure ratio in MOD-1, 2, 3 &4 for increase in intensity effect

From above fig comparing the output of excess pore pressure ratio for four models indicates there is also an increase in liquefied soil layer depth with the increase in the intensity of the input motion i.e. for

MOD-1 – Depth of liquefaction is zero.

MOD-2 – Depth of liquefaction is 1.5m from surface.

MOD-3 – Depth of liquefaction is 8m from surface

MOD-4 – Depth of liquefaction is 12m from surface

At max intensity of Loma Prieta of 0.357g in Model MOD-4 the generation of excess pore pressure is noticeable in dense sand layer. But the liquefaction doesn't reach to dense sand layer.

Effect of the type of input Motion.

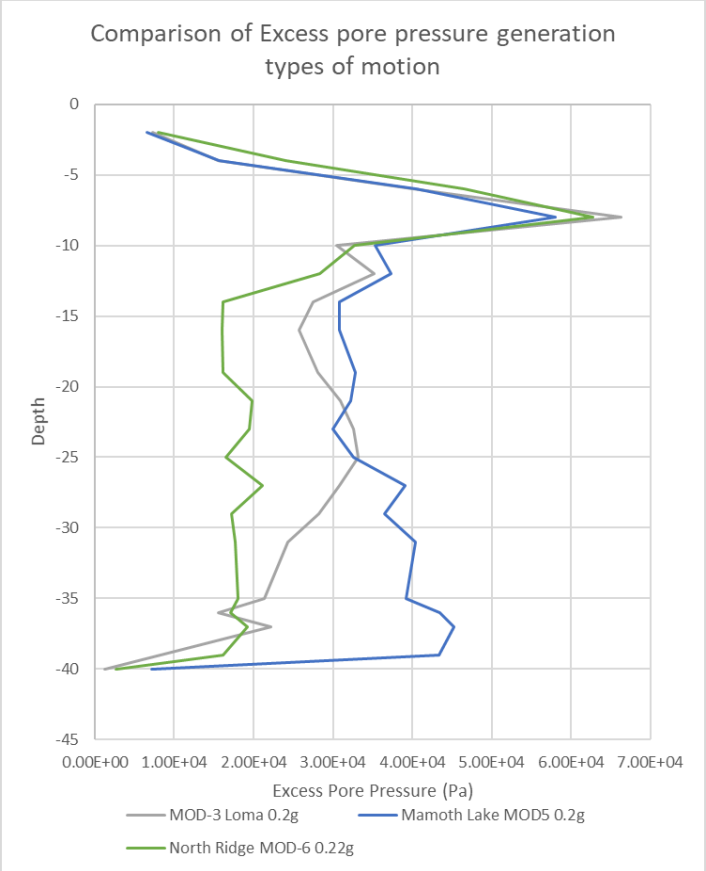

Fig 149: Comparison of Excess pore pressure in MOD-3, 5 & 6 for type of motion.

Comparing the excess pore pressure generation of MOD-3, MOD-5 and MOD-6 shows even though the modified input acceleration varies in quite range of 0.178g, 0.14g and 0.202g for Loma Prieta, Mammoth Lake and Northridge respectively, the excess pore pressure generation in them are quite close of 66.4Kpa, 58Kpa and 62.7Kpa respectively. Despite having higher intensity the pore pressure generation in North Ridge is lower than that of Loma Prieta and close to Mammoth Lake. This is due to the power generation of the Earthquake. From Fig 29, 30 and 31 is evident that the power spectrum of Northridge is lowest, thus generating lower excess pore pressure than others. The pore pressure generation patterns are also affected by the input acceleration. In both Loma Prieta and Northridge Earthquake there has been a sudden increase in pore pressure due to attaining peak in short interval of time, resulting in steep slope for excess pore pressure generation graph. Whereas a smother slope is noticeable in case of Mammoth lake. (From Fig 79, 93 and 100).

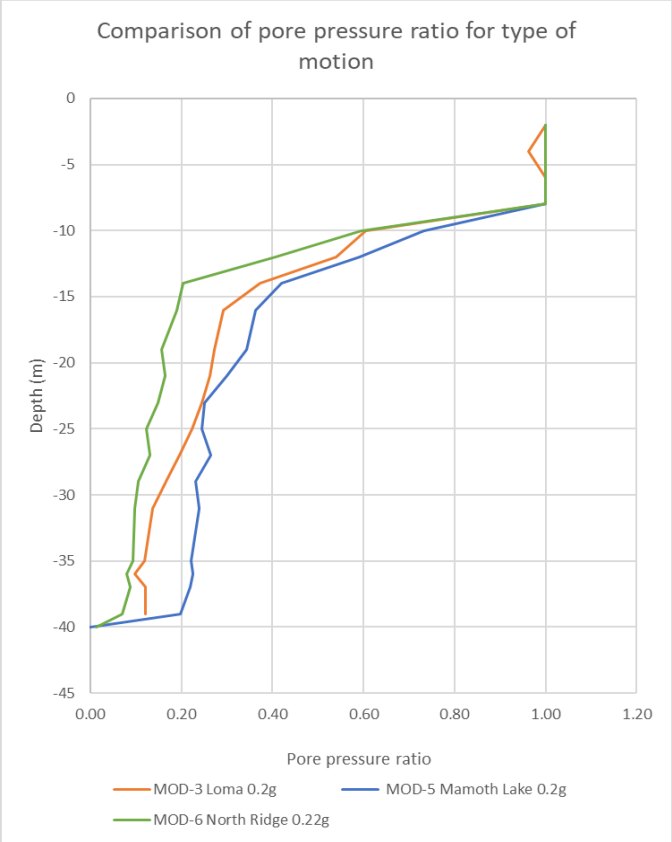

Fig 150: Comparison of Excess pore pressure ratio in MOD-3, 5 & 6 for type of motions

Comparing the excess pore pressure ratio on of MOD-3, MOD-5 and MOD-6 it has been observed that the liquefaction depth for all these are same.

Effect of increase in Top width of Embankment

For static analysis the pore pressure generation in soil increases upon loading with Embankment. The larger embankment the higher value of vertical-displacement can be seen at the crest of the model. The embankment models are quite stable on the foundation soil and shows FOS value of 1.4.

After conducting dynamic analysis the embankment comparing the excess pore pressure generation in models MOD-7, 8, 9 shows the excess pore pressure generation at the centre of the embankment increases with the increase in the width of the embankment. Even though the embankment reduces the liquefaction potential of soil immediately below it by reducing pore pressure ratio, increasing the width of the embankment, an increase of pore pressure ratio has been observed. Increase in the width of the embankment cause in increase in the drainage path of the water, causing pore water to be entrapped below it, which ultimately leads to liquefaction of the foundation soil. At edge initially the excess pore pressure generation are higher than the one at centre and also increases with the increase in width of the embankment up to 20 m. But at 30m the increase in excess pore pressure generation reduces, this reduction is due to the fact that the water is unable to percolate due to increase in drainage length.

At free field location the excess pore pressure generation remains constant irrespective of width of embankment.

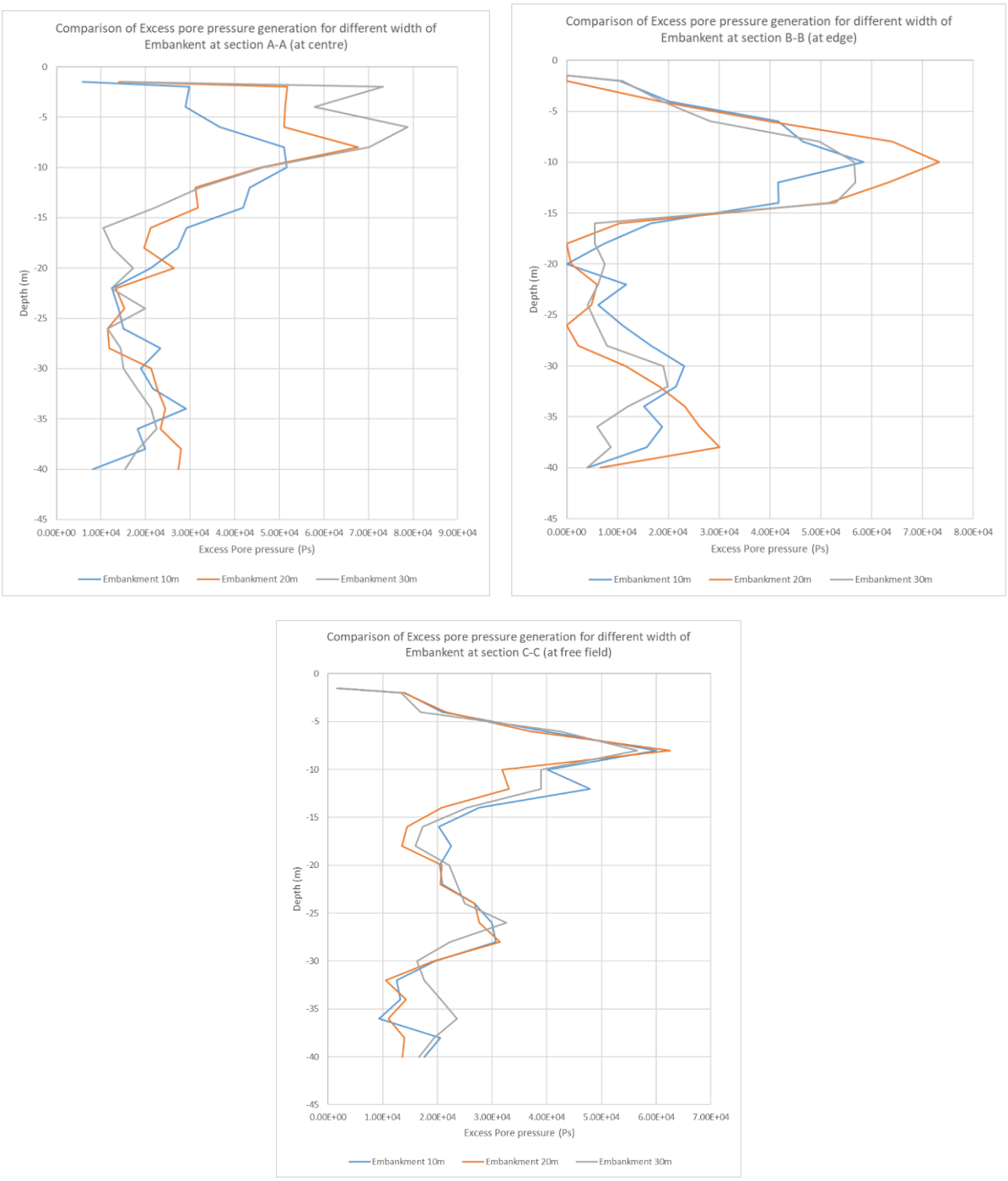

Fig151: Comparing the excess pore pressure in the model at three different sections in MOD-7, MOD-8 and MOD-9

From the above data as the model excess pore pressure increases at the centre below the embankment the pore pressure ratio of the model also increases causing the increase in the depth of liquefiable soil layer as observed from Fig given below where depth is 0, 2, and 4 mtr respectively at 10m, 20m and 30m width of the embankment.. At free field the pore pressure ratio remains constant irrespective of the width of the embankment.

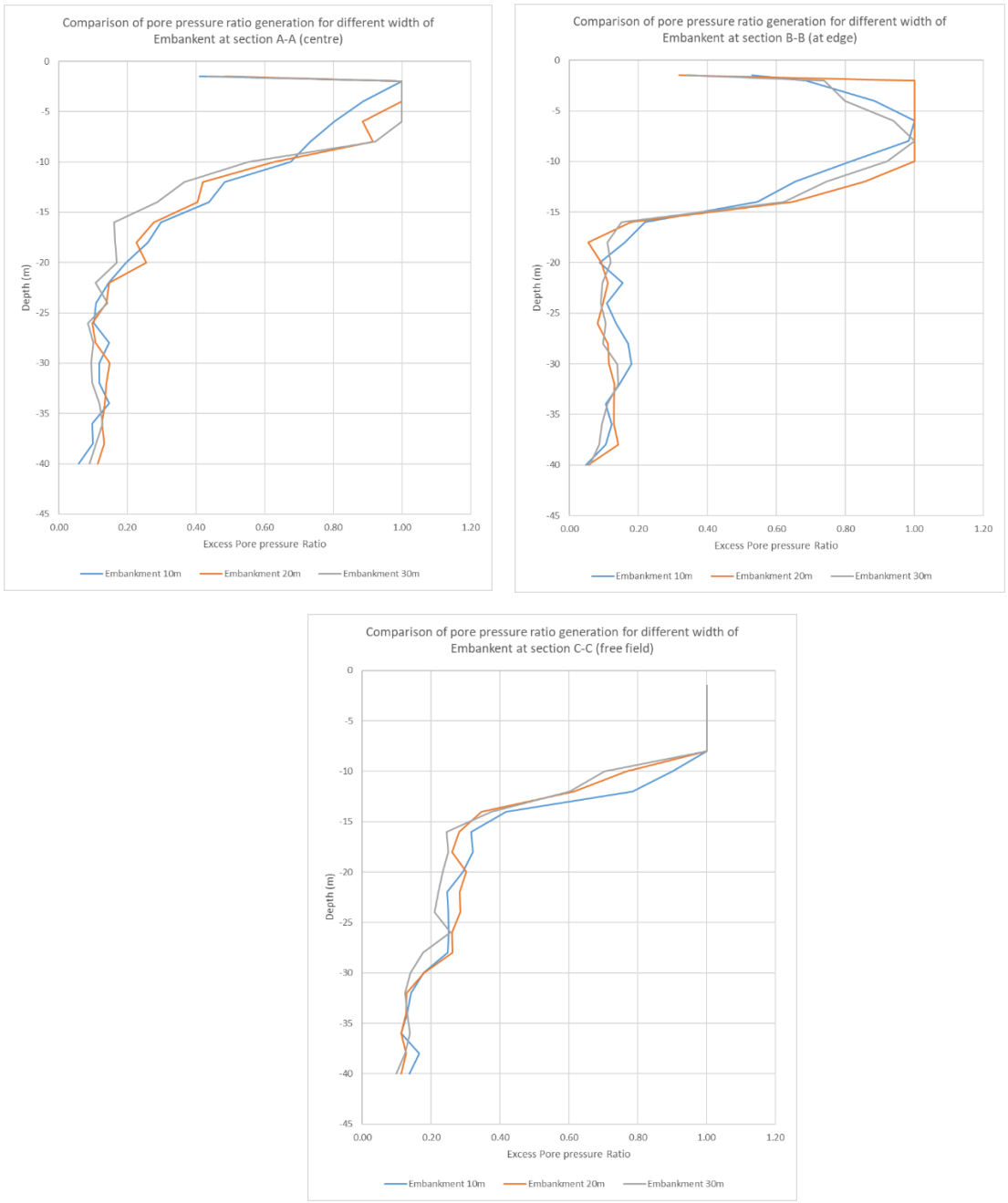

Fig152: Comparing the pore pressure ratio in the model at three different sections in MOD-7, MOD-8 and MOD-9

Effect of variation in Height of Liquefiable layer

After dynamic analysis comparing the pore pressure generation data of Model MOD-10, MOD-3, MOD-11 and MOD-12 where the height of Liquefiable layer is varied between 5m, 9m, 15m and 20m. The excess pore pressure generation increase with the increase in the height of the liquefiable layer as evident from below comparison. The depth at which maximum excess pore pressure generation occurs also seems to increase with the increase in layer height.

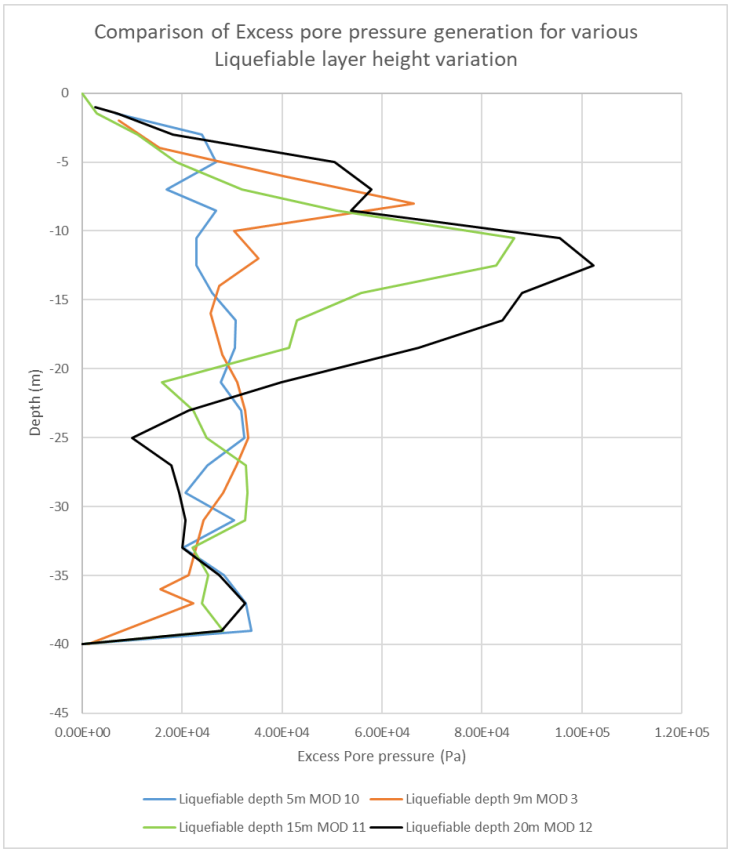

Fig 153: Comparing the Excess pore pressure generation in the model of various liquefiable layer height in MOD-10, MOD-3, MOD-11 and MOD-12

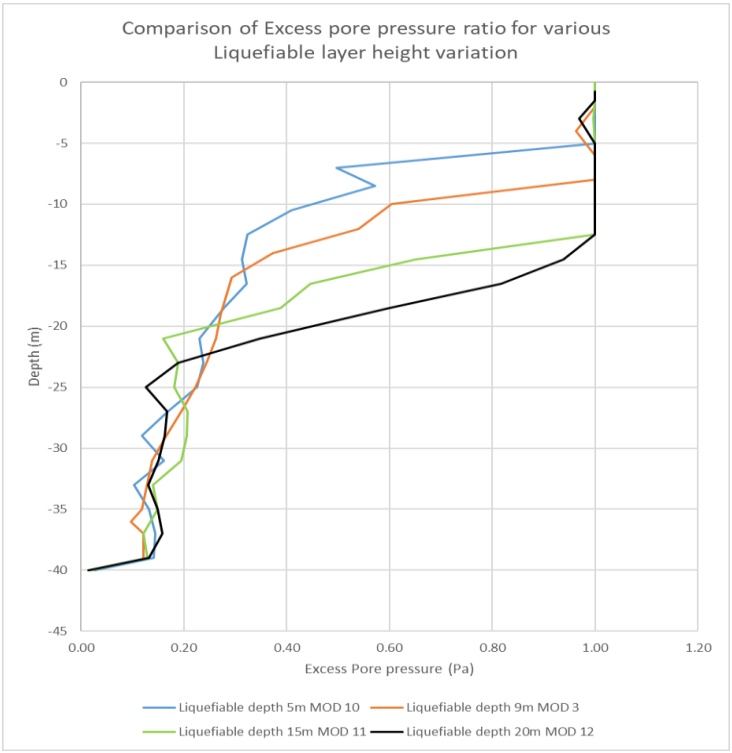

Fig 154: Comparing the Excess pore pressure generation in the model of various liquefiable layer height in MOD-10, MOD-3, MOD-11 and MOD-1

By comparing the excess pore pressure ratio of the model MOD-10, MOD-3, MOD-11 and MOD-12 it has been observed that depth of the liquefied soil increases as height of the liquefiable layer is increased i.e. 5m, 8m, 12m and 12.5m respectively.

Chapter 5

5.1 Concluding Remarks

In the above study a parametric variation is done on the stratified sandy soil deposit by increasing the intensity of input motion, type of motion used, loading it with embankment of variable width and increasing the height of the liquefiable layers. Using the data obtained from the parametric variation study under static and dynamic loading condition on the stratified soil following remarks have been drawn.

1. Under static loading condition soil remains stable and no appreciable vertical displacement can be seen. Under static condition the pore pressure generation in soil is 451KPa. Upon embankment loading on stratified sandy soil deposit a increase in the pore pressure by 32 KPa, 38 KPa and 40 KPa was observed under static condition for 10m, 20m and 30m wide embankment.
2. With the increase in the width of the embankment an increase in the vertical displacement a crest of 6mm, 6.5mm and 7.5mm is observed under static loading. Similarly horizontal displacement has also increased.
3. Static analysis with increase in Liquefiable soil layer height shows very small change in effective stress and total stress in soil.
4. After static stability of the model are checked they have been subjected to dynamic loading. Under dynamic loading a parametric variation is done by increasing the intensity of the input motion in Models MOD-1, MOD-2 MOD-3 and MOD-4, by using scaled input motion of 0.05g, 0.1g, 0.2g and 0.357g of Loma Prieta. With the increase of the intensity of the loading for each model the pore pressure generation and liquefaction tendencies of soil increases. An increase in the depth of the liquefied layer has also occurred for higher intensity of input motion.
5. Another variation done is by using different input motions. In Model MOD-3 0.178g of Loma Prieta has been used, for MOD-5 0.14g of Mammoth Lake was chosen and for MOD-6 0.21g of North ridge has been used. Comparing their pore pressure generations shows similar intensity of excess pore pressure generation. Irrespective of the diversity in intensity there pore pressure generation patterns are similar. This add upto the fact that power of the input motion influences the extent of the liquefaction in soil. Due to lower power amplitude of North Ridge it requires higher intensity to cause same liquefaction effect, caused by Mammoth Lake at lower intensity.
6. Comparing the Peak ground Acceleration vs depth for Models MOD-1, MOD-2 MOD-3 and MOD-4 show similar pattern in the amplification of ground motion at surface of soil
7. For Embankment under dynamic loading the parametric variation is done by increasing the top width of the Embankment for model MOD-7, MOD-8 and MOD-9 by 10m, 20m and 30m respectively. After completion of dynamic analysis is has been observed that the vertical displacement at crest increase with the increase in the width of the embankment i.e. for 10m, 20m and 30m top width the displacement is of 150mm, 250mm and 500mm

8. The ratio of the acceleration at the top of crest in embankment to the acceleration at the base is the amplification ratio. For MOD-7,MOD-8 and MOD-9 the amplification ratio of the input motions are 1.06, 1.17, and 1.03 respectively
9. With the increase in top width of the embankment the pore pressure under dynamic loading increase with increase of width i.e. for 10m, 20m and 30m the excess pore pressure are 51.7Kpa, 67.6Kpa and 78.7Kpa respectively at the center of the embankment. This increase in pore pressure with the increase in top width of the embankment is due to the fact of longer drainage path for entrapped pore pressure, causing the liquefaction failure of the foundation soil.
10. For the last parametric variation the height of the liquefiable layer have been increased by 5m, 9m, 15m and 20m in model MOD-10, MOD-3 MOD-11 and MOD-12. Comparing the pore pressure generation pattern shows increase in excess pore pressure generation as the height of the liquefiable soil increases. The excess pore pressure ratio pattern also indicates toward increase in depth of the liquefied layer with the increase in height.

The above points have been concluded from the parametric study of the stratified soil deposit. Further study will be required to generalise these patterns.

5.2 Future Scope

In future, the study can be extended considering foundation at the top of liquefiable soil and investigating the interaction between soil and foundation. Furthermore the interaction of pile foundation in stratified soil deposit can also be studied.

References:

- Ali Asgari, Aliakbar Golshani & Mohsen Bagheri (2014) "Numerical Evaluation of Seismic Response of Shallow Foundation on Loose Silt and Silty Sand" Journal of Earth System Science DOI: 10.1007/s12040-013-0393-9.
- Ahmad Asaadi & Mohammad Sharifipour (2015) " Numerical simulation of liquefaction susceptibility of soil interacting by single pile" International Journal of Mining and Geo-Engineering Vol.49, No.1, June 2015, pp.47-56.
- Aparna Kanth B. K. Maheshwari (2017) "Effect of Frequency of Loading on Pore Pressure in Solani Sand" Indian Geotechnical Conference 2017 GeoNEst.
- Aleš Oblak , Mirko Kosi , Antonio Viana Da Fonseca and Janko Logar (2019) "Fragility Assessment of Traffic Embankments Exposed to Earthquake-Induced Liquefaction"
- Aleš Jishnu , Mirko Kosi , Antonio Viana Da Fonseca and Janko Logar (2020) "Fragility Assessment of Traffic Embankments Exposed to Earthquake-Induced Liquefaction"
- Byrne, P. M. (1991). A cyclic shear-volume coupling and pore-pressure model for sand in proceedings. Second International Conference on Recent Advances in Geotechnical Earthquake Engineering and Soil Dynamics, St. Louis, Paper N.˚ 1.24, 47–55.
- Eleyas Assefa Dr. Li Jian Lin, Dr. Costas I. Sachpazis, Dr. Deng Hua Feng, Dr. Sun Xu Shu & Xiaoling Xu(2017) "Slope stability evaluation of the railway Embankment using stochastic finite element and Finite difference method" Journal of Geotechnical Engineering
- Giri, D., & Sengupta, A. (2010). Performance of Small-Scale Model Slopes in Shaking Table Tests. Indian Geotechnical Conference, GEOtrendz. IGS Mumbai Chapter & IIT Bombay.
- H.Dash & T.G.Sitharam (2016) "Effect of frequency of cyclic loading on liquefaction and dynamic properties of saturated sand" International Journal of Geotechnical Engineering; Doi.org/10.1080/19386362.2016.1171951
- Issa Shooshpasha & Mohsen Bagheri (2012) " The effects of surcharge on liquefaction resistance of silty sand" ; Arabian Journal of Geosciences
- Itasca (2015) User's guide for FLAC version 8.1. Itasca India Consulting, Nagpur: India
- Kaustav Chatterjee & Deepankar Choudhury (2012) " Variations in shear wave velocity and soil site class in Kolkata city using regression and sensitivity analysis" Nat Hazards (2013) 69:2057–2082
- Martin, G. R., Finn, W. D. L., and Seed, H. B. (1975). "Fundamentals of liquefaction under cyclic loading." J. Geotech. Eng. Div., 101(5), 423–438
- Mehdi Derakhshandi, Ellen M. Rathje, Kenan Hazirbaba, S.M. Mirhosseini (2007). "The effect of plastic fines on the pore pressure generation characteristics of saturated sands" Article in Soil Dynamics and Earthquake Engineering
- Nima Ranjbar Malidareh & Asskar Janalizadeh Choobbasti (2008) " Mitigation of Liquefaction Using Stone Columns" : Electronic Journal of Geotechnical Engineering
- N. Dinesh, K. Rajagopal and Subhadeep Banerjee (2016) "Study Of Constitutive Models For Cyclic Liquefaction In Sand" Indian Geotechnical Conference IGC2016.
- Nath SK, Adhikari MD, Maiti SK, Devaraj N, Srivastava N, Mohapatra LD (2014) Earthquake scenario in West Bengal with emphasis on seismic hazard microzonation

of the city of Kolkata. India Nat Hazard Earth Sys 14:2549–2575. doi.org/10.5194/nhess-14-2549-2014

- Omar Vargas, Ricardo Ortiz And Francisco Flores (2014) "Liquefaction Analysis Using Pore Pressure Generation Models During Earthquakes".
- Pradipta Chakrabortty, A.D.Pandey, S. Mukerjee and Ashish Bhargava (2004) "Liquefaction Assessment For Microzonation Of Kolkata City" 13th World Conference on Earthquake Engineering
- Rashid Zandian, Reza Imam and Arash Azizi (2009) "Modeling sand behavior using a critical state model implemented in FLAC".
- Raj Banerjee Sanku Konai, Aniruddha Sengupta & Kousik Deb (2017) "Shake Table Tests and Numerical Modeling of Liquefaction of Kasai River Sand"; Geotech Geol Eng (2017) 35:1327–1340; DOI 10.1007/s10706-017-0178-z
-
- Seed, H. B., Martin, P. P., and Lysmer, J. (1975). "The generation and dissipation of pore-water pressures during soil liquefaction." Geotechnical Report No. EERC 75-26, Univ. of California, Berkeley, CA.
- Shashank Bhatnagar, Sunita Kumari and V. A. Sawant (2015) "Numerical Analysis of Earth Embankment Resting on Liquefiable Soil and Remedial Measures" an International Journal of Geomechanics
- Sankar Kumar Nath & Nishtha Srivastava & Chitralekha Ghatak & Manik Das Adhikari & Ambarish Ghosh & S. P. Sinha Ray (2017) "Earthquake induced liquefaction hazard, probability and risk assessment in the city of Kolkata, India: its historical perspective and deterministic scenario" DOI 10.1007/s10950-017-9691-z
- 25. Surya P and Midhun Raj S N (2019) "Analysis for Pore Pressure Buildup Using UBCSand Model" 2019 JETIR May 2019, Volume 6, Issue 5.

- T. G. Sitharam & L. Govindaraju (2007) Pore pressure generation in silty sands during cyclic loading, Geomechanics and Geoengineering: An International Journal, 2:4, 295-306.
- Wayan Sengara & Ahmad Sulaiman (2020) "Nonlinear Dynamic Analysis Adopting Effective Stress Approach of an Embankment Involving Liquefaction Potential"; E3S Web of Conferences 156, 02018 (2020)
- Yu-liang Lin ,Feng Shi,Xiao Yang, Guo-lin Yang & Li-min Li (2016) "Numerical analysis on seismic behavior of railway earth embankment: A case study" Journal of Central South University volume 23, pages906–918 (2016).